

Sapling Dynamics and Forest Composition Along Environmental Gradients

DISSERTATION ZUR ERLANGUNG DES DOKTORGRADES
DER NATURWISSENSCHAFTEN (DR. RER. NAT.)
DER FAKULTÄT FÜR BIOLOGIE UND VORKLINISCHE MEDIZIN
DER UNIVERSITÄT REGENSBURG

vorgelegt von:

LUKAS HEILAND

aus
Bad Langensalza

im Jahr
2023

Das Promotionsgesuch wurde eingereicht am:
6. Juli 2023

Die Arbeit wurde angeleitet von:
PROF. DR. LISA HÜLSMANN

Unterschrift:

Acknowledgements

Thanks to the best advisors, Lisa Hülsmann and Georges Kunstler, for their great trust and sharp criticism. Thanks to Volker Peckhaus, Andreas Vogel, Norbert Hölzel, Till Kleinebecker, Hans Joosten, John Couwenberg, Martin Schnittler, and Otti Wilmanns for continuously changing my path. Thanks to the Bavarian Ministry of Science and the Arts for funding this work and the project BayForDemo within the Bavarian Climate Research Network (bayklif).

Danksagungen

Danke an alle, die mich auf dem Weg zu dieser letzten Hausaufgabe begleitet haben. An Mama, Papa, und Henni für bedingungslose Geduld und Liebe. An Mathilda, Philipp, Adele, und Mathilde für die Aussicht auf eine bessere Welt (ohne Hausaufgaben). An Janis, Niclas, Sabrina, Robert, Lukas, Stjepan, Tobi, Lisa M., Lisa W., Hanna, und Leo für Heimat, Gespräche, und die Getränke. Für schöne Ablenkungen neben der Arbeit an Johannes, Max, und Amaël.

LUKAS HEILAND
Regensburg
Juli 2023

Contribution statement

The three central chapters of this thesis have been or will be submitted as research articles to scientific journals with contributions of different co-authors.

Chapter 2

Heiland, L., G. Kunstler, P. Ruiz-Benito, A. Buras, J. Dahlgren, L. Hülsmann (2022). Divergent occurrences of juvenile and adult trees are explained by both environmental change and ontogenetic effects. *Ecography* 2022 (3). <https://doi.org/10.1111/ecog.06042>

- **L. He.**, **L. Hü.**, and **G.K.** conceptualized the manuscript and developed the methods. **P.R.B.**, **J.D.**, and **L. He.** curated the NFI data. **A.B.** contributed the methodology and preparation of the climate data. **L. He.** carried out the simulations, analyzed the data, and wrote the first draft. **L. He.**, **L. Hü.**, **G.K.**, and **P.R.B.** interpreted the results. All authors contributed ideas and to writing in the revision of the manuscript.

Chapter 3

Heiland, L., G. Kunstler, V. Šeben, L. Hülsmann (accepted). Which demographic processes control competitive equilibria? Bayesian calibration of a size-structured forest population model. *Ecology and Evolution* 2023.

- **L.He.**, **L.Hü.**, and **G.K.** conceptualized the study. **L.He.**, with advice from **L.Hü.** and **G.K.**, developed the methods. **L.He.** and **V.Š.** curated the NFI data. **L.He.** wrote the software and the first draft. All authors contributed conceptual ideas and to writing the final manuscript.

Chapter 4

Heiland, L., G. Kunstler, L. Hülsmann (in preparation). Explaining the environmental pattern of beech predominance with variation of demography.

- **L.He.**, together with **L.Hü.** and **G.K.**, conceptualized the study and developed the methods. **L.He.** wrote the software and the first draft. All authors contributed to writing of the draft.

Contents

1	Introduction	1
2	Divergent occurrences of juvenile and adult trees are explained by both environmental change and ontogenetic effects	3
2.1	Introduction	4
2.2	Methods	6
2.2.1	Two-life stage simulation model	7
2.2.2	Analyses of European national forest inventory data	8
2.3	Results	14
2.3.1	Simulated divergent occurrences	14
2.3.2	Divergent occurrences in NFIs	14
2.4	Discussion	18
2.4.1	Simulated divergences between life stages	18
2.4.2	Attributing juvenile divergence to temporal range shift or ontogenetic effects	19
2.4.3	Divergent occurrences between life stages in European forests	19
2.4.4	Conclusions	23
3	Which demographic processes control competitive equilibria? Bayesian calibration of a size-structured forest population model	25
3.1	Introduction	25
3.2	Methods	27
3.2.1	JAB model	28
3.2.2	NFI data	31
3.2.3	Prior parameter distributions	33
3.2.4	Bayesian calibration of the JAB model	34
3.2.5	Posterior simulations	35
3.2.6	HMC sampling	36
3.3	Results	36
3.3.1	Estimates of demographic rates	36
3.3.2	Initial state and extrapolated competitive equilibria	37
3.3.3	Counterfactual equilibria with switched parameters	39
3.4	Discussion	43
3.4.1	Estimates of demographic rates	43
3.4.2	Predominance at the competitive equilibrium	44

CONTENTS

3.4.3	Which species-specific differences in demographic rates lead to pre- dominance?	45
3.4.4	Prospects for the JAB model	46
3.4.5	Conclusions	46
4	Explaining the environmental pattern of beech predominance with variation of demography	49
4.1	Introduction	50
4.2	Materials and Methods	52
4.2.1	JAB Model	52
4.2.2	Data	53
4.2.3	Short time series from NFI data	53
4.2.4	Environmental variables	54
4.2.5	Fitting the JAB model with environmental variation of demographic rates	55
4.2.6	Posterior simulations from the fitted JAB model	57
4.3	Results	60
4.3.1	Estimates of demographic rates	60
4.3.2	Environmental variation of demographic rates	60
4.3.3	Equilibria in environmental space	61
4.3.4	Effect of demographic environmental variation on equilibria	61
4.4	Discussion	66
4.4.1	Species differences of demographic rates	66
4.4.2	Theoretical predictions and simulated competitive equilibria in envi- ronmental space	67
4.4.3	How do environmentally-varying rates control predominance?	68
4.4.4	Conclusions	69
5	Discussion	71
I	Supplementary Material for Chapter 2	i
II	Appendices to Chapter 3	iii
A	Methods	iii
A.1	NFI data	iii
A.2	Accounting for varying sampling areas with offsets	iv
A.3	Species' regional abundance for predicting seedling input	vi
A.4	Prior inference on seedling recruitment	vi
B	Code repository	viii
C	Data repository	viii
D	Supplementary tables	viii
E	Supplementary figures	xii
III	Supplementary Material for Chapter 4	xvii
A	Supplementary Methods	xvii
A.1	JAB model description	xvii
A.2	Species' regional abundance for predicting seedling input	xix

CONTENTS

A.3	Offsets for scaling area-standardized model states to observed counts	xx
B	Supplementary Tables	xxi
C	Supplementary Figures	xxvi
Bibliography		xxxvii

Understanding where species occur is without doubt one of the central question in ecology (MACARTHUR, 1972; SUTHERLAND *et al.*, 2013). To describe the occurrence of species dependent on environmental variables, ecologists have used abundance response curves (ELLENBERG, 1952; WHITTAKER, 1967; TER BRAAK and PRENTICE, 1988). To explain the abundance response of species with the variation of the underlying demographic processes to the environment (MAGUIRE, 1973; SCHURR *et al.*, 2012; NORMAND *et al.*, 2014), process-explicit species distribution models have been proposed (SDM; e.g., HIGGINS *et al.*, 2012; SCHURR *et al.*, 2012; NORMAND *et al.*, 2014; PIRONON *et al.*, 2017; KUNSTLER *et al.*, 2021; SCHULTZ *et al.*, 2022).

In forest ecology, however, a contradiction between theory and modelling practice has been striking: On one hand, the crucial role of juvenile trees, i.e. seedlings and saplings, for tree establishment and species composition has been widely accepted (GRUBB, 1977; YOUNG *et al.*, 2005; LINES *et al.*, 2019). It has furthermore been recognized, that saplings often respond differently to the environment than their conspecific adults (ERIKSSON, 2002; BERTRAND *et al.*, 2011; NI and VELLEND, 2021), which leads to the conclusion that different environmental responses of saplings can control forest species composition. On the other hand, process-explicit models that aim to explain tree species occurrence by environmental variation of demographic rates (VANDERWEL *et al.*, 2017; SCHULTZ *et al.*, 2022, e.g.), rarely include demographic processes at the seedling and sapling stage (PRICE *et al.*, 2001; HANBURY-BROWN *et al.*, 2022; KÖNIG *et al.*, 2022), thus ignoring the different responses of early life stages to the environment. Disregarding the dynamics of young trees in particular could lead to wrong forecasting of future species distributions. Despite forecasting being one of the main selling points of process-explicit species distribution models in the first place (BUCKLEY *et al.*, 2010; PAGEL and SCHURR, 2012; ZURELL *et al.*, 2012; THUILLER *et al.*, 2013; MEROW *et al.*, 2014).

To overcome this limitation and to gain better insight into forest dynamics, this work lays out an argument in three main chapters to include the environmental response of saplings in forest models. First, in Chapter 2, we establish that juvenile trees frequently occur under different conditions along environmental gradients compared to adults, which can be attributed to ontogenetic effects. Consequently, in Chapter 3, a simple process-

explicit model is proposed that includes demographic processes at the sapling stage. It is further demonstrated how the model can be used to forecast competitive equilibria in a two-species system. To synthesize the two chapters before, in Chapter 4, the model is applied to explain environmental variation of species composition with environmental variation of demographic rates of saplings and adult trees. Finally, in conclusion (Chapter 5), the implications of the findings for forest ecology on the one hand and for ecological modelling on the other hand will be discussed.

Divergent occurrences of juvenile and adult trees are explained by both environmental change and ontogenetic effects

2

Abstract

Recent climate warming has fueled interest into climate-driven range shifts of tree species. A common approach to detect range shifts is to compare the divergent occurrences between juvenile and adult trees along environmental gradients using static data. Divergent occurrences between life stages can, however, also be caused by ontogenetic effects. These include shifts of the viable environmental conditions throughout development (“ontogenetic niche shift”) as well as demographic dependencies that constrain the possible occurrence of subsequent life stages. Whether ontogenetic effects are an important driver of divergent occurrences between juvenile and adult trees along large-scale climatic gradients is largely unknown. It is, however, critical in evaluating whether impacts of environmental change can be inferred from static data on life stage occurrences. Here, we first show theoretically, using a two-life stage simulation model, how both temporal range shift and ontogenetic effects can lead to similar divergent occurrences between adults and juveniles (*juvenile divergence*). We further demonstrate that *juvenile divergence* can unambiguously be attributed to ontogenetic effects, when juveniles diverge from adults in opposite direction to their *temporal shift* along the environmental gradient. Second, to empirically test whether ontogenetic effects are an important driver of divergent occurrences across Europe, we use repeated national forest inventories from Sweden, Germany, and Spain to assess *juvenile divergence* and *temporal shift* for 40 tree species along large-scale climatic gradients. About half of the species-country combinations had significant *juvenile divergences* along heat sum and water availability gradients. Only a quarter of the tree species had significant detectable *temporal shifts* within the observation period. Furthermore, significant *juvenile divergences* were frequently associated with opposite *temporal shifts*, indicating that ontogenetic effects are a relevant cause of divergent occurrences between life stages. Our study furthers the understanding of ontogenetic effects and challenges the practice of inferring climate change impacts from static data.

2.1 Introduction

Recently, global climate change has put rapid external pressure on ecosystems (WALTHER *et al.*, 2002; FEEHAN *et al.*, 2009; LINDNER *et al.*, 2010). In addition, European ecosystems have experienced regional changes in land-use practices (SMITH *et al.*, 1999; HODGSON *et al.*, 2005; TURNER *et al.*, 2007). In response to pressure from environmental change, species can shift their ranges. Plant species have been shown to shift ranges over time in response to land-use change (e.g., CUDLÍN *et al.*, 2017; PERRING *et al.*, 2018), and there has been elevated interest in climate change-driven range shifts—in particular in tree species (e.g., LENOIR *et al.*, 2008; CHEN *et al.*, 2011; GIBSON-REINEMER and RAHEL, 2015).

In order to show climate-driven range shifts in trees, many recent studies have compared the occurrence of different size classes within a species along environmental gradients (e.g., LENOIR *et al.*, 2009; MONLEON and LINTZ, 2015; SMITHERS *et al.*, 2018). In these studies, tree size is assumed to reflect tree age, so that larger trees are used as a proxy for conditions further in the past, compensating the lack of historical tree occurrence data. Many studies have found that the distribution of smaller trees (here called “juveniles”) was shifted to higher elevations (e.g., LENOIR *et al.*, 2009; WASON and DOVCIK, 2017), higher latitudes (e.g., WOODALL *et al.*, 2009; MONLEON and LINTZ, 2015), or lower temperatures compared to the distribution of larger “adult” trees (e.g., BELL *et al.*, 2014; MATHYS *et al.*, 2018). Given that trees are sessile organisms with long life cycles, it is assumed that their ranges respond slowly to environmental pressure. And since the size class of juvenile trees has faster turnover than adults, under a changing environment the range of juveniles is thought to track the niche conditions more closely (MONLEON and LINTZ, 2015). Consequently, divergent occurrences of two size classes or life stages are commonly interpreted as an indicator of a temporal range shift of the entire population because juveniles have established in a new range (e.g., PEÑUELAS *et al.*, 2007; SMITHERS *et al.*, 2018).

Assuming that divergent occurrences of juveniles and adults result from temporal change alone is however problematic. During ontogeny, i.e. the progress through stages of development (GATSUK *et al.*, 1980), here reflected by size classes, the occurrence of trees can also be influenced by different types of ontogenetic effects (Figure 21). In particular, one of these ontogenetic effects, different responses of life stages to the environment, sometimes referred to as “ontogenetic niche shift” (e.g., WERNER, 1984; PARISH and BAZZAZ, 1985), can cause divergent occurrences of juveniles and adults as well (ERIKSSON, 2002; YOUNG *et al.*, 2005; MIRITI, 2006; BERTRAND *et al.*, 2011; NI and VELLEND, 2021). Ontogenetic niche shift is a likely mechanism acting on tree species (e.g., STOHLGREN *et al.*, 1998; CAVENDER-BARES and BAZZAZ, 2000; BERTRAND *et al.*, 2011), because a tree species’ phenotype undergoes marked change during its life history from seedling to adult stage (e.g., THOMAS and WINNER, 2002; AUGSPURGER and BARTLETT, 2003; LUSK, 2004; NIINEMETS, 2006; NIKLAS and COBB, 2010; VITASSE, 2013; LEUSCHNER and MEIER, 2018). This is why MÁLIŠ *et al.* (2016) have recently highlighted that divergent occurrences between juvenile and adult trees can not simply be interpreted as temporal range shifts. Instead, they have demonstrated that observed distributional differences between seedlings and adults along an elevation gradient in the Western Carpathians are better explained by their life stage than temporal range shift (see also SITTARO *et al.*, 2017). Nevertheless, subsequent studies have interpreted ontogeny as a proxy for time when analyzing range shifts in trees on larger scales (WASON and DOVCIK, 2017; MATHYS *et al.*, 2018; SMITHERS *et al.*, 2018), while the relative importance of ontogenetic effects for divergent occurrences along large-scale climatic gradients remains

still unknown.

Here, we evaluate at a continental scale whether impacts of climate and land-use change on tree species ranges can be inferred from static data, by dissecting which processes are important drivers of divergent occurrences of tree life stages across Europe: temporal range shifts or ontogenetic effects. Expanding on the argument of MÁLIŠ *et al.* (2016) who concentrated on the ontogenetic effects niche shift, niche expansion and contraction, we analyze an additional ontogenetic effect: demographic dependencies between life stages, which can also lead to divergent occurrences of juvenile and adult trees (Figure 21).

To understand how ontogenetic effects can cause divergent occurrences of life stages in environmental space, it is necessary to, first, clarify the distinction between Hutchinson niche and occurrence of a species and, second, break down the Hutchinsonian niche concept to life stages:

The Hutchinson niche is a hypervolume in environmental space representing the environmental conditions where the entire population of a species is potentially able “to survive and reproduce” (HUTCHINSON, 1957). But the actually observable occurrence space of a species is not equivalent to the niche (SOBERÓN and PETERSON, 2005): limited dispersal will reduce occurrence compared to the niche, not all niche conditions might actually be realized in geographical space, and finally, in a changing environment, occurrence can be out of equilibrium and trailing the niche conditions.

Second, the niche concept can be applied to individual life stages within a population. MAGUIRE (1973) introduced the analytical view of breaking down the niche into multiple hypervolumes representing the responses of ontogenetic stages to the environment, here called “ontogenetic niches”. Ontogenetic niches can be defined analogously to the fundamental niche (HUTCHINSON, 1957) of a whole population: As the fundamental niche comprises the environmental conditions at which an ideal population would persist independent of dispersal and species interactions (HUTCHINSON, 1957; SOBERÓN and PETERSON, 2005), we define ontogenetic niches as the environmental conditions where ideal populations of life stages would persist if they were independent of all other life stages. Thus, independence of other life stages is a key distinguishing property of ontogenetic niches compared to life stage occurrences, which are necessarily interdependent through transitions between them.

Independent shift, expansion or contraction of niches between life stages through different demographic responses to the environment (GRUBB, 1977; PARISH and BAZZAZ, 1985; MIRITI, 2006; BERTRAND *et al.*, 2011; VECCHIO *et al.*, 2020) can lead to observed divergent occurrences between juveniles and adults (BERTRAND *et al.*, 2011; PIRONON *et al.*, 2017). The occurrence of a life stage, however, is constrained by the occurrence of earlier life stages (YOUNG *et al.*, 2005) and the environmentally-dependent probability of proceeding to later life stages. Demographic dependencies between life stages can therefore also lead to divergent occurrences of life stages.

Here, we aim to disentangle the contribution of temporal range shift and ontogenetic effects to the patterns of divergent occurrences between juvenile and adult trees (*juvenile divergence*; Figure 21), with regression models applied to both theoretical data from simulations and empirical data from repeated forest inventories. First, we explore with a theoretical two-life stage simulation model how life stage occurrences along an environmental gradient respond to temporally shifting environmental conditions and ontogenetic effects. Our simulations illustrate how both temporal range shift and ontogenetic effects can cause divergent occurrences of two life stages, and how temporal range shift and ontogenetic niche shift can act simultaneously. Second, we empirically evaluate with a regression model whether

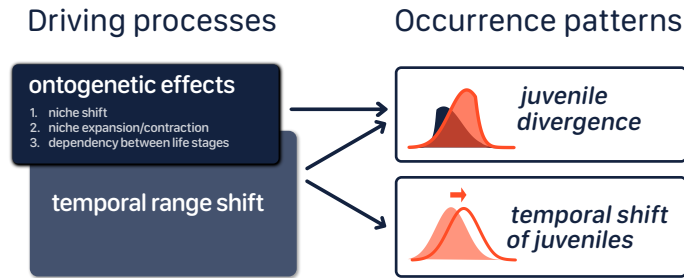


FIGURE 21: Ontogenetic effects and temporal range shift can have different observable effects on occurrence patterns of sessile organisms like trees: *Juvenile divergence*, i.e. the observed difference of juvenile occurrence compared to adult occurrence along an environmental gradient, can be driven by both ontogenetic effects and advancing juveniles under a temporal range shift of the entire population. An observed *temporal shift* of juveniles along the gradient, however, unambiguously indicates a temporal range shift.

temporal range shifts or ontogenetic effects are responsible for *juvenile divergences* observed along two large-scale climatic gradients, i.e. long-term averages of heat sum and water availability, across European forests. To this end, we estimated the effect of time and life stage on species' occurrence centers along each climatic gradient using two repeated surveys of national forest inventories (NFIs) from Sweden, Germany, and Spain. Since the vast majority of forests in these countries have been managed (McGRATH *et al.*, 2015), we expect that the estimated occurrences of life stages will be impacted by management and thus that *temporal shifts* could emerge from both climate change and changes in management regime (e.g., forest encroachment at higher altitudes after abandonment; AMÉZTEGUI *et al.*, 2010). To attribute the pattern of *juvenile divergence* to either temporal range shift or ontogenetic effects, we propose a framework of hierarchical tests, that takes advantage of the observed *temporal shifts* of juveniles from repeated surveys and compares differences in occurrence patterns instead of trying to infer different niches. Applying this framework to occurrence patterns of tree species along two large-scale climatic gradients, we assess the relevance of ontogenetic effects compared to environmental change-driven temporal range shifts for divergent occurrences between life stages in Europe. Our results challenge the common practice of inferring climate change impacts on tree species from divergent occurrence of tree life stages using static data.

2.2 Methods

We used a two-life stage population model to show with theoretical simulations how temporal range shifts and ontogenetic effects can drive divergent occurrences between life stages and how these can be detected with beta regression models. We used the same beta regression models with data from three NFIs to empirically quantify temporal range shifts and ontogenetic effects in European forests. All simulations and data analyses have been performed with R (version 4.0.2; R CORE TEAM, 2020).

2.2.1 Two-life stage simulation model

For a simple model of a population with two interdependent life stages, we used ordinary differential equations expressing the transitions between two states, abundances of juveniles and adults. Juvenile J and adult A abundances were coupled via growth, i.e. transition rate g , and regeneration rate r . The life stages' carrying capacities k (juveniles), \hat{k} (adults), expressing density dependence within life stages, and their respective density-independent mortality rates m , \hat{m} were modeled as a function of a theoretical environmental gradient \vec{e} . The environmental gradient was discretized into n equal-width cells, so that the abundance change rates in the i^{th} cell were described by

$$\frac{dJ_i}{dt} = (rD_i - m(t, e_i) \cdot J - gJ_i) \left(1 - \frac{J_i}{k(t, e_i)}\right) \quad (2.1)$$

$$\frac{dA_i}{dt} = (gJ_i - \hat{m}(t, e_i)) \cdot \left(1 - \frac{A_i}{\hat{k}(t, e_i)}\right). \quad (2.2)$$

D represents the diaspores dispersed from A that are recruited into J . Dispersal was modelled as a centered rolling average of A with window width d , so that the i^{th} cell of D was the average of the d cells around the i^{th} cell of A .

To simulate ontogenetic niches, we made the parsimonious assumption that two demographic parameters related to survival are dependent on the environmental gradient: the carrying capacity k , which expresses density-dependent survival, and the density-independent mortality m , so that both density-dependent and density-independent niche effects were accounted for. The responses to the environment were bell-shaped for carrying capacity and reversely bell-shaped for mortality, scaled by the same environmental response function f . This way, carrying capacity k reaches its maximum K and density-independent mortality m its minimum M under the same optimal environmental conditions:

$$k, \hat{k}(t, e) = K \cdot f(t, e) \quad (2.3)$$

$$m, \hat{m}(t, e) = M \cdot (1 - f(t, e)) \quad (2.4)$$

$$f(t, e) = \exp\left(-\frac{1}{2} \left(\frac{e - \mu(t)}{\sigma}\right)^2\right) \quad (2.5)$$

$$\mu(t) = a_\mu + b_\mu t \quad (2.6)$$

Different positions of the demographic niches per life stages were thus achieved by life stage-specific a_μ . As indicated by the function argument t , the demographic responses k and m could not only have different position parameters μ per life stage but could also vary with time by altering μ with the slope b . Temporally shifting the environmental driver of the demographic response relative to the original time was thus achieved by linearly shifting the response function f with time.

To simulate initial life stage abundances prior to any temporal environmental change, populations of both life stages were let grown from a very low and environmentally-constant abundance state $J = A = 0.5$ at time $t = 0$ to a stable state at $t = 10000$. We simulated three scenarios of shifts by varying the life stage-specific niche position μ and the temporal slope b to yield visibly diverging occurrences (for parameterization see Supplementary Table S1.1 in Supporting Information): (A) Temporal shift of the environment was simulated by

linearly shifting the response function over time with a slope $b_\mu > 0$ (Figure 23 A). (B) Ontogenetic niche shift was simulated by assigning juveniles and adults a different optimum value a_μ for the response function f (Figure 23 B). (C) The joint effect of temporally shifting environment and ontogenetic niche shift was simulated by first running the model to a stable state with ontogenetic niche shift as in case B, and then altering the stage response functions over time with the same temporal shift of the environment acting on both life stage populations, while the two different ontogenetic niches remained offset (Figure 23 C). In all three shift scenarios, the maximal carrying capacity was kept at $K = 10000$ for juveniles and $\hat{K} = 7000$ for adults to reflect that the carrying capacity decreases with tree size (Figure 23 A–C). In addition, to explore the effect of demographic dependency on occurrence widths of both life stages, even with equal environmentally-dependent mortality, we simulated one further scenario without any temporal or ontogenetic shifts or changes of niche width (Figure 23 D) using the same response function f , carrying capacity K , and mortality M for juveniles and adults.

To detect temporal shifts and juvenile divergence in the simulated data we used the same regression method used in the empirical analyses (see Section 2.2.2.3). We generated presence data by randomly resampling values of the theoretical environmental gradient with a sampling probability proportional to the abundance. The resulting distribution of environmental values is equivalent to an “occurrence distribution of environmental values” at presences, as used with the empirical analyses (Section 2.2.2.3) and shown as probability density curves in Figure 23 a–c.

To visualize ontogenetic niches (Figure 23 A–D, dashed lines), defined as the environmental space where ideal populations of juveniles or adults would persist if they were independent of each other (Section 2.1), we simulated two independent models for each life stage for each scenario. Each life-stage was simulated from the same model with the same environmental response as the size-structured populations, but to remove the interdependence between life stages, regeneration r was simulated from J itself instead of D , and transition g was simulated from A instead of J .

Ordinary differential equations were integrated with `lsoda` as provided by the package ‘deSolve’ (version 1.28; SOETAERT *et al.*, 2010). For model code see Supplementary Material S2 in Supporting Information.

2.2.2 Analyses of European national forest inventory data

2.2.2.1 Tree species data

To infer occurrence patterns of juvenile and adult trees in Europe, we used two repeated national forest inventory (NFI) surveys from three countries (Figure 22): Sweden, Germany, and Spain (survey design detailed in FRIDMAN *et al.*, 2014; RIEDEL *et al.*, 2017; RUIZ-BENITO *et al.*, 2017). The geographical extent of the countries is spanning a broad climatic gradient of arid, warm temperate, and boreal climates (КОТТЕК *et al.*, 2006). The survey repetitions were selected from two (Sweden) or three (Germany and Spain) repetitions to cover the maximum time period per species. This resulted in different periods between two surveys per sample plot and country (see Supplementary Tables S1.2, S1.4, and S1.5 in Supporting Information): 10 years in Sweden (periodically-regular and geographically-random rolling surveys between 2003 and 2017), 10 or 25 years in Germany (two out of three full surveys in 1987, 2002 and 2017, depending on species), and varying period between 14 and

34 years in Spain (survey dates between 1980 and 2017). To ensure that a constant environmental sampling space for species presences was maintained across survey repetitions, we included only those plots that had been surveyed at both times.

We used presence data for two life stages of 40 tree species. Trees were classified as *juveniles* when their height was below 130 cm in Sweden and Germany, and when their diameter at breast height (DBH) was below 2.5 cm in Spain. The lower sampling bounds for small trees were 10 cm height (Sweden), 20 cm height (Germany), while there was no lower bound in Spain. Different definitions of juveniles per country were necessary because small trees were counted in different size classes in the three NFIs (for sampling thresholds see Supplementary Table S1.3 in Supporting Information). Trees were classified as *adults* in all three NFIs when their height was above 130 cm and their DBH exceeded 15 cm, resulting in a size gap between juveniles and adults.

Since taxonomic concepts, the set of species, and the sampled life stages within species changed over the repeated inventory surveys, tree observations were subset to maintain a constant environmental sampling space across life stages and surveys based on the following criteria within countries: (1) survey repetitions were included for a species, when both life stages had been sampled, (2) two surveys were chosen to cover the longest possible time period, and (3) species had to be present on at least 20 plots per life stage and survey.

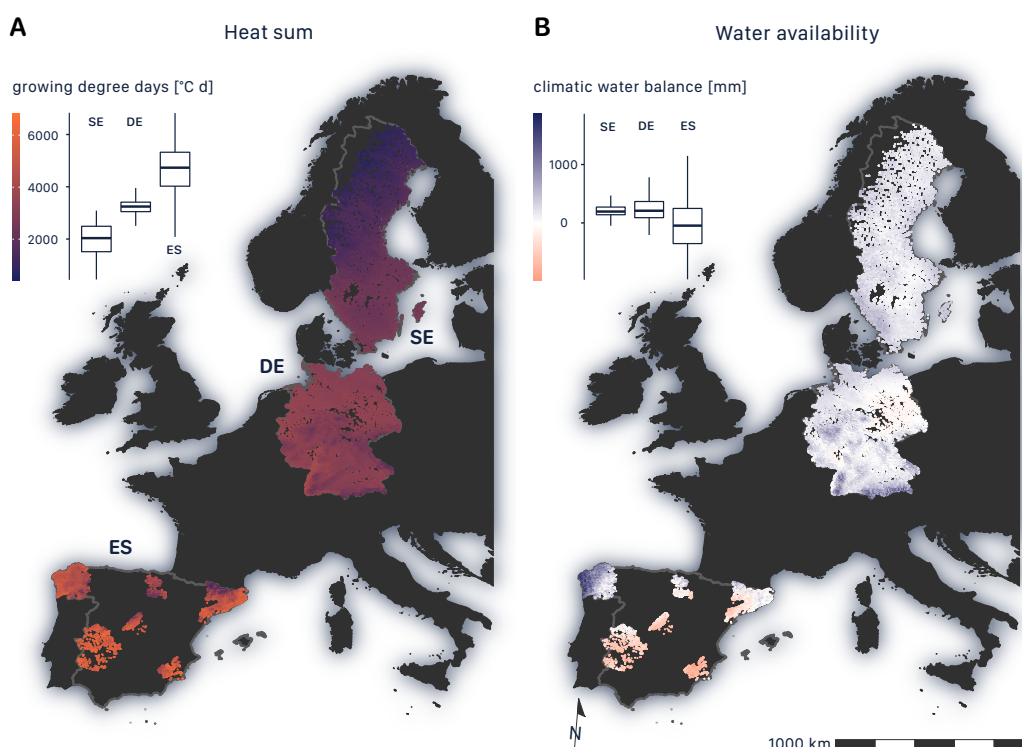


FIGURE 22: Tree plot locations of the three national forest inventories (NFIs)—Sweden (SE), Germany (DE), Spain (ES)—coloured by the climatic variables (A) heat sum (growing degree days) and (B) water availability (climatic water balance). Box plots show the distribution of climatic variables by country. The map projection is a Lambert azimuthal equal-area projection.

2.2.2.2 Climatic variables

To assess occurrence of both tree life stages along large-scale climatic gradients, we used long-term averages of heat sum and water availability. These variables are widely considered key climatic determinants of plant and vegetation distribution at larger scales (climatic water availability: e.g., WOODWARD and WILLIAMS, 1987; GUISAN *et al.*, 2007; heat sum: e.g., WOODWARD, 1988; SYKES *et al.*, 1996). Both variables were derived from long-term averages over the period 1979–2013 from the CHELSA high resolution climatologies (KARGER *et al.*, 2017), which comprise 12 monthly averages over the entire 34 years at a spatial resolution of 30 arcsec (1 km).

Heat sum was measured as growing degree days (GDD) within the frost-free period. To obtain GDD from the monthly climatologies, daily values for mean and minimum temperature were derived from the corresponding monthly values by linear interpolation. For interpolation, the differences between the values of two consecutive months were divided by the number of days between the 15th of the two months to obtain an average daily change rate. Daily temperatures between the two boundary dates were then calculated by cumulatively adding the daily changes to the climatology of the first of the two boundary dates. Daily mean temperature values were summed up from the first day following latest spring frost (as determined using daily minimum temperatures) until the day before the earliest autumn frost to obtain GDD [$^{\circ}\text{C d}$].

Water availability was measured as annual climatic water balance, i.e. the difference between precipitation and potential evapotranspiration (THORNTON, 1948). First, monthly climatic water balance was obtained from the climatologies by calculating potential evapotranspiration according to Hargreaves (HARGREAVES, 1994) as implemented in the package ‘SPEI’ (BEGUERÍA and VICENTE-SERRANO, 2017) using minimum and maximum temperatures, precipitation, and latitude. The monthly climatic water balance [mm] was then summed up over all months to obtain annual water availability.

Environmental variable values at the locations of sample plots were extracted from the raster cell covering the respective point using the `extract` function from package ‘raster’ (HIJMANS, 2020). This resulted in sampled climatic gradients ranging over heat sums from 453 to 6819 $^{\circ}\text{C d}$, and water availability from -966 to 1863 mm (Figure 22).

Using static gradients of long-term climatic variables to compare species distributions through time will lead to species shifting their range along the gradients under the assumptions of temporal climate change and tracking of climatic niches. Growing degree days significantly increased in Europe between 1950 and 2010, in particular in the Mediterranean region (SPINONI *et al.*, 2015). Increasing temperatures in southern Europe have increased drought frequency through higher evapotranspiration, while drought frequency has decreased in northern Europe through increased precipitation between 1958 and 2014 (STAGGE *et al.*, 2017). Since both, heat sum and water availability, have changed in Europe throughout the NFI survey periods, species are expected to shift along the static gradients, e.g., towards colder conditions along the heat sum gradient.

2.2.2.3 Estimates of *juvenile divergences* and *temporal shifts* from beta regression models

To infer the effects of time and life stage on centers of tree occurrence along climatic gradients, we fitted beta regression models (FERRARI and CRIBARI-NETO, 2004) with the package ‘glmmTMB’ (version 1.0.2.1 BROOKS *et al.*, 2017).

Most of the studies that compare the occurrences of different life stages compare the means or quantiles of the environmental variables at the occurrences of the life stages (e.g., LENOIR *et al.*, 2009; BELL *et al.*, 2014; MONLEON and LINTZ, 2015; MÁLIŠ *et al.*, 2016; SITTARO *et al.*, 2017; WASON and DOVCIÁK, 2017). Here, we use an analogous approach where the long-term climatic variables at plot locations where a species was present, i.e. the occurrence distribution of climatic variables, were taken as response variables of regression models. Pivoting the climatic variables from predictors to the responses and comparing the distribution centers, has several advantages compared to fitting a more complicated species distribution model with abundance or occurrence as the response: (1) As the sampling intensities (area) of juvenile trees and adults are different (in addition to changing intensities across countries and surveys; see Supplementary Table S1.3 in Supporting Information), reducing the data to presences and then taking the occurrence distribution of climatic variables will yield the same distribution regardless of the sampling intensity, which is independent of the environmental gradient. But NI and VELLEND (2021) have shown by resampling that extreme quantiles (e.g., the 95th percentile of heat sum) will underestimate the occurrence width of juveniles, when their sampling intensity in NFIs is lower than that of adults. We avoid the bias that is introduced by extreme quantiles by using the more robust centers of distributions along a climatic gradient as responses of the beta regression models. Although occurrence centers are not as sensitive to environmental changes as range margins, the occurrence centers will still reflect changes over the full distribution, including the margins. (2) Comparing the effects that a predictor has on the position of these distributions is straight-forward in regression models for which hypothesis tests are readily available. However, using a species distribution model with occurrence or abundance as a response for the same objective, would require first to harmonize the data by modelling (partly unknown) different sampling intensities, then to reduce the possible resulting response curves to a central measure, and third develop hypothesis tests to compare the effect of time or life stage on this central measure.

Occurrence distributions of climatic variables were scaled across surveyed plots including all countries and species to have the range $[\epsilon, 1 - \epsilon]$ (with computer precision $\epsilon = 2.220446 \cdot 10^{-16}$), so that the environment along the entire sampled European gradient was expressed as a variable between zero and one. We used a beta-distribution, which has two properties that account for different shapes that the occurrence distributions of climatic variables can take over a climatic gradient with fixed limits: (1) the distribution can be symmetrical or skewed, and (2) the distribution can have high or even maximal density towards one of the limits of the gradient, which reflects that the sampled range can be a sub-sample of the entire range of a species. Hence, the expected value y (position along the gradient expressed by parameter μ) and the shape (width and skewness expressed by precision parameter ϕ , which was unconstrained to provide any skewed shape) of the occurrence distribution of climatic variables were made dependent on `life stage` (juvenile or adult), `time` (year of the survey), and their interaction: $y \sim \text{time} * \text{life stage}$, with a dispersion model for the shape $\sim \text{life stage} * \text{time}$ (R-style notation, WILKINSON and ROGERS, 1973). This can be written as a beta model with mean μ and precision parameter ϕ :

$$y \sim B(\mu = p + X\beta, \phi = q + X\gamma) \quad (2.7)$$

where p, q are the respective intercepts, β, γ are vectors of coefficients, and the design matrix X consists of a column vector for time θ , as well as a dummy-coded vector of the

two life stage levels λ and their interaction with time:

$$X = \{[\theta][\lambda][\theta \cdot \lambda]\} \quad (2.8)$$

Models were fitted independently per country and species, but the response (the respective climatic variable) and time were scaled with data pooled across all countries, so that the effect sizes are comparable across countries and species. To account for the geographical clustering of sample plot locations in the Spanish NFI (Figure 22), the factor region was included as an additional fixed effect in the models for Spain. The continuous predictor time (year of the survey) was first centered at the level of independent models, i.e. per species (within cluster for Spanish data) within country, and then scaled linearly in such a way that the most frequent sampling period, 25 years, corresponded to the range between -0.5 and $+0.5$. This way, the slope for time estimates the average linear shift over 25 years, independently for each species–country combination. This harmonization makes the effect sizes for time comparable across countries and species, while the uncertainty of the estimates still depends on the original time period between surveys.

Model assumptions were checked with simulated quantile residuals provided by the package ‘DHARMA’ (HARTIG, 2020), and consequently three out of the 58 fits for heat sum and none of the fits for water availability were discarded because they violated the assumption of a beta-distributed error (see Supplementary Material S3 in Supporting Information).

To quantify *temporal shifts* and *juvenile divergences*, we used marginal effects of time and life stage on the position parameter μ , as well as post-hoc significance tests ($Pr(> |z|) = p < 0.05$) provided by the package ‘emmeans’. The differences in marginal means of the two life stages (approximately equivalent to the difference between life stage-level intercepts; Figure 23 a–c) was interpreted as the divergence of juveniles compared to adults (*juvenile divergence*). The marginal trend of juvenile occurrence over time (approximately equivalent to the slope over time within the juvenile stage level; Figure 23 a–c) was interpreted as the *temporal shift*. Species-specific *juvenile divergences* and *temporal shifts* were averaged per country by weighting with the inverse of the associated squared standard error $\frac{1}{SE}$, and the frequency of effect directions was counted (Figures 24 B–D and 25 B–D). Since both, *juvenile divergence* and *temporal shift* were transformed to the response scale, they can readily be interpreted as a change of occurrence center in % along the entire sampled gradient across all three countries, where 0% corresponds to the minimum and 100% to the maximum of the environmental gradient.

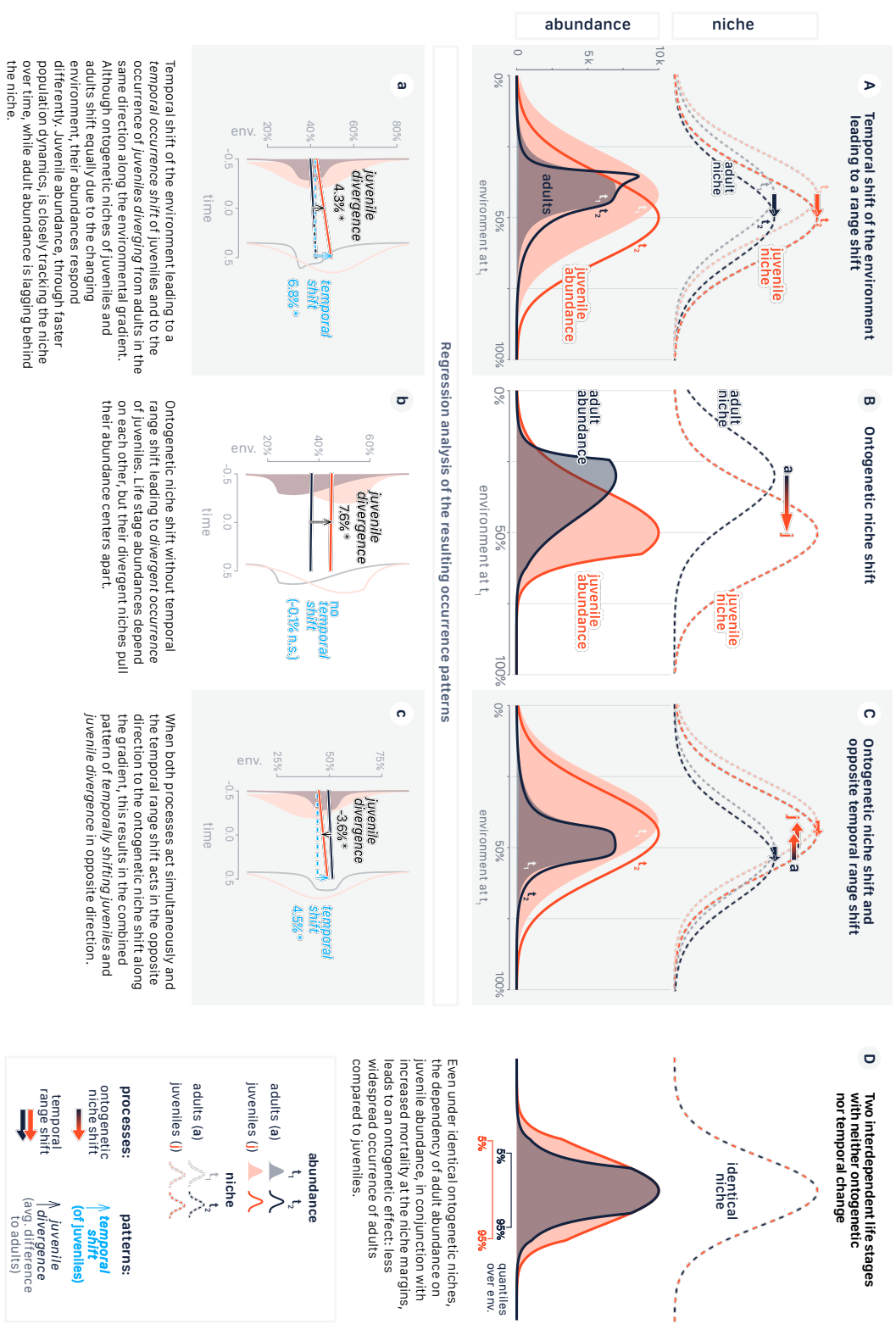


FIGURE 23: Simulated abundances of trees along an environmental gradient under (A) temporal range shift, (B) ontogenetic niche shift, (C) opposite temporal range shift and ontogenetic niche shift, and (D) under no shift at all. The three scenarios of shifts (A–C) lead to specific divergence patterns in beta regression of the occurrence distribution of environmental variables, i.e. the environmental values sampled proportional to abundance, here shown as probability densities (a–c), while scenario D illustrates the ontogenetic effect of the demographic dependency between life stages.

2.3 Results

2.3.1 Simulated divergent occurrences

Simulations of the two-life stage population model showed that both environmental-change driven temporal range shift and ontogenetic niche effects, in particular ontogenetic niche shift, can cause divergent occurrences of juveniles from adults. The simulated data from three different scenarios of shifts led to three different combinations of occurrence patterns detected by the beta regression: (A) Temporal environment shift resulted not only in a *temporal shift* of juveniles, i.e. the shift of juvenile occurrence over time along the environmental gradient, but also in *juvenile divergence* in the same direction, i.e. the difference between marginal means of occurrence from adults to juveniles (Figure 23 A). (B) In contrast, ontogenetic niche shift led to *juvenile divergence* only—in the direction of the ontogenetic niche shift (Figure 23 B). Ontogenetic niche shift and temporal range shift can act simultaneously. (C) Only when both processes acted in opposite directions, they could be disentangled because they led to oppositely directed *juvenile divergence* and *temporal shift* (Figure 23 C).

In addition to ontogenetic niche shift, our simulations demonstrate another ontogenetic effect: Under stable environmental conditions, the occurrence width can contract from juveniles to adults due to the demographic dependency of the adult on the juvenile population, even when the niche width remains constant over ontogeny (Figure 23 D). Despite identical ontogenetic niches of juveniles and adults, the environmentally-dependent mortality led to a stable state population where juveniles occurred more widespread towards the extreme conditions of the environmental gradient. Adults occurred in a smaller range because the increased juvenile mortality at the niche margins also decreased transition from juveniles to adults.

2.3.2 Divergent occurrences in NFIs

In the three European countries, tree species had both significant *temporal shifts* of juveniles over the respective time periods between surveys and significant *juvenile divergences* along the two gradients of long-term climatic variables. Significant *temporal shifts* were less frequent—24% (heat sum) and 21% (water availability) of all 55 species-country combinations—than significant *juvenile divergences*—53% (heat sum) and 48% (water availability) of the cases—(Figure 24 C and 25 C). The effect sizes of *juvenile divergence* and *temporal shift*, scaled to express changes over 25 years, were similar with up to 6.6% of the entire climatic range across all surveyed plots in all three countries. Most strikingly, the overall frequency of significant *juvenile divergences* associated with an opposite *temporal shift* was similar to the frequency of significant *divergences* associated with a *temporal shift* in the same direction along both heat sum (59% versus 41% of the significant *juvenile divergences*; Figure 24 D) and water availability (39% versus 61%; Figure 25 D).

The predominant direction of *juvenile divergences* along heat sum strongly varied between countries: All five significant *juvenile divergences* in Sweden had juveniles occurring in colder conditions than adults, while eight out of ten significant *juvenile divergences* in Spain were to warmer conditions (Figure 24 C and D). In Germany, the direction of *juvenile divergences* along heat sum was balanced. This pattern was also observed in the average *juvenile divergences* over all species per country with *juvenile divergence* towards colder in Sweden and warmer in Spain, and moderately colder in Germany (Figure 24 B) – and even

within species: Juveniles of, e.g., *Fagus sylvatica* and *Quercus robur* diverged towards warmer conditions in Spain but towards colder conditions in the other countries.

Along water availability, juveniles commonly occurred in drier conditions than adults across all countries. This pattern was consistent across averages per country (Figure 25 B) and frequencies of significant *juvenile divergences*. Of the significant *divergences*, 100% (Sweden), 67% (Germany), and 60% (Spain) were towards drier conditions (Figure 25 C). Equally, all of the significant *juvenile divergences* in opposite direction to the *temporal shift* were towards drier conditions (Figure 25 D), and many of the species with significant *juvenile divergences* in more than one country shifted exclusively to drier conditions: *Sorbus aucuparia*, *Populus tremula*, *Quercus petraea*, and *Pinus sylvestris* (but cf. *Castanea sativa* and *Quercus robur*).

Significant *temporal shifts* (Figures 24 C and 25 C) only occurred in Germany and Spain, not in Sweden, the country with the shortest period between observations of 10 years (see Supplementary Tables S1.4 and S1.5). Average *temporal shifts* per country were consistently towards colder and predominantly towards drier conditions across countries (Figures 24 B and 25 B). There were significant *temporal shifts* in all directions along the two gradients, but a small majority was towards colder and drier conditions (Figures 24 C and 25 C). Certain species had extraordinary large *temporal shifts* (around 5% of the gradient range): *Castanea sativa*, *Pseudotsuga menziesii*, *Prunus serotina*, *P. padus*, and *Larix decidua* in Germany; and *Pseudotsuga menziesii* in Spain.

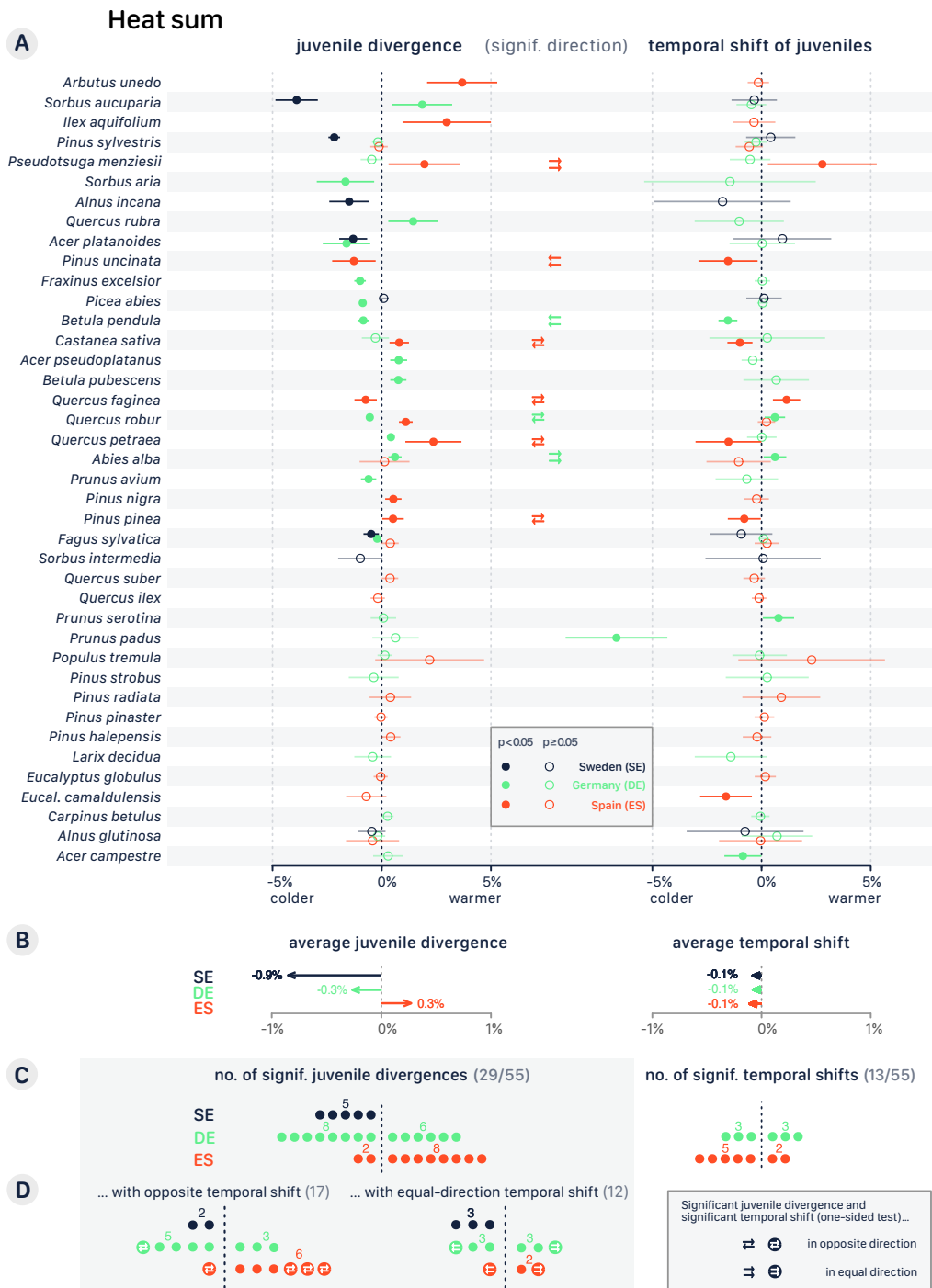


FIGURE 24: *Juvenile divergence* and *temporal shift* of juvenile trees along a European heat sum gradient: (A) Effect sizes by species and country in % of the full gradient range across all three countries, ordered by effect size and significance of the *juvenile divergence*. Pairs of arrows mark those significant *juvenile divergences* that are associated with a significant *temporal shift* (one-sided test) and whether the effects are in equal or opposite direction. (B) Average effect sizes by country and direction, weighted by the inverse of the squared standard error. (C) Count of significant *juvenile divergences* and significant *temporal shifts* by country and direction. (D) Comparison of the frequency between significant *juvenile divergences* with associated opposite *temporal shift* and with equidirectional *temporal shift* (additional significant tests for direction of the temporal shift are emphasized with arrow symbols). Significance of the estimates was tested with a two-sided test, significance of the directions with a one-sided test ($Pr(> |z|) = p < 0.05$).

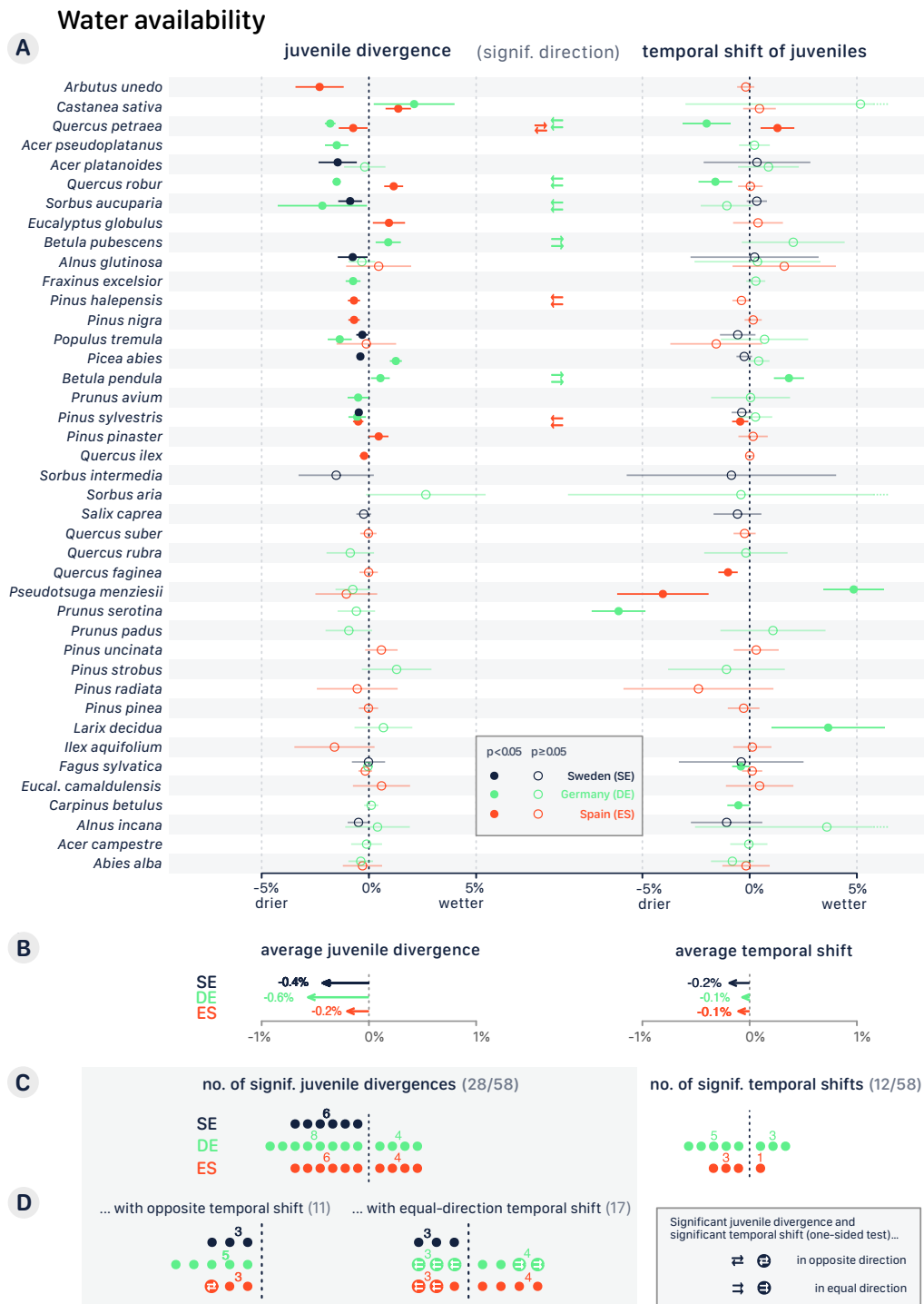


FIGURE 25: **A)** *Juvenile divergence* and *temporal shift* of juvenile trees along a European water availability gradient: **(A)** Effect sizes by species and country in % of the full gradient range across all three countries, ordered by effect size and significance of the *juvenile divergence*. Pairs of arrows mark those significant *juvenile divergences* that are associated with a significant *temporal shift* (one-sided test) and whether the effects are in equal or opposite direction. **(B)** Average effect sizes by country and direction, weighted by the inverse of the squared standard error. **(C)** Count of significant *juvenile divergences* and significant *temporal shifts* by country and direction. **(D)** Comparison of the frequency between significant *juvenile divergences* with associated opposite *temporal shift* and with equidirectional *temporal shift* (additional significant tests for direction of the temporal shift are emphasized with arrow symbols). Significance of the estimates was tested with a two-sided test, significance of the directions with a one-sided test ($Pr(> |z|) = p < 0.05$). Large confidence intervals were cut off only at the upper limit of 6.5%, as indicated by dotted error bars.

2.4 Discussion

Both temporal range shift and ontogenetic effects, such as ontogenetic niche shifts, can lead to similar divergent occurrences of juveniles and adults along an environmental gradient, as demonstrated by our two-life stage simulation model. The analysis of European NFI data revealed that significant *juvenile divergences* were as frequently opposite to *temporal shifts* as they were in the same direction. This is a strong indication that *juvenile divergence* can not simply be interpreted as a sign of environmental change-driven range shift, but that ontogenetic effects frequently play a major role in divergences between juveniles and adults.

2.4.1 Simulated divergences between life stages

Our simulations illustrate how both temporal shifts of the environment and ontogenetic niche shifts can cause divergent occurrences between life stages, and how the demographic dependency of life stages alone can lead to differently widespread occurrences. Many empirical studies, however, assume that different occurrences are exclusively the result of a temporal shift caused by environmental changes (e.g., ZHU *et al.*, 2014; MATHYS *et al.*, 2018). This is based on the assumption that, when species change their ranges to maintain niche conditions, juveniles will respond faster and track these conditions more closely than adults (MONLEON and LINTZ, 2015). These temporal range shifts that become evident as shifts of occurrence centers can also include shifts that only occur at either the leading margins, i.e. juveniles filling a new range, or at the trailing margins, i.e. juveniles regressing where adults persist (LENOIR *et al.*, 2009). Under ongoing environmental shift, juveniles will permanently lead the trailing adults throughout time. This permanent and increasing *juvenile divergence* is illustrated in Figure 23 A, where the environment had already been shifted before the first observation so that juveniles do not only diverge on average (Figure 23 a, *juvenile divergence*), but already at the first observation (Figure 23 a, at $t_1 = -0.5$). Permanent *divergence* through time alone can thus not be interpreted as necessarily caused by ontogenetic niche shift either. Inferring ontogenetic niche shifts from permanent divergence of life stages may however be considered if there are only negligible *temporal shifts* over a long period (cf. MÁLIŠ *et al.*, 2016).

As shown in our simulations, the pattern of divergent occurrences can also emerge when the niche shifts between ontogenetic stages (Figure 23 B). Ontogenetic niche shifts, i.e. juvenile plants requiring or enduring different environmental conditions to grow or survive than adults of the same species, have been reported in many empirical studies (ERIKSSON, 2002; MIRITI, 2006; EWALD, 2007; MÁLIŠ *et al.*, 2016; ANDIVIA *et al.*, 2020). In addition, it is also possible that observed divergences between life stages could reflect ontogenetic niche shift of unobserved life stages. These life stages include, e.g., ontogenetic niche shifts of seedlings below the sampling threshold, the germination of seedlings (VALDEZ *et al.*, 2019; VECCHIO *et al.*, 2020), but even the environmentally dependent ability of trees of to produce the life stage of seeds (ROSBAKH *et al.*, 2018; BAJOCCHO *et al.*, 2021). Furthermore, other ontogenetic effects like ontogenetic niche contraction or expansion (ERIKSSON, 2002; BERTRAND *et al.*, 2011), and the demographic dependency between life stages can lead to juvenile divergences, when the sampled geographical range does not include the entire niche (Section 2.4.3.3). Evidence of life stage divergence (as illustrated in Figure 23 a and b; *juvenile divergence*) can therefore not simply be interpreted as a result of temporal change but ontogenetic effects must also be considered as a potential cause.

2.4.2 Attributing juvenile divergence to temporal range shift or ontogenetic effects

Since both processes, temporal range shift and ontogenetic effects, can cause divergent occurrences between life stages along the climatic gradient, the observed pattern of *juvenile divergence*, i.e. the difference in centers of adult and juvenile occurrence along the gradient averaged over time, can not directly be attributed to either one of the processes (Figure 21). The challenge of attributing *juvenile divergence* to either temporal range shift or ontogenetic effects can be partly overcome with repeated surveys. With repeated observations, the trend of juvenile occurrence over time can be quantified and directly be interpreted as a temporal shift (Figure 23 a, *temporal shift*). When temporal range shift and ontogenetic effects act simultaneously, they can either be directed in the same direction, amplifying *juvenile divergence*. But they can also act in opposite direction, leading to *juvenile divergence* that is opposite to the direction of the *temporal shift* (Figure 23 C) or even to divergences that cancel each other out (for a discussion of the consequences for inference see Section 2.4.3.1). These associations of directions provide a tool for inferring ontogenetic effects within species: If a species has significant *juvenile divergence* associated with a significant *temporal shift* in opposite direction, we can attribute the *juvenile divergence* to ontogenetic effects because the divergence has not likely emerged from the temporal range shift. In addition, the frequencies of *juvenile divergences* and associated directions of *temporal shifts* can be used for inference within a set of species: Comparing the overall frequencies of *juvenile divergences* with opposite to those with equidirectional *temporal shifts* is an indication of the relative contribution of ontogenetic effects and temporal range shifts to observed divergences between life stages.

2.4.3 Divergent occurrences between life stages in European forests

2.4.3.1 Temporal range shifts and ontogenetic effects are at least equally relevant for divergent occurrences

There were about twice as many significant *juvenile divergences* than significant *temporal shifts* along both climatic gradients across species and the three NFI countries. Significant estimates of juvenile *temporal shift* in 24% (heat sum) and 21% (water availability) of all species–country combinations are a unequivocal indicator of temporal range shifts. The high frequency of juvenile divergences—observed in 53% (heat sum) and 48% (water availability) of all cases—is however no sufficient evidence of ontogenetic effects, such as ontogenetic niche shifts. Ontogenetic effects and temporal range shift can both cause *juvenile divergences*, and furthermore, the significance of a *temporal shift* depends on the length of the observed time period, which varies between species–country combinations (Supplementary Tables S1.4 and S1.5). Particularly in Sweden the short observation period of only 10 years could lead to *temporal shifts* that are not significant. But the contribution of ontogenetic effects to *juvenile divergences* can be inferred from the direction of associated *temporal shifts* within the same species (Section 2.4.2).

At the individual species level, we found significant *juvenile divergences* in opposite direction to the *temporal shift* for five species along the heat sum gradient and for one species along the water availability gradient. These *juvenile divergences* can clearly be attributed to ontogenetic niche shifts, because they could not have arisen from the temporal range shift. The overall importance of ontogenetic effects, however, is probably greater than ap-

parent from these individual cases, because our rigorous test for ontogenetic effects within species will exclude several cases. For instance, ontogenetic niche shifts and other ontogenetic effects will not be detected when no significant *temporal shift* occurred simultaneously in opposite direction to the ontogenetic niche shift. Additionally, even if ontogenetic niche shift and temporal shift were in opposite directions, the juvenile divergence could become too small to be significant under fast temporal shifts. Fast shifting juveniles can diminish the divergence caused by ontogenetic effects so that both processes cancel each other out, and they could even overtake the slowly shifting adults along the gradient, so that not every opposite ontogenetically-caused divergence can be observed as *juvenile divergence* in the opposite direction to the *temporal shift*.

To further evaluate the relative importance of ontogenetic effects for *juvenile divergences* across all species and countries, the odds of a *juvenile divergence* being associated with a *temporal shift* in opposite direction rather than in the same direction can be considered, regardless of significance or effect size of the *temporal shift*. Assuming that all *juvenile divergences* were caused only by temporal range shifts, all observed patterns of *temporal shifts* would be in the same direction as the *juvenile divergences* (the odds would converge to 0). In contrast, if we assume that all *juvenile divergences* were caused by ontogenetic effects—and the temporal range shift was an additional independent process not causing any divergences—the directions of the *temporal shifts* of juveniles would split equally among equidirectional and opposite patterns of *temporal shift* (the odds would converge to 1).

In our results, the odds of *temporal shifts* opposite to the *juvenile divergence* are $17 : 12 = 1.42$ along the heat sum gradient and $11 : 17 = 0.64$ along the water availability gradient. This suggests that along both gradients the majority of juvenile divergences are unlikely caused by a temporal range shift, and in the case of heat sum there are even more juvenile divergences opposite to the temporal shift than expected from independent processes ($1.42 > 1$). We can thus conclude that ontogenetic effects, like ontogenetic niche shifts, are at least as relevant for causing divergent occurrences of life stages as environmental change-driven temporal range shifts.

That occurrence centers of tree species' life stages can diverge along an environmental gradient because of ontogenetic niche shift has been suggested by other empirical studies (URBIETA *et al.*, 2011; ZHU *et al.*, 2014; MÁLIŠ *et al.*, 2016). The importance of ontogenetic effects for divergent occurrences of tree life stages has far-reaching consequences for scientific inference: environmental change impacts can not simply be inferred from static data on occurrence of tree life stages. Having established that both temporal range shifts and ontogenetic effects exist in European forest tree species, we will discuss plausible causes of those processes in the following sections.

2.4.3.2 Temporal shifts in response to environmental change

Under climate warming with increased evaporation, tree species are expected to shift over time towards colder and wetter conditions along static long-term climatic gradients to maintain the conditions of their climatic niche. In line with this expectation, temporal range shifts towards long-term colder conditions have been reported for several species based on repeated observations at northern range limits (e.g. BOISVERT-MARSH *et al.*, 2014; SITARO *et al.*, 2017) or at high elevations along mountain slopes (e.g., JULIO CAMARERO and GUTIÉRREZ, 2007; DU *et al.*, 2018). As expected from climate change-driven range shifts, the average *temporal shifts* in the three NFI countries were consistently towards colder con-

ditions. For instance, *Prunus padus*, *P. avium*, *Betula pendula*, and *Pinus uncinata* (but cf. AMÉZTEGUI *et al.*, 2010) shifted towards colder conditions. *Prunus padus* had a particularly pronounced shift in Germany, probably due to its effective long-distance seed dispersal (NESTBY, 2020). Contrary to expectations, average *temporal shifts* along water availability were mainly towards drier conditions (Figures 24 B and 25 B). This may be partly explained by regional differences in long-term trends of climatic water availability, e.g., decreased drought frequency in northern Europe (SPINONI *et al.*, 2015; STAGGE *et al.*, 2017). The *temporal shifts* in Sweden were not significant for any of the species, probably due to the comparatively short period between surveys (10 years; see Supplementary Tables S1.4 and S1.5), which leads to larger uncertainties in the *temporal shift* estimates. Across all countries, individual species significantly shifted towards both colder and warmer (8 : 5) and drier and wetter (8 : 4) conditions. This adds to the body of studies that have found inconsistent directions among species in the divergence between adults and juveniles (RABASA *et al.*, 2013; WASON and DOVCIAK, 2017; O’SULLIVAN *et al.*, 2020) and in temporal shifts from repeated observations (WOODALL *et al.*, 2013; GIBSON-REINEMER and RAHEL, 2015). Although hypotheses have been proposed about how climate warming can cause shifts to warmer and drier conditions along long-term climatic gradients—like competitive release at the warmer margin or other climate-driven habitat modifications that indirectly allow for range shifts (LENOIR *et al.*, 2010; CRIMMINS *et al.*, 2011)—it is problematic to assume that any temporal range shift is driven by climate warming.

Instead, the set of species associated with many of the most pronounced temporal shifts suggests a connection to land-use change, including (1) introduction and promotion of individual species through forestry and (2) management regime change. First, silviculturally introduced species are likely to change their range to new environmental conditions because the climatic conditions at planting locations frequently differ from their actual niche conditions (RUIZ-BENITO *et al.*, 2012). Unsurprisingly, introduced timber species are responsible for almost all of the large *temporal shifts* in Germany and Spain (Figure 24 and 25; Germany: *C. sativa*, *P. menziesii*, *P. serotina*, *L. decidua*; Spain: *P. menziesii*). The exotic conifer species *P. menziesii* has naturalized and expanded in mountainous regions in Germany (KNOERZER, 1999) and Spain (BRONCANO *et al.*, 2005). *L. decidua* has been planted outside the native range within central Europe (JANSEN and GEBUREK, 2016). The deciduous species *C. sativa* (SEEMANN *et al.*, 2001) and *P. serotina* have been introduced in Germany, where *P. serotina* in particular has become invasive (STARFINGER *et al.*, 2003). Second, in addition to introduction and promotion of individual species, changing forest management regimes, especially abandonment, has been changing species composition of forests, e.g., through giving up traditional fire management in Spain (SEIJO *et al.*, 2018) or coppice management in central Europe (MÜLLEROVÁ *et al.*, 2015). Consistently, native, resprouting species that had benefited from these traditional management regimes, e.g., *Quercus spp.* and *Carpinus betulus* also show significant *temporal shifts*. Overall, the underlying drivers of range shifts—climate, land use, or any other temporal pressure—can not be inferred from the effect of time on the occurrence distributions of environmental variables alone, and the underlying causes remain speculative.

2.4.3.3 More widespread occurrence of juveniles along European climatic gradients

Juveniles generally occurred in more extreme conditions than adults within countries and therefore along a wider range of the entire European climatic gradients (Figure 24). The

number of *juvenile divergences* per direction and country along a latitudinal gradient from low mean heat sum in Sweden towards high mean heat sum in Spain followed a striking opposite pattern (Figure 22): Although in Sweden plant productivity may be limited by heat sum (WOODWARD, 1987), all *juvenile divergences* were towards colder conditions. In Spain, however, where plant productivity is more likely limited by evapotranspiration associated with high heat sum (e.g., LARCHER, 2003), the majority of *juvenile divergences* were towards warmer conditions. Germany, where the directions of *juvenile divergences* along heat sum were balanced (Figure 24 C, also takes an intermediate position on the heat sum gradient. Along water availability, juveniles overwhelmingly diverged towards drier conditions (Figure 25 C), which—again—is a divergence towards more hostile conditions, because at a large scale only drought but not climatic water excess is a limiting factor for tree growth in Europe (e.g., KOTTEK *et al.*, 2006). *Juvenile divergences* towards more hostile growing conditions were also expressed in the per-country average *juvenile divergences*, and particularly distinct in the significant *juvenile divergences* opposite to the *temporal shift*, which are even more likely to correspond to definite ontogenetic effects (Figures 24 and 25 D).

This pattern—more widespread occurrence of juveniles along large-scale climatic gradients—can be caused by ontogenetic niche shifts but also by other ontogenetic effects, namely (1) ontogenetic niche contraction from juveniles to adults, including (2) the special case of reduced growth at niche margins, but also by (3) demographic dependency between life stages. First, changes in width of the viable conditions along environmental gradients over life history, i.e. ontogenetic niche expansion and contraction, have widely been evoked as an explanation of observed differences in occurrence widths (e.g., STOHLGREN *et al.*, 1998; COPENHAVER-PARRY *et al.*, 2020a). In particular, wider juvenile occurrence has been explained by ontogenetic niche contraction (ERIKSSON, 2002; YOUNG *et al.*, 2005; QUERO *et al.*, 2008; BERTRAND *et al.*, 2011; MÁLIŠ *et al.*, 2016), which can emerge through more severe mortality of adults under the same conditions. For example, BERTRAND *et al.* (2011) have suggested that species' niches ontogenetically converge towards better nutritional conditions because the nutrient demand of adults may be higher. Furthermore, it has been shown that larger trees are more susceptible to drought-induced mortality (BENNETT, 2015), partly because ontogenetically increasing leaf area is directly linked to higher evapotranspirative demand (BURAS *et al.*, 2018). This will result in juvenile occurrences at environmental conditions that can not supply the development into adults, which can be regarded as sink populations (SOBERÓN and PETERSON, 2005). Second, reduced growth at the niche margins can be interpreted as a special case of ontogenetic niche shift or niche contraction, when ontogenetic progression is not measured in terms of age but, as in this case, in terms of size as a measure for the progress through stages of development (GATSUK *et al.*, 1980). If under extreme water- or heat supply-limited conditions growth rates are diminished (COOMES and ALLEN, 2007), or trees adaptively never exceed certain sizes at the niche margins (e.g., LINES *et al.*, 2012), small individuals are more likely to be found at extreme climate conditions than larger individuals, leading to an ontogenetic niche change between size stages. Relatively higher abundance of small-sized trees toward climate extremes is an additional challenge to any approach using static data on tree size as a substitute for age to infer temporal shifts of range limits (e.g., RABASA *et al.*, 2013; MATHYS *et al.*, 2018).

Third, adults can occur under narrower and less extreme environmental conditions than juveniles simply because the abundance of adults is not only determined by their own ontogenetic niche, but also dependent on the abundance of earlier life stages (YOUNG *et al.*, 2005). Adults are confined to the intersection of their own ontogenetic niche with that of prior life

stages, potentially limiting adult occurrence to a smaller range on the gradient than any of these “filters” (YOUNG *et al.*, 2005) alone. In our two-life stage simulation (Figure 23 D), we have shown that the effect of narrower occurring adults due to the dependency on juvenile abundance even arises under ontogenetically identical niches of juveniles and adults, if, due to environmentally-dependent mortality alone, disproportionately fewer juveniles transition to adults at the niche margins (see ZHU *et al.*, 2014, “turnover effect”).

While only the first of the three mechanisms—ontogenetic niche contraction—is ontogenetic niche change or shift in the strict sense, all of them are ontogenetically acting effects: For all three mechanisms, trees transition less frequently to later life stages at the niche margins, leading to the same pattern of more widely occurring juveniles along environmental gradients. Any one of these processes—acting individually or simultaneously—could thus be responsible for the observed *juvenile divergence* towards colder in Sweden, towards hotter in Spain, and towards drier conditions across all three countries.

Here, instead of modelling life stage’s niches, we modelled the change in the occurrence distribution of climatic variables over time and per life stage, because this allows for differences in sampling protocols between life stages and countries (see Section 2.2.2.3) as well as the fact that the sampling does not cover the entire climatic range of all species. Without these data limitations, however, a niche modelling approach that characterizes ontogenetic niches would be preferable to accurately predict species occurrences. Furthermore, to separate the ontogenetic effects that act on the occurrences of life stages into ontogenetic niche differences and demographic dependencies between life stages, an ontogenetic niche modelling approach will also have to account for these demographic dependencies. For example, recently, it has been discussed whether juvenile trees have wider or narrower ontogenetic niches than adult trees (BERTRAND *et al.*, 2011; COPENHAVER-PARRY *et al.*, 2020a; NI and VELLEND, 2021). We have shown that to answer this question, the vital performance of life stages along environmental gradients has to be assessed separately, because occurrence of a particular life stage is also constrained by its dependency on other life stages.

2.4.4 Conclusions

We conclude that divergent occurrences between life stages are caused by both temporal range shifts and ontogenetic effects—including ontogenetic niche shift, expansion or contraction, and demographic dependency between observed or unobserved life stages. That *juvenile divergences* associated with temporal range shifts in opposite direction are as frequent as divergences in the same direction, indicates that ontogenetic effects are at least as relevant for divergent occurrences between life stages as temporal range shifts.

The important role of ontogenetic effects at the continental scale emphasizes that impacts from changing climate on forest ecosystems can not simply be inferred from divergent occurrence of life stages in static data on tree occurrences. Instead, future studies should recognize demographic dependencies between life stages and that early tree life stages can have different ontogenetic niches than adult trees that could cause even more sensitive responses to environmental change (GRUBB, 1977; LINES *et al.*, 2019).

Which demographic processes control competitive equilibria? Bayesian calibration of a size-structured forest population model

3

Abstract

In forest communities, light competition is a key process for community assembly. Species' differences in seedling and sapling tolerance to shade cast by overstory trees is thought to determine species composition at late-successional stages. Most forests are distant from these late-successional equilibria, impeding a formal evaluation of their potential species composition. To extrapolate competitive equilibria from short-term data, we therefore introduce the JAB model, a parsimonious dynamic model with interacting size-structured populations, which focuses on sapling demography including the tolerance to overstory competition. We apply the JAB model to a two-“species” system from temperate European forests, i.e. the shade-tolerant species *Fagus sylvatica* L. and the group of all *other* competing species. Using Bayesian calibration with prior information from external Slovakian national forest inventory (NFI) data, we fit the JAB model to short timeseries from the German NFI. We use the posterior estimates of demographic rates to extrapolate that *F. sylvatica* will be the predominant species in 94% of the competitive equilibria, despite only predominating in 24% of the initial states. We further simulate counterfactual equilibria with parameters switched between species to assess the role of different demographic processes for competitive equilibria. These simulations confirm the hypothesis that the higher shade-tolerance of *F. sylvatica* saplings is key for its long-term predominance. Our results highlight the importance of demographic differences in early life stages for tree species assembly in forest communities.

3.1 Introduction

Among the species interactions that shape community composition, competition is one of the most important in forest ecosystems (TILMAN, 1982; GOLDBERG and BARTON, 1992). While in recent years, the role of facilitation in species assembly has been increasingly acknowledged (BRUNO *et al.*, 2003; PRETZSCH *et al.*, 2013; SIMHA *et al.*, 2022), trees in forests

are subject to exceptional levels of competition for light. Tree species are in an evolutionary arms race with other plants and acquired slowly-growing woody structures as a means of increasing their access to light with increasing height (CLEMENTS *et al.*, 1929; GIVNISH, 1988; KEDDY, 2001). Not only does the upper hand in height lead to an advantage for assimilating carbon that is size-symmetric, but harvesting light that comes from above means excluding trees below, which is a size-asymmetric competitive advantage for larger trees (SCHWINNING, 1998). Hence, the differential ability of tree recruits to tolerate the shading effect of the competing overstory is a key determinant of tree species assembly in forests (EMBOG, 1998), in addition to competitiveness for belowground resources such as water and nutrients (PUTZ and CANHAM, 1992; COOMES and GRUBB, 2000).

Evidence from around the world suggests that high shade-tolerance of saplings is a mechanism for individual tree species to attain predominance in forests at the competitive equilibrium, i.e. the equilibrium of species abundances as the result of interacting demographic processes in the absence of major disturbances (PICKETT, 1980). Instances, where species with shade-tolerant saplings tend to be predominant in late-successional forests are common across climate zones and clades, e.g.: *Tsuga canadensis* (L.) CARRIÈRE in temperate forests (eastern North America; ROGERS, 1978; see also CANHAM, 1989), *Sloanea woollsii* F. MUELL. in subtropical rainforests (eastern Australia; BAUR, 1957; FLOYD, 1990), and *Gilbertiodendron deweyrei* DE WILD. in tropical lowland forests (Ituri Forest of Zaïre; HART, 1995). Shade-tolerant tree species, whose recruits are viable under a closed canopy over long periods, are generally contrasted with “pioneer” species that are only able to regenerate after a disturbance has opened the canopy (WHITMORE, 1989). These different recruiting strategies highlight the crucial importance of the sapling stage for competitive exclusion, which can finally lead to predominance at the competitive equilibrium.

In temperate European forests, *Fagus sylvatica* L. (European beech, hereinafter abbreviated “*Fagus*”) is traditionally thought to be the shade-tolerant tree species that dominates at competitive equilibrium (WATT, 1923; ELLENBERG, 1963). *Fagus* saplings can survive particularly well under shading (PETROVSKA *et al.*, 2021a), so that *Fagus* is thought to naturally predominate, at least in environments at submontane elevations without higher abiotic stress or major disturbances (ELLENBERG, 1963). That *Fagus* would potentially predominate in Central European forests, has however not been tested with data at a large scale. This kind of test is impeded by the fact that in reality the Central European landscape has been altered by humans, ever since *Fagus*’ ongoing post-glacial immigration (?MAGRI, 2008), so that *Fagus* is not de facto the predominant tree species: KNAPP (2008) estimates that currently only 4.5% of Germany is covered with beech forests, in contrast to their projected natural cover of about 66%.

Given that only data from disturbed and managed forests are available, models can be used to project which species will predominate at the competitive equilibrium. Not all models, however, are suited to the task: Along the spectrum between correlative (statistical) and process-based models (DORMANN *et al.*, 2012a), purely correlative models have the advantage that they can be easily fitted to data. Correlative models, however, have the disadvantage that they cannot be used for extrapolating states outside the domain of the data, and furthermore, they can only rarely be used for inference on the underlying processes (KORZUKHIN *et al.*, 1996; DORMANN *et al.*, 2012a). On the other extreme, process-based dynamic vegetation models can extrapolate potential community states outside the data domain by assuming that the same processes act universally, but are often hard to fit to data as they require a multitude of parameters to be calibrated (KORZUKHIN *et al.*, 1996;

HARTIG *et al.*, 2012). Several modelling attempts have been undertaken to extrapolate the equilibrium forest vegetation with relatively complex process models that concentrate on larger trees, but neither explicitly consider the role of the sapling stage nor quantify the role of sapling demography (e.g., PRENTICE *et al.*, 1993; BUGMANN and SOLOMON, 2000; BADECK *et al.*, 2001). However, the critical role of recruitment processes in determining forest composition has recently led to calls for explicit modelling of these processes (PRICE *et al.*, 2001; KUNSTLER *et al.*, 2009; HANBURY-BROWN *et al.*, 2022; KÖNIG *et al.*, 2022).

Here, to extrapolate long-term competitive equilibria from short-term forest dynamics, we propose the JAB model, a simple dynamic population model that includes species interactions and a sapling stage. The JAB model explicitly represents the species-specific response of saplings to competition from the overstory with a two-layer size structure (e.g., as in LUNDQVIST, 1995; CORDONNIER *et al.*, 2019). Besides the competition response to the overstory, the sapling dynamics in the model include key demographic processes, like competition effects among saplings, growth, and seedling recruitment. In contrast, the competition between trees of the overstory is only represented by a simple density-dependent population model. Thus, being based on demographic processes but decisively parsimonious, the JAB model combines the advantages of the correlative and process-based modelling: It is relatively easy to fit to data while still being suited for predicting competitive equilibria (see also CLARK *et al.*, 2020) and inferring the role of individual demographic processes (see also BRISCOE *et al.*, 2019).

We apply the JAB model by fitting it to data from the German national forest inventory (NFI), using Bayesian calibration with prior parameter distributions based on external information from the Slovakian NFI data. For the question at hand, “will *Fagus sylvatica* be predominant at the competitive equilibrium?” we group all *other* tree species into one population and let them compete with *Fagus* to project the population states at the competitive equilibria. To test the hypothesis that the higher tolerance of *Fagus* saplings to competition from the overstory is key in its predominance, we simulate and compare the predominance in counterfactual competitive equilibria where demographic parameters have been switched between *Fagus* and *others*.

3.2 Methods

Here, we present the JAB model (Section 3.2.1) and the NFI data that were used for its calibration (Section 3.2.2 and A.1). Using a Bayesian calibration approach, we facilitated the fit of the model by constraining the seedling recruitment rates with prior parameter distributions, which were inferred by regression with auxiliary data from the Slovakian NFI (Sections 3.2.3 and A.4). With the inferred priors, we used an observation model to fit the JAB model to count data (Section 3.2.4), linking the area-standardized basal area states in the model to angle count data with basal area-related offsets (Section 3.2.2.2 and A.2). Finally, we simulated data from the fitted JAB model for inference about competitive equilibria and their drivers (Section 3.2.5).

All data analyses were performed with R (version 4.0.5; R CORE TEAM, 2021). All models have been written in the language stan (version 2.30.1; STAN DEVELOPMENT TEAM, 2022) and were fitted with the package cmdstanr (version 0.5.3; GABRY and ČEŠNOVAR, 2021) and the default Hamiltonian Monte Carlo (HMC) algorithm (Section 3.2.6).

3.2.1 JAB model

The JAB model is a dynamic model with competition effects that includes an explicit juvenile stage (Figure 31; for code see B). The JAB model describes populations of species that are logistically limited by the same resource (GAUSE, 1932) but differs from a classical competitive Lotka-Volterra model in four main aspects: (1) size-structured populations, (2) basal area growth, (3) reduced complexity of competition effects, (4) influx from outside the populations.

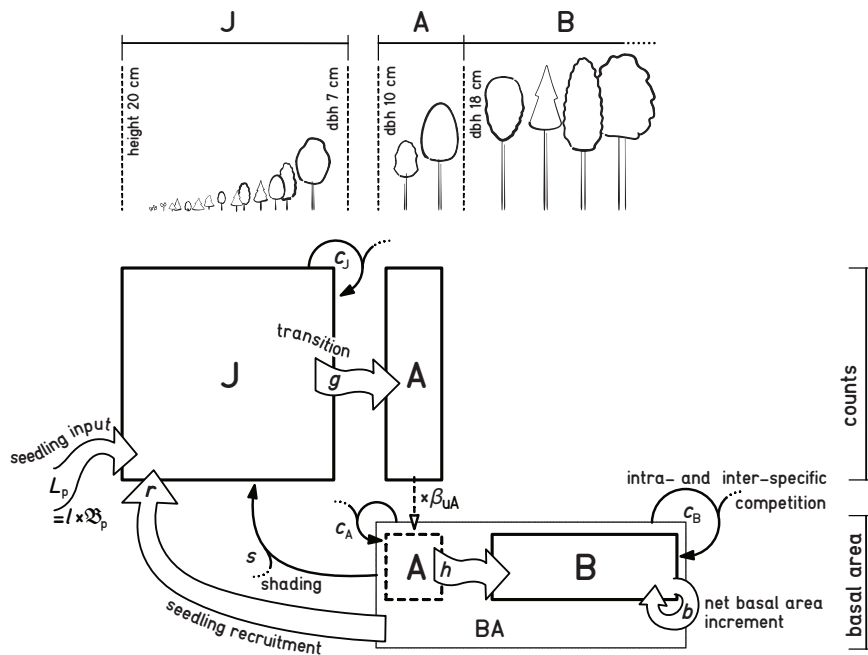


FIGURE 31: The JAB model represents three different size stages of a tree population (J, A, B) and demographic processes, including the competitive interactions between size stages and multiple species. There are processes that contribute to population growth: seedling input into the population from temporal or spatial dispersal L_p (dependent on regional basal area \mathfrak{B}_p), within-population seedling recruitment r , transitions from a smaller to a larger stage (g , h), and the net basal area growth b . The processes that limit population growth comprise the competition effect from the total sum of the sapling stage J on species-specific J (c_J), the competition from the sum of A and B, i.e. the total basal area of all species BA, on A and B (c_A , c_B), as well as the asymmetric competition from BA on J (“shading” effect s). The choice of thresholds between size stages is informed by the size classes in the data. In the German NFI small trees between height 20 cm and dbh 7 cm were counted, while trees with dbh > 10 cm were additionally measured in terms of basal area, so that intermediary size stage A acts as a mediator between count data for J and the basal area data for B. The factor β_{uA} , i.e. the upper basal area of a tree in A, converts A from counts to basal area.

In the JAB model, populations are structured into three size stages that interact: the juvenile stage J, representing the understory, and the stages A and B, jointly representing the overstory (Figure 31). Partitioning tree populations into understory and overstory, we can express asymmetric competition between the two fundamentally different forest layers (SCHWINNING, 1998): the understory is affected by the shading of the overstory, while the overstory is directly exposed to light and unaffected by the understory (VALLADARES and

NIINEMETS, 2008; ANGELINI *et al.*, 2015; CORDONNIER *et al.*, 2019; DE LOMBAERDE *et al.*, 2019). The overstory (BA) is divided into A and B to enable conversion between measures of tree abundance in the sapling stage J, which is quantified as a count density, and the final stage B, which is represented in terms of basal area. The count density in J reflects the common measure of sapling inventories in NFI (see Section A.1.1), whereas the basal area in the overstory stage B is a common measure for timber growth and competition (BIGING and DOBBERTIN, 1992). The size stage A functions as an intermediary between J (only counts) and B (only basal area) by having counts that are converted to basal area with a conversion factor. The JAB model represents growth as transition rates in absence of competition: from the understory stage J to the intermediary stage A (parameter g) and from A to B (parameter h). In addition to transitions from A, the final stage B has intrinsic basal area growth (parameter b ; Table 31).

To reduce the complexity of competition compared to a full Lotka-Volterra model, we represented only the differences in species' response to competition, assuming a similar competition effect among species (simplifying from a matrix of n^2 parameters to parameter vectors of n competing species). More specifically, species are affected by the competition from the sum of the basal area of all species within their respective layers, i.e. they have a different competitive response to the sum of all inter- and intraspecific competition (vectors of species-specific parameters c_J, c_A, c_B). In applying this competition structure, we assume that the difference in competitive response between species is much more important than their difference in competitive effect (TILMAN, 1982; GOLDBERG and LANDA, 1991; GOLDBERG, 1996). The asymmetric competition from the overstory BA on J is represented by the "shading" parameter s .

In the JAB model, there are two different sources of seedling recruitment: (1) local recruitment that is proportional to the local conspecific basal area (parameter r), and (2) external seedling input. The external seedling input L_p represents all long-term persistence of diaspores and long-distance dispersal into a subpopulation that is not explained by the local conspecific basal area of a plot p . It is proportional to a measure of long-term and large-scale distribution of the species \mathfrak{B}_p with the coefficient and parameter l (detailed in A.3).

Table 31: Parameters of the JAB model and their explanation. The parameters generally link two model states, so that there is an effect acting from some model state on another that can be positive or negative (indicated in column "direction").

Stage	Symbol	Explanation	Effect from ...	on	(direction)
J	l	seedling input from large-scale and long-term basal area average to specific J	\mathfrak{B}	J	+
	r	seedling recruitment from the local basal area to specific J	BA	J	+
	c_J	competition effect from total count of juveniles on specific J	sum J	J	-
	s	competition effect from total basal area on specific J	sum BA	J	-
J/A	g	transition due to survival and growth from specific J to specific A	J/A	A/J	+/-
A	c_A	competition effect from total basal area on specific A	sum BA	A	-
A/B	h	survival and growth from specific A to specific B	A/B	B/A	+/-
B	b	net basal area increment of specific B dependent on specific B (also includes mortality)	B	B	+
	c_B	competition effect from all basal area on specific B (includes both mortality and growth reduction)	sum BA	B	-

Based on these principles, we implemented the JAB model as a discrete-time iteration rule in `stan`, with hyperbolic density dependence (see WATKINSON, 1980; ELLNER, 1984; LEVINE and REES, 2004), similar to a Lotka Volterra-type model formulation in DIN (2013). The iteration rule comprises a set of four equations (Equations 3.1–3.4) that relate states at year $t + 1$ to states at year t . Here, in accordance with the software implementation, we

provide a vectorized formulation of the model, where all variables, including the parameters, and the stages J [ha^{-1}], A [$\text{m}^2 \text{ha}^{-1}$], B [$\text{m}^2 \text{ha}^{-1}$], and BA [$\text{m}^2 \text{ha}^{-1}$] are vectors with length n (number of species). These vectors are operated on with element-wise multiplication \odot and division \oslash ; the operator sum reduces the stages to a scalar, representing the total abundance of a stage across species.

$$J_{t+1} = L_p + r \odot BA_t + (J_t - g \odot J_t) \oslash [1 + c_J \text{sum}(J_t) + s \text{sum}(BA_t)] \quad (3.1)$$

$$A_{t+1} = g \odot J_t \oslash [1 + c_J \text{sum}(J_t) + s \text{sum}(BA_t)] + (A_t - h \odot A_t) \oslash [1 + c_A \text{sum}(BA_t)] \quad (3.2)$$

$$B_{t+1} = h \odot A_t \cdot \beta_{uA} \oslash [1 + c_A \text{sum}(BA_t)] + (1 + b) \odot B_t \oslash [1 + c_B \text{sum}(BA_t)] \quad (3.3)$$

$$BA_{t+1} = A_{t+1} \odot \beta_{mA} + B_{t+1} \quad (3.4)$$

All parameters ($r, c_J, s, g, c_A, h, b, c_B$, and $L_p = l\mathfrak{B}_p$) are generally assumed to be positive, so that all model states are strictly positive at any time (in fitting the model, this will be ensured by exponentiating the parameters sampled on a log-scale; Section 3.2.4.1). The four equations, representing size stages, are coupled through states of other stages, so that changes in one state propagate in discrete time steps, e.g., from BA to J to A to B. The fractions of trees that survive and grow in the absence of competition from J to A and from A to B are expressed by the transition rates g and h ($\in (0, 1)$), respectively. The counts in A are transformed to basal area at two different occasions: (1) In the transition to B, the counts are converted by factoring in the basal area of one tree at the threshold between A and B, a species-independent scalar factor β_{uA} , which is dependent on the threshold diameter at breast height (dbh; Equation 3.3); (2) the combined basal area BA is calculated by multiplying the counts within A with a vector of the corresponding mean basal areas β_{mA} , which are species-specific constants from the data (Equation 3.4; *Fagus*: 0.01586m^2 ; *others* 0.01611m^2).

All stages (J, A, and B) are logistically limited by interspecific tree density: The sapling stage J is limited by the competitive effect from the total basal area across species BA (s) and from the total counts within the same stage (c_J), while the stages A and B are only limited by the competitive effect of BA (c_A, c_B). This limitation is implemented by dividing the states with a denominator that is slightly greater than 1: $[1 + c_J \text{sum}(J_t) + s \text{sum}(BA_t)]$ and $[1 + c_{A,B} \text{sum}(BA_t)]$, for understory and overstory respectively. Not only the stage abundances are limited, but also the growth processes are density-dependent. The growth rates under competition are expressed by the density-dependent terms $g \oslash [1 + c_J \text{sum}(J_t) + s \text{sum}(BA_t)]$, $h \oslash [1 + c_A \text{sum}(BA_t)]$, and $b \oslash [1 + c_B \text{sum}(BA_t)]$, respectively (Table 32).

Overall, this leads to a system of populations that are in an arms race from a disturbed state towards a competitive equilibrium: Depending on their seedling recruitment (L_p and r), through transition (g, h) and net basal area increment (b) populations can intrinsically only grow or stagnate. This assumes that density-independent mortality is negligible in J and A, and that density-independent mortality in B is included in b and does not exceed basal area growth in the long term. Thus, the model is built on the assumption that populations of *Fagus* and *others* are viable in the given environmental range. Although, populations can never go extinct, they can decline through interspecific competition (c_J, s, c_A, c_B). These properties enable the JAB model to extrapolate species composition under the assumption

that species composition is mainly determined by a competitive equilibrium (ELLENBERG, 1963).

3.2.2 NFI data

To fit the JAB model to observed tree populations of *Fagus* and *others*, we used data from two different national forest inventories (NFI): the Slovakian NFI with one survey (2015–2016) and the German NFI with three repeated surveys (main years 1987, 2002, 2012; Table S1).

Data from the Slovakian NFI, which include observations of seedlings with height 10–20 cm, were used to infer prior probability distributions for the seedling recruitment rate r (for details on the Slovakian NFI data see Section A.1.2).

Subsequently, the short-term time series data from the German NFI were used to fit the JAB model to repeated observations of aggregated populations (for details on the German NFI data see Section A.1.1).

3.2.2.1 Tree size classes J, A, and B

To calibrate the JAB model with data from the German and the Slovakian NFI, trees were grouped into size classes corresponding to the stages of the JAB model. The stage J included all trees between height 20 cm and dbh 7 cm in the German NFI (Table S2). For stages A and B represented in basal area in the JAB model, we included all trees with a dbh above 10 cm, which is the lower size threshold for the angle count sampling in the German NFI. The threshold between A and B was set to dbh 18 cm. Because the lower dbh threshold of angle counts, and correspondingly the upper threshold for sapling counts, was changed from 10 cm in 1987 to 7 cm in 2002 in the German NFI, counts for saplings of this size were not available for all NFI years creating a size gap between J and A. Despite this gap, in the JAB model fit, we treat the count data in size class J as a proxy for all trees between height 20 cm and dbh 10 cm. For inferring the seedling recruitment rate from the Slovakian NFI, the basal area was summed up over the same size classes A and B (BA) and was used as a predictor for the count density of a size class right below J, seedlings of height 10–20 cm.

For analyzing the potential predominance of *Fagus sylvatica* with the JAB model, trees were split up into *F. sylvatica* and all *others*, a binary classification for which we will use “species” as a shorthand. Within species and size class, stage abundances were calculated per plot by summing up the counts in J and A, and adding up the basal area in A and B.

3.2.2.2 Accounting for varying sampling areas

To model tree abundances recorded with varying sampling areas using a count process in the likelihood of the JAB model (Section 3.2.4.2) as well as in the models for prior inference (Section 3.2.3), we used different offsets. In general, the offsets o convert the model states \hat{x} , which are abundances standardized per hectare, to the scale of observed counts x :

$$x \sim o \hat{x} \tag{3.5}$$

Different offsets were used depending on the type of the abundances in the model and the corresponding data: for the offsets that scaled the basal area states in the model to count data from the angle count method see Section A.2.1; for the offsets that scaled counts in the model to counts on different fixed areas see Section A.2.2. Because all NFI sampling

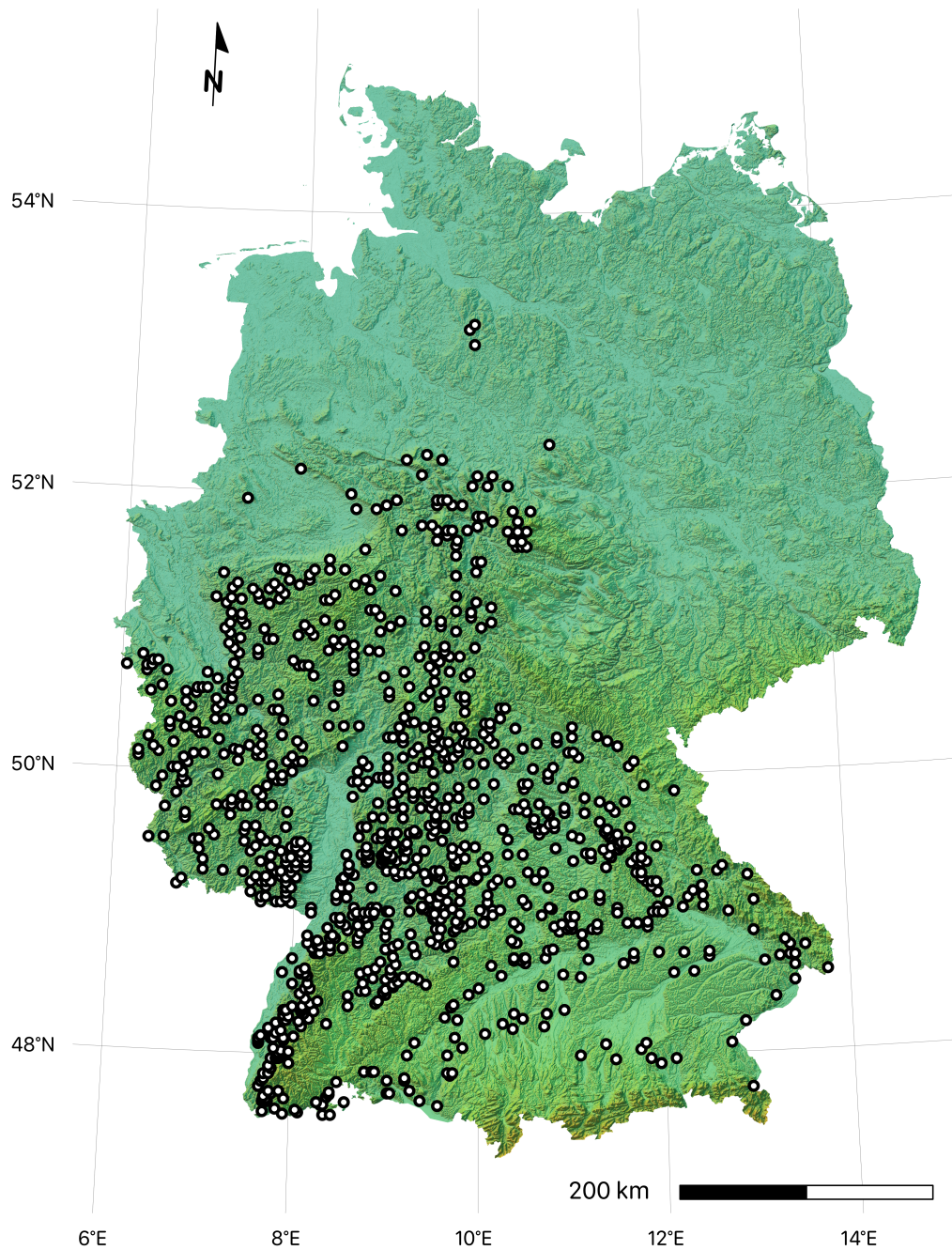


FIGURE 32: Locations of the 1000 randomly selected NFI clusters in Germany. Each cluster consists of one to four sampling plots, depending on whether the location was forested. One random plot per cluster was selected if its elevation was at 100–600 m, if there was any observation of both *Fagus* and *others*, if the observation period included all of the three surveys (1987, 2002, and 2012; which excludes former East Germany), and if there were no records of management within the period. Each selected plot (cluster) is represented by one subpopulation in the JAB model. The map projection is Lambert Conformal Conic, the color shading indicates elevation and relief.

protocols made observation areas dependent on size or abundance, the offsets for zero observations had to be derived separately (see Section A.2.3).

These offsets account for the varying sampling intensity that also affects the variance of observations. Furthermore, using a count process with offsets is (1) preferable over modelling a continuous response for the basal area because it reflects the actual observation process with discrete numbers of trees (even when being multiplied with a tree-specific basal area), and (2) preferable over upscaling the small sampling areas to a common area because this would break distributional assumptions by deflating small counts in the data, e.g. when a plot size is one fourth of the common standard area 1 hectare, the smallest measured count per hectare would be 4.

3.2.3 Prior parameter distributions

Prior to fitting the JAB model to aggregated population data from the German NFI, we estimated priors from several sources. First, we used external information from Slovakian NFI data to directly estimate species-specific uncertainty distributions for seedling recruitment r (Table S5). The regression method for inferring priors on r from the density of small seedlings with height 10–20 cm in the Slovakian NFI is detailed in A.4. The uncertainty of the estimated species-specific parameter distributions was expanded with a factor (see Section A.4) and then used as priors to constrain the model. Second, in addition to the estimated species-specific priors, we specified vague and species-unspecific priors for all other parameters of the JAB model (Section 3.2.3.2). Further, we specified several regularizing priors for technical parameters, detailed in Section 3.2.4. For parametric specifications of prior distributions for the model parameters see Table 32.

3.2.3.1 Propagating the estimated priors

We propagated the fitted posterior parameter distributions for the species-specific recruitment rate r (see Section A.4) as priors in the JAB model fit. We first visually checked the posteriors for normality and then fitted a closed-form maximum likelihood estimate of the normal distribution (`fitdistr()` in the R package ‘MASS’ version 7.3; RIPLEY, 2022) to the posterior HMC samples of species-specific $\log r$. To express the additional uncertainty due to historical and geographical differences in Slovakia (see Section A.1.2), the fitted standard deviations of $\log r$ were multiplied with a factor 4. Finally, the multiplied standard deviations, together with the means of the distributional fits, were passed on to species-specific normal priors of the parameter $\log r$.

3.2.3.2 Other vague priors for model parameters

In addition to the species-specific priors on seedling recruitment that were directly inferred from auxiliary data ($\log r$), vague and species-unspecific normal priors were provided for all other log-transformed parameters of the JAB model ($\log l$, $\log c_J$, $\log s$, $\log g$, $\log c_A$, $\log h$, $\log b$, $\log c_B$; Table 32). These priors were specified (1) to improve the convergence of the model fit by reducing the parameter space, (2) in accordance with prior predictive checks of the resulting stage abundances, (3) and to express some prior beliefs: The limiting parameters $\log c_J$, $\log c_A$, and $\log c_B$ express the expectation that the competition response of J to J c_J is relatively small and that it increases for larger trees parameters c_A and c_B . The belief that “shading” $\log s$ has a stronger effect on J than c_J was expressed with a vague

prior ($\mu = -6$, $\sigma = 2$). Priors for transition rates express the belief that the fraction of ingrowth relating to saplings J ($\log g$: $\mu = -5$, $\sigma = 2$) is smaller than ingrowth relating to the narrow size class A ($\log h$: $\mu = -4$, $\sigma = 2$). The prior for $\log b$ was based on the yearly net basal area increment estimated for surviving trees from the German NFI by (RUIZ-BENITO *et al.*, 2014) of approximately 4% ($\mu = \log 0.04 \simeq -3.2$) and thus specified with higher confidence ($\sigma = 1$). The seedling input rate l was assumed to be distributed around $\exp(4)$, which is roughly in line with the seedling input that was not explained by conspecific basal area in the regression on Slovakian data (see Section A.4 and Table S5, where the intercept $\exp(6) \lesssim k \lesssim \exp(7)$ divided by the average basal area of the respective species (Table 33 is about $\exp(4)$). Importantly, these priors were equally applied to both species, so that there is only a conservative bias regarding inference about differences between species. For both the vague and species-unspecific, as well as the inferred species-specific priors see Figure 33 and Table 32.

3.2.4 Bayesian calibration of the JAB model

3.2.4.1 Model structure

Each sample plot from the German NFI is represented as a subpopulation that changes over time in the JAB model. Each subpopulation has unknown random initial states of the three stages J, A, and B, which are fitted to the first observed state of each plot, and then simulated forward with the JAB model. The JAB model parameters (Table 31) are sampled globally, i.e. it is assumed that the simulations of all subpopulations are generated from parameters with one global uncertainty distribution, respectively. These parameter uncertainty distributions are sampled on the log-scale, informed by the corresponding priors (Section 3.2.3), and transformed with an $\exp(\cdot)$ statement to be strictly positive, before they are plugged into the JAB model (Equations 3.1–3.4). The seedling input parameter l has subpopulation specific values, $L_p = \exp(\log l) \mathfrak{B}_p$ iterated over the subpopulations or NFI plots p . This way, the regional basal area \mathfrak{B}_p informs the subpopulation-specific seedling input L_p , plugged into Equation 3.1.

To improve convergence of the model, gamma-distributed priors were specified for the unknown initial states per subpopulation. These priors express our belief that the initial states are close to the observed value in the data and avoid model fits where the initial states would significantly deviate from the data to compensate for the model dynamics due to extreme parameter combinations. The gamma distributions were parameterized with mode ν and standard deviation ζ ,

$$\beta = \frac{\nu + \sqrt{\nu^2 + 4\zeta^2}}{2\zeta^2} \quad (3.6)$$

$$\alpha = 1 + \nu\beta. \quad (3.7)$$

By specifying the mode, we set the highest probability to the observed value, and different standard deviations σ per stage dependent on the observed count κ so that $\sigma = [\text{J: } 100 + 20\kappa, \text{A: } 10 + 2\kappa, \text{B: } 1 + 0.2\kappa]$. Cases with zero observations were parameterized with expected value $E = \frac{\alpha}{\beta}$ and shape α . By setting $\alpha = 1$ and E to [J: 0.1, A: 0.02, B: 0.01] times the minimum observed value within that stage, we assumed a shape with the maximum probability always near 0 and different degrees of uncertainty for unobserved trees.

3.2.4.2 Likelihood function

The JAB model was fitted to two kinds of data, both from count processes: (1) Count data in the size classes J and A originate from a count process on varying areas per tree size, so that the area-standardized model state (counts per hectare) is related to the observations with an offset o , which is the average area of one sampling plot (see Section A.2). (2) Basal area data in size class B also originate from a count process of individual trees with varying areas, but in addition, each tree originally had an individual basal area record. Hence, to relate the model state of B (basal area per hectare) to observed counts in size class B, we used a basal area-related offset that includes both the average sampling area and a factor $\frac{c_p}{ba_p}$, which expresses how many counts c_p are added per unit of basal area ba_p on average per plot (see Section A.2.1). The offsets o transform the area-standardized and strictly positive model state (JAB) to the counts C in the data, so that for each plot p within a subpopulation c , year t (or survey r), species j , and stage s , the likelihood function is expressed by the statement:

$$C_{ptjs} \sim \text{NegativeBinomial}(JAB_{tjs} o_{ptjs}, \phi_{rjs}). \quad (3.8)$$

The precision parameter ϕ was fitted separately per stage, species, and survey. We allowed for different levels of ϕ to account for the different sampling protocols or sampling areas of the stages. Species-specific ϕ within stage were necessary because *others*—consisting of multiple species—are assumed to have a much lower dispersion in forests than the stochastic counts of a singular species—*F. sylvatica*. For the initial state, which was constrained with priors based on the first survey in the data, a separate level for ϕ than for the later observations was assumed. Since the sampling areas of size class J changed between surveys, we assumed separate levels for ϕ for all three surveys for this size class, so that overall there were six levels of ϕ in stage J, and each four levels for stage A and B. A very vague half-normal prior for the inverse of ϕ was specified to improve convergence: $\frac{1}{\phi} \sim \mathcal{H}(10)$.

3.2.5 Posterior simulations

3.2.5.1 Simulating competitive equilibria

Using the posterior probability distributions of the parameters, we simulated the JAB model forward from the initial state to obtain trajectories of model states over time (Figure 34) until final equilibrium states were reached (Figure 35). The criterion for reaching equilibrium was that the greatest species-specific relative change in basal area (BA) in the last time step should not be greater than 1%: $\max |(BA_t - BA_{t-1}) \oslash BA_t| \leq 0.001$. This numerical method for finding the equilibrium points of the JAB models is equivalent to the established procedure for numerical solution of fixed-points of a function by formulating the function as an iteration rule (BURDEN and FAIRES, 1993). In addition to the equilibrium criterion, the model was simulated over a period of at least 250 years to exclude that potential temporary extrema at the beginning of the trajectory were mistaken as an equilibrium (Figure 34), and for at most 5000 years.

3.2.5.2 Simulating counterfactual equilibria

To test the role of species-specific differences in the JAB model parameters for the equilibrium, we further simulated new equilibria from the initial state with the parameters switched

between species. Additionally, some sets of parameters whose interactions determined demographic processes were switched jointly. Jointly switched parameters include the two seedling recruitment parameters r and l , as well as parameters that appear together in a density-dependent term, i.e. g and s and c_J , h and c_A , b and c_B (Table 33). By assigning the parameter of *Fagus* to *others* and vice versa in each model run, we generated a distribution of counterfactual equilibria for each parameter and combinations to test how their species-specific differences drive competitive equilibria (Figure S4; Table 33). As a measure for the role of species-specific parameter differences in determining the predominance at the equilibrium, we calculated the percentage of cases across subpopulations and HMC samples, i.e. “posterior cases”, where either species had the majority after switching the parameters (Figure 36).

3.2.6 HMC sampling

The models, including the JAB model and the model for prior inference on seedling recruitment, were fitted with the Hamiltonian Monte Carlo (HMC) algorithm implemented by the software `stan` (version 2.21.0; STAN DEVELOPMENT TEAM, 2022). We used the default setting of 1000 iterations for both the warmup and the sampling phase, in four independent HMC chains, so that there were 4000 samples of the posterior distributions (see Table 32 for bulk effective sample size, VEHTARI *et al.*, 2021). Convergence of the four chains was checked with `stan`’s default diagnostic \hat{R} .

3.3 Results

The JAB model was successfully fitted to size class abundance data from the German NFI (HMC chain convergence for all parameters: $\hat{R} < 1.05$), conditioned on prior parameter distributions. Fitting the model with priors to short-term timeseries data, we obtained species-specific demographic rates that were used to extrapolate long-term trajectories and competitive equilibria of subpopulations (Figure 34). *Fagus sylvatica* was extrapolated to be the predominant species at the competitive equilibrium in about 94% of the posterior cases, despite being in the minority at the initial state. *Fagus*’ predominance at the competitive equilibrium was at least partially explained by its weaker response to competition from the overstory compared to *other* species (“shading” parameter s), as revealed by the fact that extrapolating new equilibria with s switched between species led to *others* predominating in 100% of the cases.

3.3.1 Estimates of demographic rates

We obtained distinct posterior estimates of demographic rates for the two species, despite all rates but r having common prior uncertainties (Figure 33, Table 32).

Of the marginal posteriors with common priors for both species (l , g , s , c_J , h , c_A , b , and c_B), external seedling input l and shading-response s were the most differentiated between species (Figure 33). Both l and s were orders of magnitude higher for *others*. The competition response within J (c_J) was however greater for *Fagus* than for *others*. The overstory parameters (c_A , h , b , c_B) were consistently more similar between species with at least some overlap of the posteriors.

Table 32: Prior and posterior distributions of JAB model parameters (mean \pm standard deviation). In addition to the growth rates g , h and b , the corresponding density-dependent (d.d.) terms are given at initial (init.) and equilibrium (eq.) state, i.e. $\log \{g \otimes [1 + c_J \text{sum}(J_t) + s \text{sum}(BA_t)]\}$, $\log \{h \otimes [1 + c_A \text{sum}(BA_t)]\}$, and $\log \{b \otimes [1 + c_B \text{sum}(BA_t)]\}$. The dispersion parameter ϕ relates to different levels of uncertainty per stage and survey.

	Posterior		Prior		bulk ESS	
	<i>Fagus</i>	<i>other</i>	<i>Fagus</i>	<i>other</i>	<i>Fagus</i>	<i>other</i>
$\log l$	4.018 ± 0.1156	5.398 ± 0.1276	4 ± 2	(common)	4149.079	3494.801
$\log r$	2.349 ± 0.1981	4.825 ± 0.1296	4.237 ± 0.5114	3.054 ± 0.7887	5115.510	4095.912
$\log c_J$	-11.56 ± 0.1798	-9.770 ± 0.9153	-10 ± 2	(common)	3594.346	2055.221
$\log s$	-8.908 ± 1.094	-1.211 ± 0.5917	-6 ± 2	(common)	4641.564	1892.538
$\log g$	-5.519 ± 0.06480	-3.591 ± 0.5471	-5 ± 2	(common)	4811.408	1923.476
$\log c_A$	-9.421 ± 1.067	-6.811 ± 0.2345	-7 ± 2	(common)	4019.090	4705.809
$\log h$	-2.683 ± 0.06066	-2.843 ± 0.06431	-4 ± 2	(common)	5840.295	3412.199
$\log b$	-4.779 ± 0.5712	-3.599 ± 0.2811	-3.2 ± 1	(common)	3655.673	2673.140
$\log c_B$	-7.287 ± 0.2391	-6.691 ± 0.1724	-7 ± 2	(common)	3578.249	2760.259
$\log g$ d.d. init.	-5.582 ± 0.06156	-5.766 ± 0.09560	.	.	5065.781	4749.521
$\log g$ d.d. eq.	-5.615 ± 0.06115	-6.188 ± 0.1124	.	.	5111.270	4339.732
$\log h$ d.d. init.	-2.686 ± 0.06120	-2.870 ± 0.06674	.	.	5896.932	3423.927
$\log h$ d.d. eq.	-2.688 ± 0.06163	-2.886 ± 0.06817	.	.	5894.770	3451.546
$\log b$ d.d. init.	-4.796 ± 0.5679	-3.629 ± 0.2763	.	.	3659.276	2672.822
$\log b$ d.d. eq.	-4.806 ± 0.5663	-3.647 ± 0.2740	.	.	3658.505	2669.801
ϕ (J Initial state)	$13810. \pm 107000.$	$25120. \pm 255000.$.	.	3418.828	4024.314
ϕ (J 2nd survey)	0.2561 ± 0.01868	0.2334 ± 0.01332	.	.	6993.445	6555.684
ϕ (J 3rd survey)	0.3029 ± 0.01842	0.2045 ± 0.01091	.	.	8347.978	7462.385
ϕ (A Initial state)	$7896. \pm 166700.$	$8034. \pm 58090.$.	.	3156.184	3574.011
ϕ (B Initial state)	$9504. \pm 74570.$	$16860. \pm 187600.$.	.	2938.323	4433.032
ϕ (A 2nd/3d survey)	2.047 ± 0.2750	1.472 ± 0.1203	.	.	7297.655	8996.458
ϕ (B 2nd/3d survey)	2.399 ± 0.2246	2.745 ± 0.1605	.	.	4900.993	7813.761

The species' sapling transition rates were reversed between conditions without competition (g) and with competition (density-dependent transition term $\log \{g \otimes [1 + c_J \text{sum}(J_t) + s \text{sum}(BA_t)]\}$; Figure S3). While transition without competition g was lower for *Fagus*, the density-dependent transition term was much higher than that of *others*, especially at the competitive equilibrium. The interspecific differences of demographic rates h and b were, however, mostly unaffected by density effects (Figure S3; Table 32)).

The marginal parameter estimates for seedling recruitment r deviated from their species-specific priors (Figure 33; Table 32). The internal seedling recruitment rate r was smaller than the prior for *Fagus* and greater for *others*, which had much greater posterior values, overall.

A multivariate representation of the posterior parameter distributions revealed strong correlations among sets of certain parameters (Figure S2): In particular, *others'* g was strongly correlated with its response to competition s and c_J (Pearson correlation 0.98 and 0.90, respectively). In addition, there were strong correlations between the two parameters determining the basal area growth in B , b and c_B , of both species, *Fagus* (0.83) and *others* (0.96).

3.3.2 Initial state and extrapolated competitive equilibria

All subpopulations across all HMC samples reached a competitive equilibrium (Section 3.2.5.1) after forward simulation over a median of 381 and a maximum of 1169 years (Figure 34).

At the initial state, *Fagus* was the less common species, only predominant in 24.0% of the cases across subpopulations and HMC samples—predominance being defined as

3. COMPETITIVE EQUILIBRIA

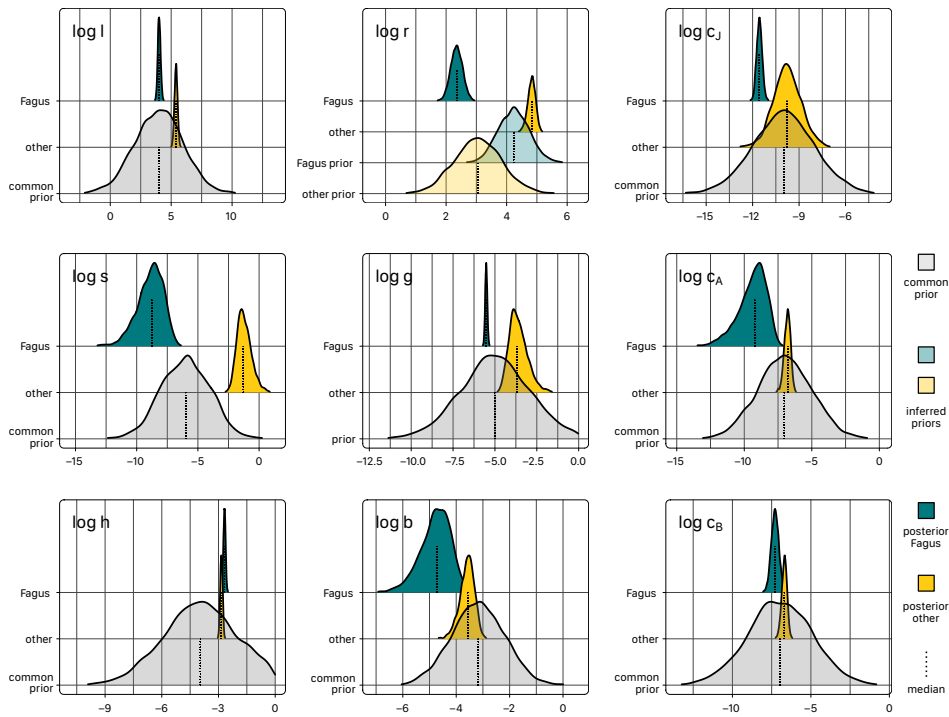


FIGURE 33: Marginal uncertainties of JAB model parameters including prior (transparent) and posterior distributions (solid) for *Fagus* and *others*. Prior to the JAB model fit, species-specific distributions for the seedling recruitment parameter $\log r$ were inferred with regression models from Slovakian NFI data and propagated as species-specific normal priors into the fit of the JAB model. The priors for all other parameters ($\log l$, $\log c_J$, $\log s$, $\log g$, $\log c_A$, $\log h$, $\log b$, $\log c_B$) were specified as common normal priors for both species (Section 3.2.3.2).

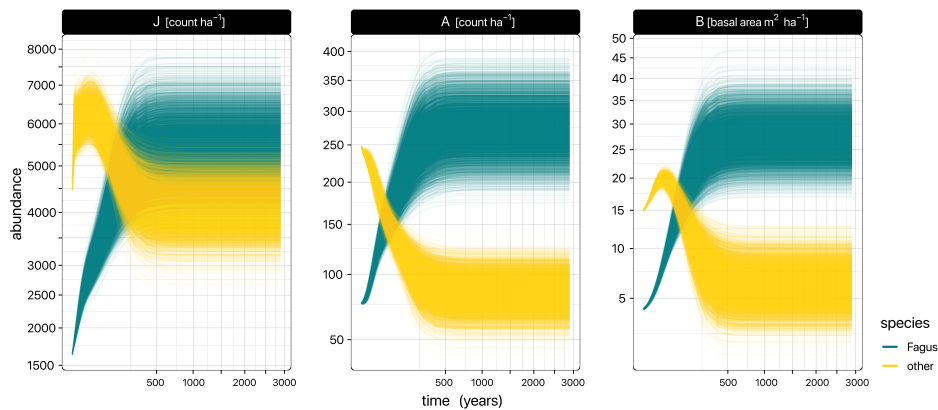


FIGURE 34: Timeline of stage abundances, simulated forward from the posterior distribution of mean initial states across subpopulations to the equilibrium. The simulations were conducted with the posterior distributions of the parameters, and with the mean per HMC sample of the subpopulation-dependent seedling input L_p . Hence, the distribution of trajectories reflects both the uncertainty of the initial states per stage, and the parameter uncertainty. Both axes are $\sqrt{\cdot}$ -transformed.

constituting $> 50\%$ of the modelled basal area (Figure 36, Table 33). Also, the mean basal area of *Fagus* was much lower at $5.1 \text{ m}^2 \text{ ha}^{-1}$ than *others*, which predominated at mean $18.4 \text{ m}^2 \text{ ha}^{-1}$ (Figure 35; Table 33). In general, the average predicted initial model states were close to the average initial observations in the data but slightly larger (Table 33).

Although initially, *Fagus* was in the minority, it became predominant in around 94% of the posterior cases at the competitive equilibrium (Figure 36; Table 33). At equilibrium, *Fagus* also superseded *others* in terms of basal area (mean 30.1 and $9.0 \text{ m}^2 \text{ ha}^{-1}$, respectively; Figure 35; Table 33). High equilibrium basal areas of *Fagus* were always correlated with low basal areas of *others*, and vice versa (Figure 35 B). Further, focusing on the distribution of the subpopulations that represented the median across HMC samples at the initial state revealed that these subpopulations, at the equilibrium state had the same distribution as the total of all subpopulations (Figure 35 A).

3.3.3 Counterfactual equilibria with switched parameters

To test the role of species differences in demographic processes for determining the competitive equilibrium, we simulated counterfactual equilibria with the parameter values switched between species (Figure 36; Table 33).

Compared to the original equilibria, where *Fagus* was extrapolated to predominate in 94% of the cases across subpopulations and HMC samples, only switching one of the limiting parameters c_J , s , c_A , and c_B led to a major change in the distribution of basal area across species and in the frequency of predominance (Table 33; Figure S4). In particular, switching the posterior estimates of s between species had the most pronounced effect (Figure 35), leading to predominance of *others* in 100.0% of the cases, i.e. reversing the predominance in all of the cases where *Fagus* would have predominated before. The limiting parameter in B, c_B , had the second greatest effect on predominance at the equilibria, leading *others* to predominate in 94.2% of the cases. Switching of L_p and r , g , and b only amplified *Fagus*' predominance.

Switching the density-dependent rates g , h , and b together with their limiting counterparts so that the results refer to the species-specific differences in the density-dependent transitions and growth together with the density effect on the states, led to a major change in predominance for the joint switch of g and c_J and s , as well as for h and c_A (Figure S5). The counterfactual equilibrium after joint switch of b and c_B , however, had a similar outcome as the extrapolated equilibrium (87.6 % *Fagus*).

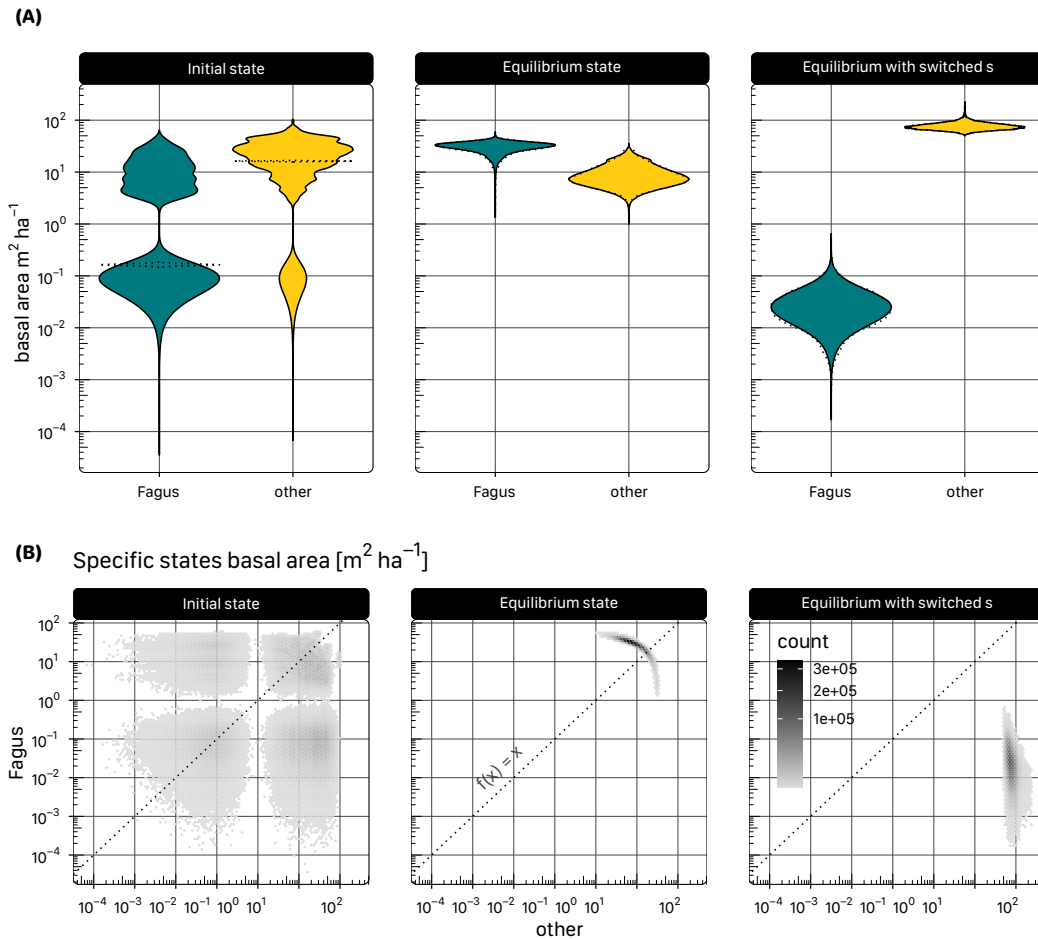


FIGURE 35: Distributions of basal area of *Fagus* and *others* at the initial state and at the equilibrium as predicted by the JAB model. In addition to the equilibrium simulated with the posterior distribution of the parameters, a counterfactual equilibrium is shown, simulated with the posteriors of the “shading” parameter s switched between *Fagus* and *others*. The state distributions include both model uncertainty, as well as spatial variability across subpopulations (NFI plots). **(A)** While the distribution of initial states of *Fagus* is mostly smaller than that of *others*, *Fagus* has the majority at at the competitive equilibrium. The dashed violins represent the model uncertainty of the median initial state across subpopulations. The identical set of subpopulations that represent the median at initial state, have equilibrium states spread along the entire range of possible states. **(B)** Predicted basal area of *Fagus* versus *others* at initial and equilibrium state. The coordinate system is divided into hexagonal bins that are colored by counts of points to indicate density. Points above the diagonal ($f(x) = x$) indicate *Fagus* predominance, points below indicate predominance of *others*. Note that all continuous axes are \log_{10} -transformed.

Table 33: Posterior distributions of initial and equilibrium abundances (stages J and A [count ha⁻¹]; B and total BA [m² ha⁻¹]) and species' predominance (mean \pm standard deviation across subpopulations and HMC samples). Equilibrium states include counterfactual simulations, where some parameters have been switched between *Fagus* and *others*.

		Fagus	others	
J	initial state data	1623.4 \pm 5361.1	4467.9 \pm 13412.	
	initial model state	1649.3 \pm 5357.6	4492.1 \pm 13406.	
	equilibrium state	5265.2 \pm 1331.1	4304.5 \pm 1272.1	
A	initial state data	72.964 \pm 209.83	245.78 \pm 453.27	
	initial model state	75.714 \pm 208.94	247.92 \pm 452.14	
	equilibrium state	262.55 \pm 67.135	92.517 \pm 33.499	
B	initial state data	4.0505 \pm 7.5868	14.872 \pm 15.390	
	initial model state	4.1454 \pm 7.6761	15.016 \pm 15.509	
	equilibrium state	25.971 \pm 6.1065	7.5556 \pm 3.9755	
BA	initial state data	5.1049 \pm 8.5159	18.395 \pm 16.071	
	initial model state	5.3459 \pm 8.6968	19.010 \pm 16.354	
	equilibrium state	30.133 \pm 7.0646	9.0462 \pm 4.4942	
	eq. sum across species	39.179 \pm 3.0684	.	
	eq. with switched l and r	84.681 \pm 9.7323	0.048748 \pm 0.028346	
	eq. with switched c_J	7.1219 \pm 8.4019	25.682 \pm 6.4551	
	eq. with switched s	0.030156 \pm 0.025767	76.468 \pm 12.579	
	eq. with switched g	131.84 \pm 69.280	0.11712 \pm 0.17244	
	eq. with switched g and s	1.0286 \pm 0.85662	36.204 \pm 7.6819	
	eq. with switched c_A	14.715 \pm 6.1191	22.331 \pm 5.6985	
	eq. with switched h	30.229 \pm 7.1389	9.2249 \pm 4.5736	
	eq. with switched h and c_A	14.086 \pm 6.0263	22.691 \pm 5.6290	
	eq. with switched b	58.235 \pm 15.821	2.2481 \pm 2.6158	
	eq. with switched c_B	7.4086 \pm 6.1813	43.081 \pm 16.073	
	eq. with switched b and c_B	26.032 \pm 6.2534	11.856 \pm 5.1306	
	Frequency of predominance	initial model state	0.23812 \pm 0.42593	0.76188 \pm 0.42593
		equilibrium state	0.94142 \pm 0.23484	0.058581 \pm 0.23484
eq. with switched l and r		1.0000 \pm 0	0 \pm 0	
eq. with switched c_J		0.10564 \pm 0.30738	0.89436 \pm 0.30738	
eq. with switched s		0 \pm 0	1.0000 \pm 0	
eq. with switched g		1.0000 \pm 0	0 \pm 0	
eq. with switched g and s		0.00022925 \pm 0.015139	0.99977 \pm 0.015139	
eq. with switched c_A		0.25013 \pm 0.43309	0.74987 \pm 0.43309	
eq. with switched h		0.93882 \pm 0.23966	0.061177 \pm 0.23966	
eq. with switched h and c_A		0.22204 \pm 0.41562	0.77796 \pm 0.41562	
eq. with switched b		0.99471 \pm 0.072535	0.0052892 \pm 0.072535	
eq. with switched c_B		0.058321 \pm 0.23435	0.94168 \pm 0.23435	
eq. with switched b and c_B		0.87634 \pm 0.32919	0.12366 \pm 0.32919	

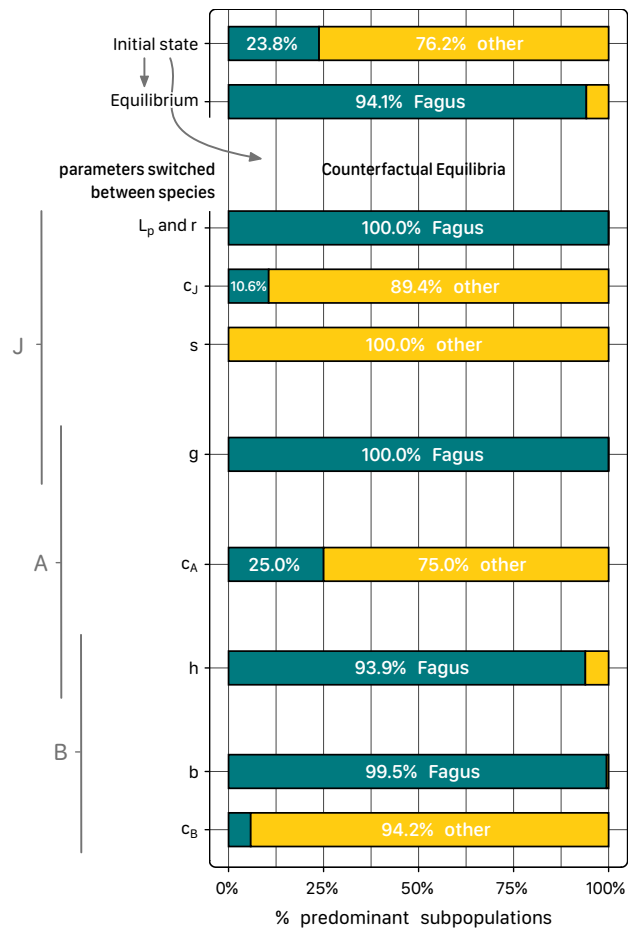


FIGURE 36: Fraction of posterior cases where either *Fagus* or *others* are the predominant species, at the initial state, at the extrapolated equilibrium, and at counterfactual equilibria with parameters switched between species. Posterior cases include the variance across subpopulations and HMC samples. The seedling recruitment parameters L_p and r were switched jointly.

3.4 Discussion

Here, we inferred species-specific demographic rates of *Fagus sylvatica* and all *other* species by fitting the JAB model to short-term timeseries data from the German NFI with prior parameter distributions for seedling recruitment based on external data from the Slovakian NFI. Using the posterior estimates of the demographic rates, we extrapolated long-term population trajectories. Consistent with the traditional consensus, *Fagus* was extrapolated to predominate across competitive equilibria, despite being in the minority at the initial state. The most important demographic process in sustaining *Fagus*' predominance is the weaker competition response of its saplings to the overstory, as demonstrated by simulations of counterfactual equilibria.

3.4.1 Estimates of demographic rates

The demographic rates, which were estimated globally across all subpopulations and different environments, revealed species-specific differences between *Fagus* and *others* (Table 32) that largely followed expectations from demographic traits at different positions along a pioneer—late-successional spectrum (WHITMORE, 1989; GRIME, 2001), especially in the sapling stage J.

Saplings of *Fagus*, consistent with the consensus on their shade-tolerance (WATT, 1923; ELLENBERG, 1963; PETROVSKA *et al.*, 2021a), were less affected by competition from the overstory (s) than saplings of the *other* species. Although the estimated effect of s also includes below-ground competition (PUTZ and CANHAM, 1992; COOMES and GRUBB, 2000), we assume the response to shading to be the most important component of the competition response of saplings to the overstory. The competition response of J to itself (c_J) was orders of magnitude smaller for *others*, even when considering the difference of units between J and BA (Table 33), which indicates that the density-dependent limitation of *others*' saplings is mainly caused by the overstory. That *others*' seedling recruitment parameters l and r had considerably higher estimates, is expected from a species mixture including pioneer species (Table S3). Especially, the external seedling input l is expected to be much lower in *Fagus sylvatica* because, compared to other tree species, it only rarely disperses over larger distances (KUNSTLER *et al.*, 2007; DOUNAVI *et al.*, 2010). In comparison to these parameters, the transition rate g , i.e. growth from stage J to A in the absence of competition, was less differentiated between *Fagus* and *others*. The overstory-related parameters (c_A , h , b , c_B) were overall more similar among species, which suggests that a major part of the demographic differentiation happens in the sapling stage J. Still, the net basal area increment b of *Fagus* was relatively slower compared to the *other* tree species, whose basal area in the German NFI mostly consists of fast-growing timber species (VOSPERNIK, 2021; Table S3).

The parameter estimates have to be interpreted in the context of two major trade-offs in the model structure, which were revealed by correlations between the posteriors of *others*' sapling parameters g , c_J , and s , as well as in the overstory between *others*' b and c_B (Figure S2). These strong correlations indicate a certain degree of equifinality, i.e. that the same model states that fit the data can be produced by multiple parameter configurations (HARTIG *et al.*, 2014), e.g., the same high basal area could be produced by either fast growth or a small competition effect. Consequently, the parameters g , c_J and s , as well as b and c_B should be interpreted in conjunction to understand their interaction, e.g., by interpreting the complete density-dependent transition term $\log \{g \odot [1 + c_J \text{sum}(J_t) + s \text{sum}(BA_t)]\}$ (Table 32)

and by jointly switching parameters between species to generate counterfactual equilibria (Section 3.4.3).

In contrast to the parameter estimate of g , the density-dependent transition term at the sapling stage $\log \{g \odot [1 + c_J \text{sum}(J_t) + s \text{sum}(BA_t)]\}$ was distinctly greater for *Fagus*. The density-dependent growth and survival terms in the overstory, however, were not fundamentally different than the density-independent rates h and b (Table 32, Figure S3). This hints at the exceptional role of competition effects on growth and survival at the sapling stage.

That the posterior estimates of seedling recruitment r deviated from the species-specific priors, indicating a conflict between the prior external information and the aggregated population data that the JAB model is fitted to, can be explained by possible biases in the estimation method, which assumes that density of small seedlings are a species-unspecific proxy for yearly seedling input (see Section A.4). Furthermore, the differences in geographical conditions and silvicultural history in Slovakia might have biased the estimates.

Overall, the population dynamics as suggested by the demographic rates of *Fagus* compared to *others* can be subsumed as slower population growth through seedling input (l , r) but overall higher sapling survival (joint effect of g , c_J , s), and predominance despite slower net basal area growth (interaction of b and c_b), which is consistent with the demographic strategy described by PETROVSKA *et al.* (2021a) as: “grow slowly, persist, dominate”.

3.4.2 Predominance at the competitive equilibrium

Fagus was extrapolated to be the predominant species in 94% of the competitive equilibria although being in the minority at the initial state, i.e. the state corresponding to the first of the German NFI surveys. This long-term extrapolation of population trajectories was based on short-term demographic rates that were estimated globally, i.e. each JAB model parameter integrated all subpopulations without being allowed to vary systematically with the environment. According to the traditional consensus, *Fagus* is very competitive under mesophilic conditions but relatively intolerant to abiotic stress like drought on the one hand, or anoxia on the other hand (ELLENBERG, 1963; MEIER *et al.*, 2011; FERNER *et al.*, 2012; LEUSCHNER, 2020). Under the assumption that physiological limitation under extreme conditions is mostly independent of species interactions, it follows that the selected plots where *Fagus* was observed at all (see Section A.1.1), do likely not only represent the environmental range where *Fagus* is able to physiologically persist but at the same time the range where it is competitive. Consequently, it is expected that *Fagus*' is also predominant in the majority of equilibria that were extrapolated from globally-inferred estimates of demographic rates on these plots.

The projected total equilibrium basal area of around $39 \text{ m}^2 \text{ ha}^{-1}$ (Table 33) lies between the total basal area reported from pristine beech-dominated forests ($\sim 36 \text{ m}^2 \text{ ha}^{-1}$ in Uholka-Shyrokyi Luh, Ukraine; STILLHARD *et al.*, 2022) and the upper limits of European forests around $50 \text{ m}^2 \text{ ha}^{-1}$ projected by MORENO *et al.* (2018). A maximum carrying capacity at the combined basal area below $50 \text{ m}^2 \text{ ha}^{-1}$ is also indicated by the line formed by bivariately associated basal areas of *Fagus*' and *others*' (Figure 35 B, center).

Uncertainty of the equilibrium states originates mostly from the posterior uncertainty of the model parameters. This is demonstrated by visualizing the equilibrium distribution for a single subpopulation (taking a population at the median of the initial state, Figure 35). Given that this single subpopulation had the same uncertainty as the total distribution of

subpopulations indicates that the equilibrium is independent of the subpopulation-specific initial state and regional basal area \mathfrak{B}_p . In conclusion, instead of the subpopulation states, the parameter uncertainty is responsible for most of the variation in the equilibria.

Comparing the means of the initial model states and the corresponding stages in the data reveals small but consistent overestimation across size classes (Table 33), which can be explained by the model assumptions for the latent model states. The initial model state was fitted to the data as a continuous, strictly-positive random variable with strong priors around the data, which were less certain for observed zeroes (Section 3.2.4.1), so that the predicted estimates are distributed more densely around the count levels, including many values close to but not zero (Figure 35 A). Nevertheless, this approach allowed the initial states to flexibly adapt to the priors on the one hand and to the model structure with transitions between stages on the other hand, so that continuous states that had corresponding zeroes in the data were likely pulled up to higher values if the priors or the other model stages made it likely.

In general, the predicted model states of the pooled species *others* are to be interpreted as an approximate environmental variable that affects the *Fagus* population, rather than a population itself. For this analysis with the focus on *Fagus*, multiple species have been aggregated into one, also resulting in a pooled estimate of the different demographic properties within the pool. This also assumes that the parameters of *others* are constant over the succession. In reality the species composition within *others* would probably change with succession towards more competitors in the pool (LORTIE *et al.*, 2004; VELLEND, 2010), e.g., *Abies alba* in colder regions (LEUSCHNER and ELLENBERG, 2017b), and consequently change the overall demographic properties of *others* towards more competitiveness. On the other hand, while the model assumes constant regional basal area \mathfrak{B}_p that informs the seedling input into the subpopulation, in reality, the regional basal area would shift towards the predominant species, which would provide *Fagus* a dispersal advantage that is not reflected in the model.

3.4.3 Which species-specific differences in demographic rates lead to predominance?

We tested the hypothesis that the weaker shading effect on saplings plays an important role in sustaining *Fagus*' predominance at the competitive equilibrium (WATT, 1923; PETROVSKA *et al.*, 2021a) with counterfactual simulations of equilibria where parameters had been switched between species (Table 33; Figure S4). The results clearly confirm the key role of the shading parameter s , which reversed all equilibria to the benefit of *others* when switched (Figure 36). Species differences in the tolerance to overstorey competition also played an important role for *Fagus*' predominance after the sapling stage, as evident from the high predominance of *others* after the switch of c_A and c_B . The species differences in growth parameters g , h , and b in the absence of competition, are all beneficial to *others*' equilibria, as indicated by *Fagus*' even greater predominance after the switch. The seedling recruitment parameters L_p and r were switched jointly because they are part of a similar process and both posteriors are beneficial for *others*, but they are trumped by the greater limiting effect of s and c_J on *others*.

The shading parameter s also had the most important role in counterfactual equilibria after joint switches of the rates g , h , and b with their limiting counterparts (Figure S5). When s is switched together with g , *others* still predominate in 100% of the cases, even though the switched g , should improve *Fagus*' dynamics. In contrast, the strong positive

effect of the shift of c_B on the abundance of *others*, disappeared when c_B and b were shifted jointly. Thus, when the correlation between c_B and b is accounted for, the joint effect of the overstory parameters does not appear to be a key determinant of *Fagus*' predominance. That the switch of s reversed all projected equilibria to the benefit of *others* is, however, not challenged by the joint switches with correlated parameters.

Overall, the demographic differentiation in the sapling stage, particularly the weaker response of *Fagus* to shading (s), is responsible for sustaining the predominance at the competitive equilibrium, which is in line with the traditional view of shade-tolerance leading to long-term predominance (WATT, 1923; ELLENBERG, 1963). Furthermore, our findings are consistent with the observation that for the recruitment success and predominance of *Fagus*, survival of saplings under shading, i.e. a smaller competitive response s to the overstory, is more important than increased growth rates (KUNSTLER *et al.*, 2005; PETRITAN *et al.*, 2007; PETROVSKA *et al.*, 2021b; for this mechanism in other shade-tolerant species see also KITAJIMA, 1994; KOBE *et al.*, 1995; CANHAM *et al.*, 1999).

3.4.4 Prospects for the JAB model

Having demonstrated the ability of the JAB model to be fitted to forest inventory data available at large spatial scales, and used for inference about the demographic processes underlying species predominance, there are multiple possible extensions of the model that could be applied in future research.

Formulated in the modelling language stan, the JAB model can be easily extended with several structural changes: (1) spatial random effects structure for the parameters, (2) temporal random effects structure for the parameters (e.g., adding random pulses to the seedling input), or (3) temporal process errors for transitions between the model states. These different structural extensions are ways to further clarify the parameter estimates by allocating some of the current variability in the parameters to the sampling structure (Section 3.4.2).

Further, the JAB model will efficiently scale up to multiple species. Calculations within the stan implementation are primitive vector operations from the software library Eigen that scale up efficiently (GUENNEBAUD and JACOB, 2010; STAN DEVELOPMENT TEAM, 2022). The number of estimated parameters will scale linearly with the number of species, because we reduced the interactions compared to a traditional Lotka-Volterra model to have only one-directional competitive effects (Sections 3.2.1).

Furthermore, species abundances along environmental gradients could be explained by linking the demographic processes in the JAB model to environmental predictors at the subpopulation level (BRISCOE *et al.*, 2019; see also SCHULTZ *et al.*, 2022). This way, questions like "How does the variation in *Fagus*' tolerance to shading at the sapling stage (parameter s) explain its variation in predominance along environmental gradients?" are readily answered with the posterior simulations that we demonstrated in Section 3.2.5.

3.4.5 Conclusions

Here, we proposed the JAB model, a parsimonious multi-species system of size-structured tree populations that concentrates on the interactions between saplings in the understory and adult trees in the overstory. We demonstrated the JAB model's ability to extrapolate credible long-term competitive equilibria from a fit to short-term time series data (see DAMGAARD, 2019). Using commonly available data from the German NFI with external

information from the Slovakian NFI allowed us to extrapolate that the competitive, shade-tolerant species *Fagus sylvatica* will be predominant at the competitive equilibrium in a two-species system of *Fagus* and all *other* tree species, although *Fagus* has been in the minority initially.

We further used the posterior parameter distributions from the JAB model fit to demonstrate with simulations that the species-specific differences in demographic processes of the sapling stage are crucial in determining the competitive equilibrium between tree species. In particular, we found strong evidence for the hypothesis that the higher tolerance of *Fagus* saplings to shading and other competition from the overstory is key for long-term predominance of *Fagus*. Our findings highlight the proposition that limitations in early ontogenetic stages constrain the potential outcomes at later stages and, in particular, the crucial role of the seedling and sapling stage for species assembly in forest communities (MAGUIRE, 1973; GRUBB, 1977; YOUNG *et al.*, 2005; HEILAND *et al.*, 2022).

Finally, the JAB model presented here can be extended to be applied in future research, like using systems of multiple species and linking the demographic processes to the environment to build demographic distribution models. The JAB model could be instrumental in improving our understanding of how demographic processes at the sapling stage control forest composition of tree species communities across the environment.

Abstract

Understanding where species occur and why is a fundamental question in ecology. For Central European forests, ecological consensus predicts that common beech *Fagus sylvatica* L. predominates at the competitive equilibrium within a specific range of soil pH and water levels, while other species dominate at less favorable conditions. The predominance of species in environmental space can be explained with the variation of demographic rates by employing process-explicit models that incorporate environmental variation.

To test the prediction that *Fagus*' predominates at favourable conditions, we fitted a parsimonious dynamic forest model (JAB model) that has interacting size-structured populations, to short time series of observed tree abundances from German national forest inventory data. By modelling the variability of demographic rates along pH and soil water gradients, we were able to reproduce the prediction and provide the first explanation for *Fagus*' predominance based on environmentally varying tree demography.

Our results largely confirm the prediction that *Fagus* outcompetes other species at a central range that extends towards more dry and less acidic conditions. This environmental pattern is explained by the environmental variation of net basal area increment of overstory trees and competition response at different sizes, rather than by rates at the sapling and intermediate sizes.

Synthesis: Through inverse calibration of a simple forest population model, we confirm a long-standing theory of potential forest vegetation in Central Europe and provide the first demographic explanation for this pattern. By employing our approach of inverse calibration of demographic rates being dependent on environmental gradients, ecological modelling can provide deeper insights into environmentally-varying dynamics and competitive equilibria between species.

4.1 Introduction

Understanding where species occur is one of the central questions in ecology (MACARTHUR, 1972; SUTHERLAND *et al.*, 2013). To describe the occurrence of species dependent on environmental variables, ecologists have used the Hutchinson niche concept (HUTCHINSON, 1957) and abundance response curves (ELLENBERG, 1952; WHITTAKER, 1967; TER BRAAK and PRENTICE, 1988). In the quest to go beyond description, ecologists since MAGUIRE (1973) have sought to explain the variable abundance along environmental gradients with the underlying environmental variation in demographic and vital processes (WATKINSON, 1985; SCHURR *et al.*, 2012; NORMAND *et al.*, 2014).

A method for explaining changing species abundance by the responses of the underlying demographic processes, is fitting process-explicit species distribution models (SDM; e.g., HIGGINS *et al.*, 2012; SCHURR *et al.*, 2012; NORMAND *et al.*, 2014; PIRONON *et al.*, 2017; KUNSTLER *et al.*, 2021; SCHULTZ *et al.*, 2022). Process-explicit SDMs received much attention a decade ago, as part of a research agenda for better forecasting range shifts under climate change (BUCKLEY *et al.*, 2010; PAGEL and SCHURR, 2012; ZURELL *et al.*, 2012; THUILLER *et al.*, 2013; MEROW *et al.*, 2014). There is, however, little evidence that these dynamic models predict species ranges much better than simple correlative SDMs, and as a consequence they are not widely used (MORIN and THUILLER, 2009; ZURELL *et al.*, 2016; BRISCOE *et al.*, 2019). But in contrast to purely-correlative SDMs, process-explicit SDMs have untapped potential as a tool for understanding why species occur where they do, dependent on environmental variables and interactions with other species (DORMANN *et al.*, 2012b; SCHURR *et al.*, 2012; THUILLER *et al.*, 2013; MALCHOW *et al.*, 2022). Moreover, it has been shown that early life stages are both critical filters for species composition (GRUBB, 1977; YOUNG *et al.*, 2005; LINES *et al.*, 2019) and that saplings can respond differently to the environment than their adult conspecifics (BERTRAND *et al.*, 2011; HEILAND *et al.*, 2022). Therefore, there have been calls for explicit modelling of seedling and sapling recruitment to capture environmental variation of forest dynamics (PRICE *et al.*, 2001; KUNSTLER *et al.*, 2009; HANBURY-BROWN *et al.*, 2022; KÖNIG *et al.*, 2022). In this study, we fit a process-explicit SDM that includes both shade-tolerance and recruitment at the sapling stage and adult dynamics. We fit the model to short forest time series to answer the question of how interspecific and environmental variation in demographic rates explains Ellenberg's 1963 theory on the predominance of the tree species *Fagus sylvatica* in Central European forests, which has remained the ecological consensus to date (e.g., FICHTNER *et al.*, 2012; MELLERT *et al.*, 2016; LEUSCHNER, 2020; CAILLERET *et al.*, 2020; PETROVSKA *et al.*, 2021a).

The Ellenberg theory states that *Fagus sylvatica* L. (common beech) is the predominant tree species at mesic soil conditions of submontane Central European forests, because it is more competitive than other species (ELLENBERG, 1963). Mesic soil conditions, i.e. conditions without extreme chemical properties and shortages or excess of water, are assumed to be physiologically optimal for most tree species, so that their *physiological response* along soil pH and water gradients would be similar among species—were it not for species interactions (ELLENBERG, 1952). In particular, *Fagus sylvatica* outcompetes other tree species at mesic soil conditions, so that their *ecological optima* are shifted towards more extreme conditions (see also KEDDY, 2001). *Fagus'* competitive demographics compared to other species include better shade-tolerance of seedlings and saplings (HEILAND *et al.*, 2023; KÄBER *et al.*, 2021), which gives rise to a positive feedback mechanism between sapling recruitment and the shading from the overstory, so that at late successional stages *Fagus* predominates at the

competitive equilibrium (LEUSCHNER and ELLENBERG, 2017b; PETROVSKA *et al.*, 2021a). However, towards the extremes of the soil gradients, *Fagus* ceases to be predominant. This species turnover can only be explained by the environmental variation of demographic rates of either *Fagus* or other tree species.

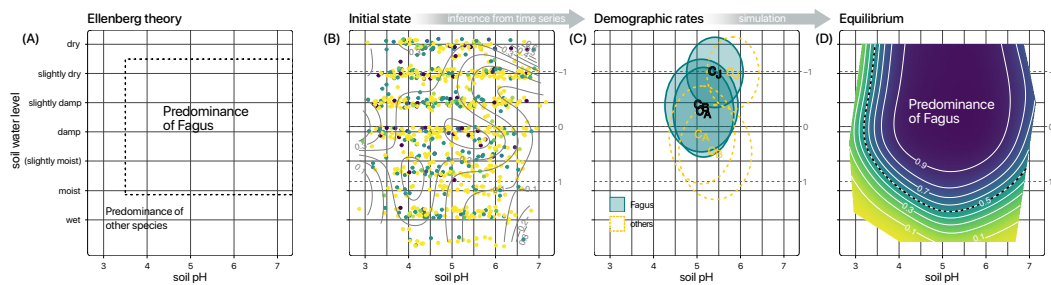


FIGURE 4I: The environmental range of predominating *Fagus sylvatica* as postulated by ELLENBERG (1963) (A) and the fraction of the total basal constituted by *Fagus* at the initial state corresponding to the first German NFI survey (B). Short time series from the NFI were used to infer the environmental variation of demographic rates. The optima (minima) of estimated growth rates are visualized by ellipses representing the standard deviations around the mean of the center parameter (C). The demographic rates were extrapolated to yield spatially-varying competitive equilibria (fraction of *Fagus* in D). Points representing forest plots in environmental space were jittered by 0.1 in both directions. Translation of the hydromorphic soil water levels to English according to LEUSCHNER and ELLENBERG, 2017a.

Although Ellenberg’s theory about predominance of *Fagus* and the *ecological response* of other tree species has been generally accepted (MELLERT *et al.*, 2016; LEUSCHNER and ELLENBERG, 2017a; CAILLERET *et al.*, 2020), there is no clear understanding how this species turnover along soil gradients is explained by variable response of demographic processes, including interspecific competition (MEIER *et al.*, 2011; MARÉCHAUX *et al.*, 2021). Furthermore, it has not yet been confirmed with large-scale data that the demographic rates of *Fagus* vary across the environment in such a way that *Fagus* would be extrapolated to dominate only at mesic conditions. We therefore ask, how does the environmental variation of demographic rates of *Fagus* and other tree species lead to the environmental variation of *Fagus*’ predominance?

To tackle this question, we use the JAB forest population model (HEILAND *et al.*, 2023). This parsimonious dynamic model explicitly includes a sapling stage and the competitive interactions between two “species”, *Fagus sylvatica* and all *other* species. We fit the model using short time series data from the German NFI, using Bayesian inverse calibration of species-specific and environmentally-dependent demographic rates (HARTIG *et al.*, 2012). This allows us to (1) infer how rates of *Fagus sylvatica* vary along soil pH and water level (defining a two-dimensional space, i.e. ecogram, ELLENBERG, 1963). We then (2) extrapolate competitive equilibria to test the prediction that *Fagus sylvatica* will predominate only at mesic conditions. Finally, (3) we use a simulation method to test which demographic rate’s variation explains *Fagus*’ predominance along soil gradients.

4.2 Materials and Methods

4.2.1 JAB Model

The JAB model (HEILAND *et al.*, 2023) is a simple dynamic forest population model that includes a sapling stage. The model concentrates on competition between multiple species and on the species-specific differences in sapling dynamics by assuming a simple two-layer size structure (see also VALLADARES and NIINEMETS, 2008; CORDONNIER *et al.*, 2019), while the interactions within the overstory are simplified to a density-dependent population model.

Table 41: Demographic rates in the JAB model and their explanation. The rates generally link two model states, so that there is an effect acting from some model state on another that can be positive or negative (indicated in column direction).

Stage	Symbol	Explanation	Effect from ...	on	(direction)
J	l	seedling input from large-scale and long-term basal area average to specific J	\mathfrak{B}	J	+
	r	seedling recruitment from the local basal area to specific J	BA	J	+
	c_J	competition effect from total count of juveniles on specific J	sum J	J	-
	s	competition effect from total basal area on specific J	sum BA	J	-
J/A	g	transition due to survival and growth from specific J to specific A	J/A	A/J	+/-
A	c_A	competition effect from total basal area on specific A	sum BA	A	-
A/B	h	survival and growth from specific A to specific B	A/B	B/A	+/-
B	b	net basal area increment of specific B dependent on specific B (also includes mortality)	B	B	+
	c_B	competition effect from all basal area on specific B (includes both mortality and growth reduction)	sum BA	B	-

The JAB model structures forest tree populations into three size stages that interact: the juvenile stage J, representing the understory, and the stages A and B, jointly representing the overstory (Fig. S1). The overstory (BA) is divided into the intermediary stage A and the final stage B, allowing conversion between count density in the sapling stage J and basal area as a measure for competition in the final stage B (BIGING and DOBBERTIN, 1992). The overstory (A and B) shades the understory, while being directly exposed to light, not affected by the understory J (ANGELINI *et al.*, 2015; CORDONNIER *et al.*, 2019; DE LOMBAERDE *et al.*, 2019). Hence, the JAB model captures asymmetric competition (SCHWINNING, 1998) between overstory and understory.

The JAB model incorporates several key demographic processes that are specific-specific (Table 41). In the sapling stage J, these include the competition response to the overstory's basal area BA (s), competition among saplings (c_J), growth and survival to stage A (g), external seedling input ($L_p = \mathfrak{B}_p l$, see Suppl. Section A.2), and seedling regeneration from the local overstory (r). Transition from stage A to B is represented by the growth and survival rate h together with a conversion factor from counts to basal area (β_{uA} , see Suppl. Section A.1). Basal area growth in the final stage B is captured by the net increment rate b . The overstory stages A and B have competition response to BA (c_A and c_B) so that all stages are logistically limited by the intraspecific tree density through different competition parameters (J: s , c_J ; A: c_A ; and B: c_B). The density-dependence applies not only to the stages but also to the growth rates g , h , and b so that in addition to these rates at the absence of competition, we provide the density-dependent growth terms $\frac{g}{1+s \text{sum}(BA)+c_J \text{sum}(J)}$, $\frac{h}{1+c_A \text{sum}(BA)}$, and $\frac{b}{1+c_B \text{sum}(BA)}$ (Table 42 and Fig. S7).

The JAB model can be fitted to short forest time series to (1) infer the role of species-specific differences in demographic rates, (2) extrapolate long-term competitive equilibria, and (3) predict the environmental variation of these processes (HEILAND *et al.*, 2023). As a demographic abundance dynamics model (BRISCOE *et al.*, 2019), the model combines the

benefits of correlative and process-based approaches, as its parsimony makes it relatively easy to fit to data yet capable of extrapolating states and simulating counterfactual scenarios (HEILAND *et al.*, 2023).

For a detailed explanation of the JAB model, see the description in Supporting Information A.1 and Fig. S1, reproduced from HEILAND *et al.* (2023).

4.2.2 Data

4.2.3 Short time series from NFI data

For fitting the JAB model we used short time-series with repeated tree counts and measurements from the German NFI (main years 1987, 2002, 2012; Table S1).

The forest plots of the German NFI are arranged on a regular quadratic grid with clusters that are 4 km apart, each consisting of four plots that are 150 m apart (TOMPPÖ *et al.*, 2010). In certain federal states, the grid may be intensified to 2.83 km or 2 km between clusters. To fit the JAB model, one randomly selected plot per cluster was used to represent a subpopulation, as the within-cluster variance of tree abundances was high, yet selecting one plot per cluster still avoids potential dependencies among the plots of one cluster.

In the German NFI, trees above 10 cm diameter at breast height (dbh) were sampled using the angle count method (RIEDEL *et al.*, 2017), which selects all trees appearing wider than a defined angle around a central observer at 1.3 m height (KANGAS and MALTAMO, 2006). Instead of a fixed area for all tree sizes, the selection with an angle leads to a sampling area that varies with dbh. This method delivers data where each counted tree has (1) a corresponding distance to the center, (2) a dbh that is equivalent to a potential sampling distance, i.e. area and sampling probability, (3) as well as a calibration factor k [$\text{m}^2 \text{ha}^{-1}$] for the sampling angle. In this study, the angle count plots were truncated to have a fixed maximum radius of 15 m (for details see Section A.3.3).

Trees were grouped into size classes corresponding to the stages of the JAB model. Stages A and B, represented in basal area in the JAB model, included all trees above the lower size threshold for angle count sampling (10 cm). The threshold between A and B was set to dbh 18 cm. Saplings between height 20 cm and dbh 7 cm were counted on circular fixed area plots with radii dependent on size class and survey and were subsumed as size class J in the analyses (Table S2). Because the lower dbh threshold of angle counts, and correspondingly the upper threshold for sapling counts, was changed from 10 cm in 1987 to 7 cm in 2002 in the German NFI, counts for saplings of this size were not available for all NFI years creating a size gap between J and A. Despite this gap, in the JAB model fit, we treat the count data in size class J as a proxy for all trees between height 20 cm and dbh 10 cm.

As the analysis is about the environmental variation of *Fagus sylvatica* we divided trees into two categories (referred to as “species” for brevity): *F. sylvatica* and all *other* species. Within each species and size class, stage abundances were calculated per plot by summing counts in J and A and adding up basal area in A and B. If one of the two species was not present on a plot that was recorded as forested in the NFI, the observation of the respective species was supplemented with 0 for each size class.

To ensure that the data were relevant for Ellenberg’s original predictions for submontane elevations and appropriate for inferring population demographics, we selected plots at elevations between 100 and 600m (which is inclusive regarding latitudinal variation; EL-

ELLENBERG, 1963) that included corresponding records of soil water level (Section 4.2.4) and with repeated observations, that were unmanaged during the observation period. Plots were selected that were surveyed thrice—in 1987, 2002, and 2012—which confines the sampled area to former West Germany. Clear cuts were ruled out by excluding plots that had tree observations in the first or second survey but only zero-observations in a subsequent survey. Plots where categories of management were recorded (sowing, planting, harvested sample trees, or damage through forestry) in the second or third survey were also excluded. Plots with missing sample trees for “unknown reasons” (category only available in the third survey) were also excluded. But contrary to HEILAND *et al.* (2023), we did not select the plots based on whether *Fagus* was present or not, to sample a greater environmental range of plots.

To reduce computational cost, a random subsample of plots was selected, stratified based on the two environmental variables used in the analysis (Section 4.2.4). The variables were split into seven uniform intervals between their minimum and maximum values, resulting in 49 bins in environmental space. To achieve an overall sample size below $n = 1200$ either $\lceil \frac{n}{49} \rceil = 25$ plots were randomly sampled per bin, or in case there were less than 25 plots, all plots were selected (Table S4). Overall with plot exclusion and sampling criteria, from 61666 plots in 21574 clusters before selection, 795 plots were sampled (Table S1).

4.2.4 Environmental variables

We matched the two soil gradients in the original formulation of the prediction on predominance of *Fagus* (ELLENBERG, 1963) by using soil pH and soil water level as environmental predictors in the model fit. For the analyses, we scaled and centered both variables. To visualize forest plots in two-dimensional environmental space, we added a consistent uniform jitter $[-0.1, 0.1]$ around the unscaled variables.

4.2.4.1 Soil pH

We used the top soil pH in CaCl_2 , provided as a spatial raster at 500 m resolution by the European Soil Data Centre (BALLABIO *et al.*, 2019). Values of the spatial raster were extracted based on the coordinates of the forest plot locations. Soil pH is commonly used as a proxy for plant nutritional conditions because it is tightly correlated with factors such as base saturation and C/N ratios (HÄRDTLE *et al.*, 2004).

4.2.4.2 Soil water level

We further used hydromorphic soil water and groundwater categories from the National Forest Soil Survey (BENNING *et al.*, 2019) at locations of the German NFI to match the soil water gradient of Ellenberg’s prediction. The categories were ranked and converted into a pseudo-ratio scale according to the levels in ELLENBERG (1963) and based expert knowledge and the category descriptions in BENNING *et al.* (2016), so that the levels between “dry” (−6.0), “damp” (0.0), and “very wet” (8.0) were uniformly spaced (see Suppl. Table S3 for ranking details). The pseudo-ratio values were averaged per plot, weighted by the respective soil layer thickness and surface area.

4.2.4.3 Environmental range

We compared the environmental range of the German NFI with the range of European distribution of *Fagus sylvatica* by extracting environmental variables at all plots used in the analysis, and at locations of *Fagus sylvatica*'s presence in Europe (Suppl. Fig. S3). As presences we used raster cells with predicted Relative Probability of Presence > 1% from The European Atlas of Forest Tree Species (<https://forest.jrc.ec.europa.eu/en/european-atlas/>; DE RIGO *et al.*, 2016). To visualize differences in pH ranges, we used top soil pH in CaCl₂ (European Soil Data Centre, Section 4.2.4.1). For comparing ranges of water availability across Europe, instead of water soil level, we used a climatic water balance, described in HEILAND *et al.* (2022).

4.2.5 Fitting the JAB model with environmental variation of demographic rates

4.2.5.1 Model subpopulation structure

In the JAB model, each forest plot is represented as a subpopulation that changes over time. Each subpopulation has random initial states of the three stages (J, A, and B), which are fitted to the first observed states of each plot, and then simulated forward. The forward-simulated yearly model states are matched to the observed data, with the discrete time t after the initial state $t = 1$ in the model to the t^{th} year after the first data survey (e.g., 1987). The subpopulation-specific demographic rates (Table 41) are generated dependent on the respective environmental variables (Section 4.2.5.2).

Using random initial states allowed flexibility for subpopulation trajectories; but to improve convergence and express different levels of certainty we constrained them with gamma priors per species, stage and subpopulation. The gamma distributions were parameterized with mode μ_γ and standard deviation σ_γ ,

$$\beta = \frac{\mu_\gamma + \sqrt{\mu_\gamma^2 + 4\sigma_\gamma^2}}{2\sigma_\gamma^2} \quad (4.1)$$

$$\alpha = 1 + \mu_\gamma\beta. \quad (4.2)$$

By specifying the mode, we set the highest probability to the observed value, and different standard deviations σ per stage dependent on the observed count ω so that $\sigma = [J: 50 + 30\omega, A: 5 + 3\omega, B: 0.5 + 0.3\omega]$. Cases with zero observations were parameterized with expected value $E = \frac{\alpha}{\beta}$ and shape α . By setting $\alpha = 1$ and E to $[J: 0.02, A: 0.01, B: 0.005]$ times the minimum observed value within that stage, we assumed a shape with the maximum probability always near 0 and different degrees of uncertainty for unobserved trees.

4.2.5.2 Environmental variation of demographic rates

Environmental variation of the JAB model rates ($r, c_J, s, g, c_A, h, b,$ and c_B) is achieved by fitting bell-shaped paraboloids dependent on the two environmental variables x (soil pH) and y (soil water level). The parabolic response of a demographic rate (f) at a subpopulation (p) is expressed as the sum of two quadratic response curves,

$$f_p = \exp\{\zeta_x(x_p - \kappa_x)^2 + \zeta_y(y_p - \kappa_y)^2 + \epsilon\}, \quad (4.3)$$

where ϵ is the extreme value of a rate, κ are the positions of the extremum along the two environmental axes x and y , ζ are the two respective spreads of the curves, and the exponentiation ensures that all JAB model rates are strictly positive.

This vertex parameterization, with five paraboloid parameters per demographic rate, makes it straight-forward to formulate prior distributions for all parameters. The extreme value ϵ is the general height of the response and is assumed to be similar to the posterior rate estimates of the JAB model published in HEILAND *et al.* (2023) (for priors see Table 42). The centers κ were assumed to conform to a normal distribution $\kappa \sim \mathcal{N}(0, 1)$. Since the environmental variables (Section 4.2.4) were scaled and centered, this expresses the belief that the extremum is positioned along the range of the respective variable with a higher probability of intermediate values. The spreads ζ determine the direction (bell shape or upside-down bell shape) and the curvature of the paraboloid along the two axes. The growth rates (r, g, h, b) were assumed to have negative ζ , indicating a maximum and slower growth towards the margins, while the limiting rates (c_J, s, c_A, c_B) were assumed to have positive ζ with a minimum and greater limitations towards the margins along both axes. The curvature is assumed to follow a half-normal prior with its greatest mass close to zero, $\pm\zeta \sim \mathcal{H}(\sigma_\zeta)$, which means that a flat response to the environment with value ϵ is the most likely case a priori. The standard deviation σ_ζ of the prior was adapted to the prior expected value for ϵ to make it comparable across demographic rates. Comparability is achieved by calculating $\sigma_\zeta = \zeta_{x,y}$ so that the exponentiated parabola would have a consistent slope $q = 0.1$ at $x, y = 1$ and for $\kappa = 0$. Given that the ζ of the respective other gradient is 0, the slope is $q = 2\zeta x \exp(\epsilon + \zeta x^2)$. Hence $\sigma_\zeta = W_0(\frac{1}{2}q \exp -\epsilon)$, where W_0 is the principal branch of the Lambert W function.

All priors were specified equivalently for both species.

In contrast, the seedling input rate l varies not with the environmental variables, but with a spatial smooth of the regional conspecific basal area, a measure for long-distance and long-term dispersal (details in Suppl. Section A.2). The regional basal area \mathfrak{B}_p informs the subpopulation-specific values, $L_p = \exp(\log l) \mathfrak{B}_p$ iterated over the subpopulations or NFI plots p .

To characterize the variation of demographic rates along environmental gradients, we took the means of the posterior log rates per subpopulation and summarized these *environmental distributions* by calculating means and standard deviations (Table 42).

4.2.5.3 Likelihood function

The JAB model states, including the unknown initial state, were fitted to the data with the same Negative Binomial likelihood function but with varying offsets and observation error.

Different offsets were used to integrate two kinds of data, both from count processes (see Suppl. Section A.3 for details): (1) Count data in the size classes J and A originate from a count process on varying areas per tree size, so that the area-standardized model state (counts per hectare) is related to the observations with an offset o , which is the average area of one sampling plot. (2) Basal area data in size class B also originate from a count process of individual trees with varying areas, but in addition, each tree originally had an individual basal area record. Hence, to relate the model state of B (basal area per hectare) to observed counts in size class B, we use a special offset that includes both the average sampling area and a factor $\frac{c_p}{ba_p}$, which expresses how many counts c_p are added per unit of basal area ba_p on average per plot. The offsets o transform the area-standardized and strictly positive model

state (JAB) to the counts C in the data, so that for each plot p within a subpopulation c , year t (or survey r), species j , and stage s , the likelihood function is expressed by the statement:

$$C_{ptjs} \sim \text{NegativeBinomial}(JAB_{tjs} \phi_{ptjs}, \phi_{rjs}). \quad (4.4)$$

We accounted for variations in sampling protocols and areas by fitting the precision parameter ϕ separately for each stage, species, and survey (Table S6). Species-specific ϕ within stage were necessary because the dispersion of a set of multiple species (*others*) is much lower than that of a single species—*F. sylvatica*, which had more stochastic abundance. For the initial state, which was initialized based on the data of the first survey, a different level for ϕ was assumed (Suppl. Table S6). Additionally, changes in sampling areas for size class J between surveys required different values of ϕ for all three surveys in this class. As a result, there were six levels of ϕ in stage J, four levels in stage A, and four levels in stage B. A half-normal prior for the inverse of ϕ was used to improve convergence: $\frac{1}{\phi} \sim \mathcal{H}(1)$.

4.2.5.4 HMC sampling

The JAB model was implemented in stan (version 2.31.0; STAN DEVELOPMENT TEAM, 2022) and fitted with the package cmdstanr (version 0.5.3; GABRY and ČEŠNOVAR, 2021) using its default Hamiltonian Monte Carlo (HMC) algorithm. We used 800 iterations for the warmup and 1000 iterations for the sampling phase, in four independent HMC chains, so that there were 4000 samples of the posterior distributions (see Table 41 for bulk effective sample size, VEHTARI *et al.*, 2021). Convergence of the four chains was checked with stan's default diagnostic $\hat{R} < 1.05$. All data preparation and posterior analyses were performed with R (version 4.2.3; R CORE TEAM, 2021).

4.2.6 Posterior simulations from the fitted JAB model

Using the posterior probability distributions of the demographic rates, we simulated competitive equilibria and the effect of demographic rates' environmental variation. The simulations were implemented in the `generated quantities` block within the stan model.

4.2.6.1 Competitive equilibria

We simulated the JAB model forward from the initial state to obtain trajectories of subpopulations over time until final equilibrium states were reached. The criterion an equilibrium was that the greatest species-specific relative change in basal area (BA) in the last time step should not exceed 1‰: $\max |(BA_t - BA_{t-1}) \oslash BA_t| \leq 0.001$. This method for finding the equilibrium points of the JAB models is equivalent to the established procedure for numerical solution of fixed-points of a function as iteration rule (BURDEN and FAIRES, 1993). The model was simulated forward at least 250 years to ensure that temporary extrema at the beginning of the trajectory were not mistaken as equilibrium (HEILAND *et al.*, 2023), and for a maximum of 6000 years. Additionally, we generated counterfactual equilibria where the regenerative rates (l , r , b) of the respective other species were set to 0, to show the potential abundant centers of each species (Suppl. Fig. S8). Further, to demonstrate the role of the shading parameter s , which had been shown to be the most important for predominance

at the equilibrium overall (HEILAND *et al.*, 2023), we simulated equilibria with s switched between species at the subpopulation level (Suppl. Fig. S8 G).

Equilibrium abundances were visualized by fitting and predicting two-dimensional smoothing splines along the two environmental axes using the `gam` function of the `mgcv` package (version 1.8; WOOD, 2021). The model was fitted to the posterior distribution with a Gaussian response for basal area and binomial response for fraction of total basal area. Predictions from the model were visualized within the convex hull that included the non-jittered positions of the observed plots. The line indicating the range of *Fagus* predominance was visualized by predicting the isocline of 50% basal area fraction at equilibria (Fig. 41 and Suppl. Fig. S8 B).

4.2.6.2 Effect of demographic environmental variation on equilibria

To quantify the effect of environmental variation of demographic rates on the competitive equilibria, we calculated the differences in *Fagus*' basal area fractions at the equilibria with and without environmental variation of demographic rates. To simulate counterfactual equilibria with a flat environmental response of demographic rates, we used the mean rate across subpopulations in all subpopulations. We obtained a posterior distribution of the *environmental variation effect* by subtracting the fraction of *Fagus* at equilibria with flat rates from those with environmentally-dependent rates, with negative differences indicating that the rates' environmental variation has a negative effect on the basal area at equilibrium. In Fig. 43, we provide a summary of the environmental variation effect for each demographic rate, represented by the mean of the absolute differences.

We further visualized the simulated environmental variation effect in environmental space using Gaussian smoothing splines, as outlined in Section 4.2.6.1 (Fig. 44 and Suppl. Figs S9). To identify credible effects, we determined the fraction of the posterior per subpopulation that was greater or smaller than 0. If more than 90% of the posterior met either condition, we determined the environmental variation effect of a subpopulation as credibly positive or negative, respectively.

Table 42: Posterior distributions of JAB model parameters, including the paraboloid parameters (mean \pm posterior standard deviation) and the environmental distribution of log demographic rates (mean \pm environmental standard deviation). Demographic rates are generated by the corresponding paraboloid parameters ϵ , κ , ζ with the respective environmental axes x (pH) and y (soil water level). In addition to the growth rates $\log g$, $\log h$ and $\log b$ the corresponding density-dependent ($d.-d.$) terms across all subpopulations are given at initial and equilibrium state, i.e. $\log(g \odot [1 + c_J \text{sum}(J_t) + s \text{sum}(BA_t)])$, $\log(h \odot [1 + c_A \text{sum}(BA_t)])$, and $\log(b \odot [1 + c_B \text{sum}(BA_t)])$.

Stage	Rate	Parameter	Explanation	Fagus	others	Prior
J	r	$\log r$	env. distribution	2.232 ± 0.1561	4.629 ± 0.1366	
		ϵ_r	extremum	2.235 ± 0.1560	4.632 ± 0.1367	4 ± 1
		$\kappa_{r x}$	center (pH)	0.0001603 ± 0.9643	0.1004 ± 0.9937	
		$\kappa_{r y}$	center (soil water)	0.008588 ± 0.9955	0.01348 ± 0.9690	
		$\zeta_{r x}$	spread (pH)	-0.0007368 ± 0.0005630	-0.0007302 ± 0.0005647	
		$\zeta_{r y}$	spread (soil water)	-0.0007352 ± 0.0005440	-0.0007166 ± 0.0005464	
	c_J	$\log c_J$	env. distribution	-12.23 ± 0.2726	-8.272 ± 0.7036	
		ϵ_{c_J}		-12.79 ± 0.3719	-8.964 ± 0.8795	-11 ± 2
		$\kappa_{c_J x}$		0.4383 ± 0.6883	0.8527 ± 0.6355	
		$\kappa_{c_J y}$		-0.9838 ± 0.6394	-0.9699 ± 0.6583	
		$\zeta_{c_J x}$		0.1329 ± 0.08853	0.1771 ± 0.1001	
		$\zeta_{c_J y}$		0.1736 ± 0.09618	0.1731 ± 0.09071	
	s	$\log s$		-9.367 ± 1.030	-0.3539 ± 0.5606	
		ϵ_s		-10.25 ± 1.216	-0.5047 ± 0.5613	-6 ± 2
		$\kappa_{s x}$		0.2164 ± 0.7749	-0.1824 ± 0.9156	
		$\kappa_{s y}$		-0.2101 ± 0.7144	1.039 ± 0.8310	
		$\zeta_{s x}$		0.2539 ± 0.2006	0.02001 ± 0.01794	
		$\zeta_{s y}$		0.3971 ± 0.3607	0.04323 ± 0.02879	
J/A	g	$\log g$	env. distribution	-5.190 ± 0.1140	-2.304 ± 0.5375	
		ϵ_g		-4.863 ± 0.1734	-2.227 ± 0.5361	-4 ± 1
		$\kappa_{g x}$		-0.3004 ± 0.7416	-0.2853 ± 0.8740	
		$\kappa_{g y}$		1.015 ± 0.5867	0.4063 ± 0.9424	
		$\zeta_{g x}$		-0.06200 ± 0.04883	-0.01870 ± 0.01612	
		$\zeta_{g y}$		-0.1155 ± 0.05590	-0.02175 ± 0.01889	
		$d.-d. \text{ term}$	at initial state	-5.224 ± 0.1109	-4.895 ± 0.1050	
			at equilibrium	-5.254 ± 0.1090	-6.053 ± 0.2159	
A	c_A	$\log c_A$	env. distribution	-8.859 ± 1.082	-6.622 ± 0.2118	
		ϵ_{c_A}		-9.551 ± 1.328	-6.756 ± 0.2456	-7 ± 2
		$\kappa_{c_A x}$		0.1756 ± 0.7395	0.1406 ± 0.8022	
		$\kappa_{c_A y}$		-0.2601 ± 0.8150	0.1530 ± 0.8889	
		$\zeta_{c_A x}$		0.3011 ± 0.2648	0.04833 ± 0.04099	
		$\zeta_{c_A y}$		0.1924 ± 0.1923	0.03918 ± 0.03615	
A/B	h	$\log h$	env. distribution	-2.835 ± 0.1221	-2.988 ± 0.07214	
		ϵ_h		-2.412 ± 0.2077	-2.823 ± 0.08453	-3 ± 1
		$\kappa_{h x}$		0.9856 ± 0.5552	-0.09541 ± 0.8960	
		$\kappa_{h y}$		0.4131 ± 0.4774	1.089 ± 0.4414	
		$\zeta_{h x}$		-0.1220 ± 0.06250	-0.01314 ± 0.01197	
		$\zeta_{h y}$		-0.1421 ± 0.08160	-0.06805 ± 0.02732	
		$d.-d. \text{ term}$	at initial state	-2.841 ± 0.1232	-3.017 ± 0.07450	
			at equilibrium	-2.850 ± 0.1250	-3.062 ± 0.08182	
B	b	$\log b$	env. distribution	-3.546 ± 1.292	-3.047 ± 0.2228	
		ϵ_b		-2.947 ± 0.4956	-3.004 ± 0.2172	-3 ± 1
		$\kappa_{b x}$		0.5314 ± 0.7471	0.006300 ± 0.9264	
		$\kappa_{b y}$		-0.4941 ± 0.9391	0.1035 ± 0.9095	
		$\zeta_{b x}$		-0.1114 ± 0.1490	-0.009622 ± 0.009471	
		$\zeta_{b y}$		-0.1498 ± 0.2490	-0.01575 ± 0.01439	
		$d.-d. \text{ term}$	at initial state	-3.576 ± 1.281	-3.078 ± 0.2171	
			at equilibrium	-3.614 ± 1.271	-3.126 ± 0.2115	
B	c_B	$\log c_B$	env. distribution	-6.754 ± 0.6812	-6.543 ± 0.1965	
		ϵ_{c_B}		-6.916 ± 0.7710	-6.600 ± 0.2057	-7 ± 2
		$\kappa_{c_B x}$		0.1291 ± 0.8907	0.4474 ± 0.8884	
		$\kappa_{c_B y}$		-0.3808 ± 0.8419	0.4679 ± 0.8594	
		$\zeta_{c_B x}$		0.04258 ± 0.04792	0.01304 ± 0.01124	
		$\zeta_{c_B y}$		0.05732 ± 0.07456	0.01776 ± 0.01516	
(J)	L_p	$\log L_p$	env. distribution	2.428 ± 0.1205	7.656 ± 0.1531	
		$\log l$		1.691 ± 0.1205	5.095 ± 0.1531	5 ± 2

4.3 Results

4.3.1 Estimates of demographic rates

The fitted paraboloid parameters (ϵ , κ , ζ ; Section 4.2.5.2) determined the JAB model parameter values at the subpopulation level (r , c_J , s , g , c_A , h , b , and c_B). The resulting *environmental distributions* of subpopulation-level rates (Section 4.2.5.2), were primarily influenced by the extreme values ϵ (Table 42).

Notably, the extreme values and environmental distributions showed the most differentiation between *Fagus* and *others* at the sapling stage J compared to the later stages (Table 42). Specifically, *others*' saplings exhibited competition response that was orders of magnitude higher than *Fagus*'s, both in terms of competition from the overstory (s) and within-sapling competition (c_J). While *Fagus* had much lower estimates for seedling recruitment (r) and external seedling input (L_p).

In the overstory stages A and B, *others* still had greater response to competition, but the species differences decreased as tree size increased from A (c_A) to B (c_B).

Regarding growth and transition rates in the absence of competition (g , h , b), the species differences varied across size classes. *Fagus* exhibited a lower fraction of saplings transitioning to stage A (g) but a higher fraction transitioning from stage A to stage B (h). The net basal area increment (b) was smaller for *Fagus* compared to *others*. These species relations generally held true for density-dependent growth terms (Section 4.2.1), except for the transition term $\frac{g}{1+s \text{sum}(BA)+c_J \text{sum}(J)}$, which was greater for *Fagus* but only at the equilibrium.

4.3.2 Environmental variation of demographic rates

Fagus showed much greater environmental variation compared to *others* in the demographic rates at the overstory stages A and B, as indicated by the standard deviations of environmental distributions on the log scale (Table 42), and the resulting paraboloids (Fig. 42). At the sapling stage J, however the environmental variation was more similar between species.

Specifically, rates that represent mortality in the JAB model, typically had the largest environmental variation per stage. The most significant variation was observed in the net basal area increment ($\log b$, including density-independent mortality) of *Fagus* in overstory stage B, ranging from a maximum of -3.5 (Table 42) to values below -4.8 (Fig. 42). The competition response in stage B ($\log c_B$) also varied from a minimum of -6.75 to values below -6.45 . In the smaller size stages, the limiting rates $\log c_A$ (stage A), and $\log s$, $\log c_J$ (stage J) also showed considerable variation, with standard deviations up to 1 on the log scale.

Across species and most demographic rates, the extreme value was positioned near the center of both the soil pH and the water level gradient (Fig. 42). The extremum for all demographic rates was located close to the center, around moderately acidic values of pH 4.5–6, with a slight tendency towards less acidic conditions indicated by positive κ_x (Table 42). In contrast, along the soil water gradient, there was more variation in the position of the extrema across species, as reflected by larger absolute values of κ_y .

The density-dependent growth terms (4.2.1), exhibited variations in environmental space similar to the corresponding growth rates (h and b). The density-dependent transition term for saplings $\frac{g}{1+s \text{sum}(BA)+c_J \text{sum}(J)}$, however, had a minimum at the center under equilibrium

conditions, expressing the pattern of the two limiting rates s and c_J together with the equilibrium abundance, instead of g (Suppl. Fig. S7).

4.3.3 Equilibria in environmental space

At the simulated equilibria, *Fagus* predominated (basal area fraction $>50\%$) at the central region of the environmental space and its fraction of basal area decreased towards the margins (Fig. 41, Suppl. Fig. S8). Even though, at the initial state, *Fagus* was at only 14% on average (Table S7) with the highest fractions of *Fagus* found at marginal regions (Suppl. Fig. S8 A). Especially at the wet and at the acidic margin, *Fagus* decreased steeply, resulting in predominance of other species at the equilibrium. However, at the dry margin, the equilibrium basal area fraction of *Fagus* showed minimal decline.

In counterfactual equilibria where *others* were absent due to simulations without their regeneration, *Fagus* remained the most abundant species in the central region of the environmental space. However, in the absence of *Fagus* regeneration, *others* no longer exhibited the highest abundance at the margins but instead showed a similar abundance at the central region previously occupied by *Fagus*. Simulating equilibria while switching the shading response (s) between species, revealed that *Fagus* would only locally gain a maximum of 50% of the basal area and would never become the predominant species (Suppl. Fig. S8 G).

4.3.4 Effect of demographic environmental variation on equilibria

Demographic rates of *Fagus* mostly had a much larger environmental variation effect compared to *others*, i.e. greater absolute mean difference in basal area fractions at equilibria with environmentally-varying demographic rates compared to equilibria with flat mean rates (Fig. 43). The most pronounced effects were observed in *Fagus*' overstory stage B, specifically in the limiting rate c_B and the net basal area increment b . The combined environmental effect of these two rates also had the largest overall impact. The next largest effect was observed in the sapling stage J, in the rate c_J . The combined effect of g and the limiting rates c_J and s also had considerable influence. In contrast, at the intermediate stage A, the rates of growth (h) and competition (c_A) were not as influential. Interestingly, for *Fagus*, both the seedling recruitment (r) and seedling input rate (L_p) exhibited minimal effects on the environmental variation of equilibria.

The environmental variation effects in *others* were considerably smaller compared to *Fagus*, and in the overstory rates the relative ranking of their magnitudes closely resembled that of *Fagus*. Specifically, the rate c_B had the most significant effect, followed by b . However, overall in *others*' the equilibria were primarily influenced by the seedling input rate L_p and the shading parameter s . On the other hand, it is worth noting that the rate with the smallest environmental variation effect across species was seedling recruitment r .

Analyzing the environmental patterns of the three most significant effects (rates b , c_J , c_B) reveals a response that is consistent with the fitted paraboloids (Section 4.3.2). The environmental variation of these rates has a positive effect on *Fagus*' basal area in a central region within its range of predominance, while the range of credibly positive effects is even narrower within (90% of the posterior differences > 0). Outside the range of predominance, towards the margins, the effect changes to negative, although this negative effect is only credible for a few subpopulations at the very edges (see Fig. 44). Notably, the fourth most significant effect, the sapling transition rate g in *Fagus* (Suppl. Fig. S9), exhibited

a deviating environmental pattern. The strongest positive effect was observed under moist and more acidic conditions whereas a negative influence of declining g was observed towards dry conditions. The environmental effect of the seedling input L_p , despite being the most important within *others*, showed no systematic environmental variation (Suppl. Fig. S11).

The combined environmental variation effects of the sapling rates g , c_J , and s , the rates of the intermediate stage h and c_A , as well as the rates of the final stage b and c_B , exhibit an amplified pattern. These combined effects have a greater magnitude and higher credibility compared to their individual effects, indicating a stronger influence on the system (Suppl. Fig. S10).

For the environmental patterns of environmental variation effects for all rates see (Suppl. Fig. S9).

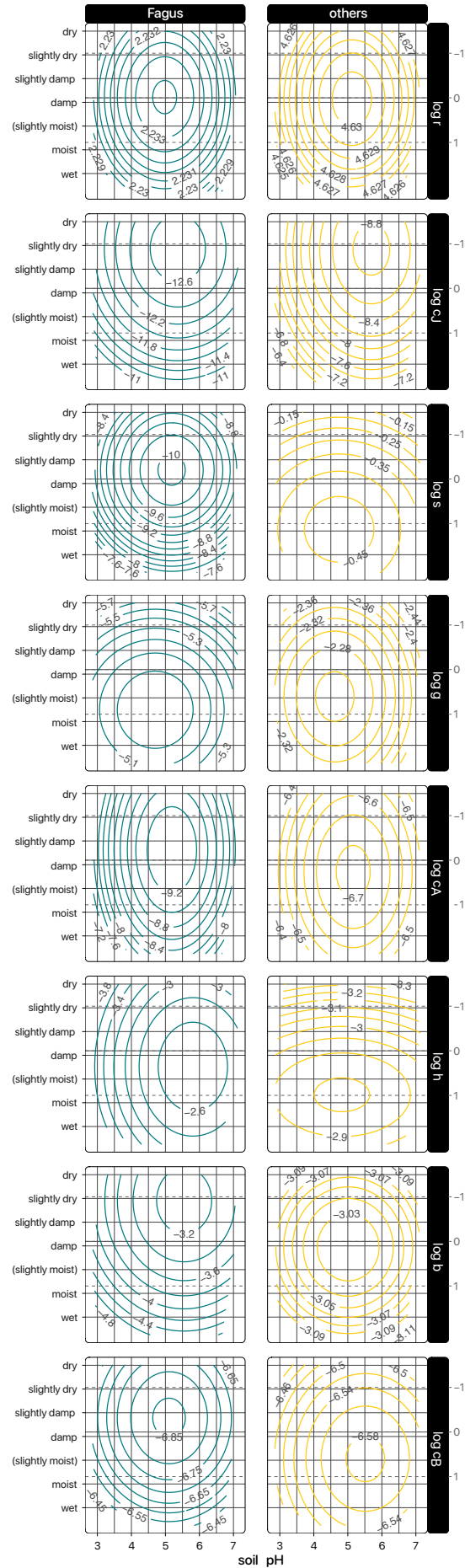


FIGURE 42: JAB model demographic rates in environmental space. The contours show the mean predicted values from the posterior distribution of polynomials (Section 4.2.5.2).

























mean absolute environmental variation effect			
	Fagus	others	incl. in Fig. 4
L_p	0.0088 	0.0258 	
r	0.0007 	0.0005 	☑
c_J	0.0670 	0.0048 	☑
s	0.0219 	0.0123 	☑
g	0.0459 	0.0068 	
$g \& c_J \& s$	0.0828 	0.0120 	
c_A	0.0220 	0.0066 	
h	0.0098 	0.0104 	
$h \& c_A$	0.0241 	0.0098 	
b	0.0745 	0.0117 	☑
c_B	0.0617 	0.0199 	☑
$b \& c_B$	0.1107 	0.0229 	

FIGURE 43: Magnitude of the environmental variation effect per demographic rate and the combined effects of rates in density-dependent terms. The magnitude is indicated by the mean of the absolute effects.

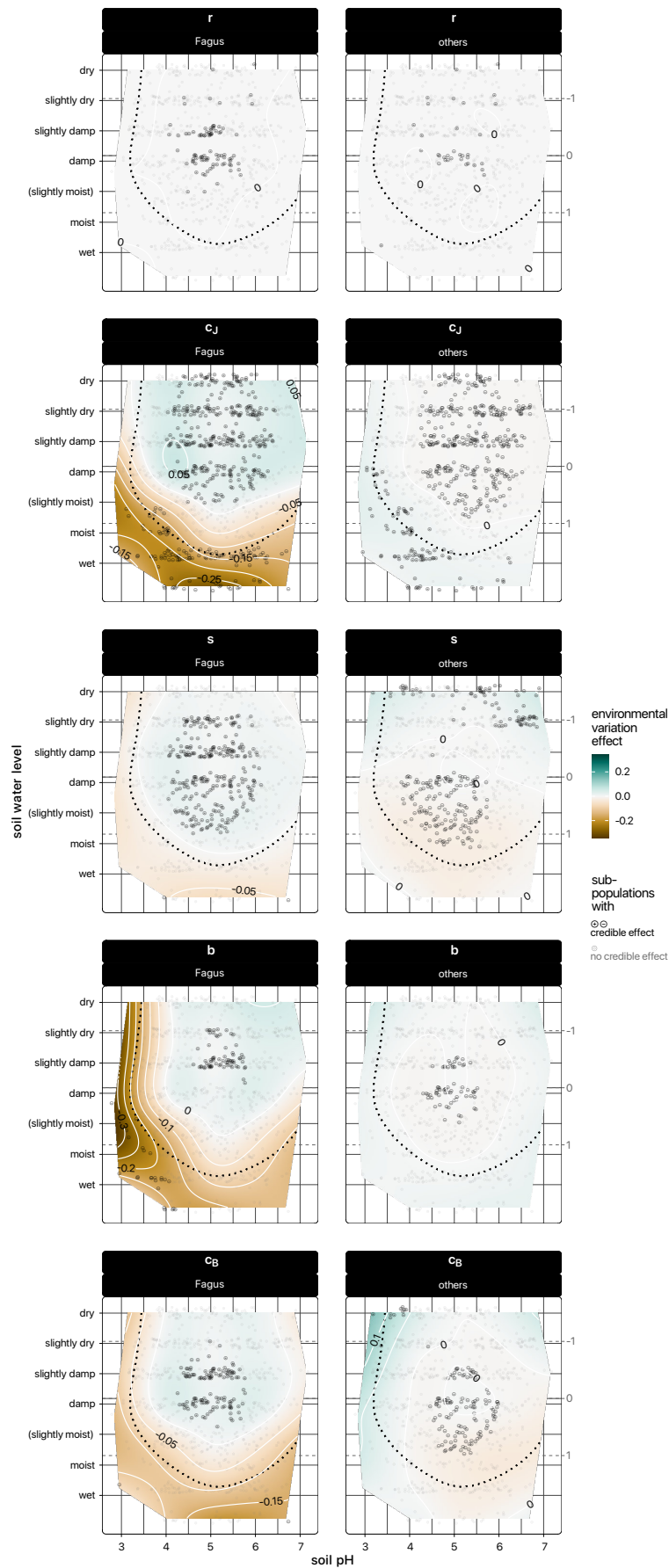


FIGURE 44: Environmental variation effect of the demographic rates r , c_J , s , b , and c_B . Dark point characters indicate credible effects at subpopulations (90% of the posterior either $>$ or $<$ 0). The dashed line indicates the range of *Fagus*' predominance.

4.4 Discussion

4.4.1 Species differences of demographic rates

Environmental distributions of demographic rates revealed differences between the two species (Section 4.3.1, Table 42) aligning with expectations based on respective positions along a spectrum between pioneer species (*others*) and a late-successional species (*Fagus*; WHITMORE, 1989; GRIME, 2001; see also HEILAND *et al.*, 2023). The environmental distributions are determined by the paraboloid parameters, primarily the extreme value ϵ , but also spread ζ , and center κ , as discussed in Section 4.4.3).

Consistent with the original theory by Ellenberg (ELLENBERG, 1963, Section 4.1), saplings of *Fagus* were less affected by competition from the overstory through shading and below-ground competition (s) than saplings of the *other* species (see also WATT, 1923; PETROVSKA *et al.*, 2021a; HEILAND *et al.*, 2023). The competition response of *others*' saplings to itself (c_J) was significantly smaller, indicating that density-dependent limitation in *others* is mainly caused by the overstory. Higher estimates of seedling recruitment r in *others* was expected due to the high fraction of pioneer species (Table S5). *Fagus* seedling regeneration however, was mainly driven by local basal area (r) due to rare long-distance dispersal (KUNSTLER *et al.*, 2007; MILLERÓN *et al.*, 2013; AXER *et al.*, 2021). That the overstory-related parameters (c_A , h , b , c_B) became increasingly similar among species with increasing tree size suggests that a major part of the demographic differentiation happens in the sapling stage J.

While the estimate for the sapling transition rate g in the absence of competition was smaller for *Fagus*, the corresponding density-dependent transition term at the equilibrium, $\frac{g}{1+c_J \text{sum}(J)+s \text{sum}(BA)}$, was notably higher compared to *others* (Table 42). This suggests that shading and other density effects play a significant role in influencing growth and survival at the sapling stage, particularly for *others*.

The distinct posterior estimates of demographic rates for the two species are remarkable, given that all prior uncertainties were equal among species (Table 42). Hence, any differences between species' parameter estimates are informed by the data.

It is important to exercise caution when interpreting the species differences in demographic rates because (1) the JAB model has simplifications regarding possible sources of mortality and moreover (2) there is potential equifinality in the model structure. Specifically, density-independent mortality is only included in the net increment b of stage B, while in stages J and A only experience density-dependent mortality (see HEILAND *et al.*, 2023). These simplifications might result in underestimating growth rates in stages J and A compared to a system with density-independent mortality. Furthermore, correlations in the posterior estimates of particular rates, e.g., the extrema of overstory rates ϵ_b and ϵ_{c_B} , reveals a trade-off in the model structure that can lead to equifinal results, i.e. that the same model states that fit the data can be produced by multiple parameter configurations (HARTIG *et al.*, 2014). Consequently, the rates b and c_B , should be interpreted together considering their interactions. To address this, we interpret the demographic rates that lead to the abundance within one stage in conjunction. e.g., g , s and c_J , as well as h and c_A . Specifically, we compare the estimates with the full density-dependent growth terms, e.g. $g \odot [1 + c_J \text{sum}(J_t) + s \text{sum}(BA_t)]$ (Table 42), and we jointly average parameters for computing their joint environmental variation effect (Section 4.4.3).

Carefully interpreting the potential equifinal processes within one stage together, we can

still conclude with certainty that *Fagus* benefits significantly from higher sapling survival (joint effect of g , c_J , s) enabling its predominance despite slower net basal area growth (interaction of b and c_b).

4.4.2 Theoretical predictions and simulated competitive equilibria in environmental space

4.4.2.1 *Fagus* predominates at the center of environmental space

Our findings provide strong evidence for Ellenberg’s original theory on predominance of *Fagus*. *Fagus* is the predominant tree species at a central to dry region of the environmental space, as inferred from environmentally-dependent demographic rates with short time series from the German NFI (Section 4.3.3; Fig. S3), only slightly deviating from the predictions of ELLENBERG (1963).

Our equilibrium simulation shows that *Fagus* predominates in a central region that extends towards both the neutral extreme along the pH axis and the dry extreme along the soil water level axis (Section 4.3.3). The wider distribution of rate extrema along soil water compared to pH for both species may contribute to the broader abundance along the soil water axis (Fig. S8), suggesting a complementary effect. While the original prediction by ELLENBERG (1963) also has *Fagus*’ extending to alkaline conditions, the original predictions suggests a switch in dominance at the dry margins, whereas our results only show minimal decline of *Fagus*’ abundance. This discrepancy may be attributed to three limitations of the data at the dry edge: First, in contrast to Ellenberg’s formulation the scale available to this study only has the level “dry” and does not differentiate “very dry” (BENNING *et al.*, 2019; Suppl. Table S3; ELLENBERG, 1963). That the soil water level data is too undifferentiated at the dry edge is also indicated by the much higher number of sampled forest plots at the dry compared to the wet edge (Suppl. Table S4). Second, the sampled data range covers a relatively moist portion of *Fagus*’ range, as evident from the distribution of climatic water balance of the German National Forest Inventory plots compared to the broader range in the European Atlas of Forest Tree Species (means and standard deviations: 215.8 ± 193.5 vs. 158.3 ± 343.9 mm a⁻¹; Suppl. Fig. S3; DE RIGO *et al.*, 2016). Third, there may be a selection bias in the cultural landscape where extremely dry areas that could be forested (typically with predominance by *Quercus* spp.), have consistently been turned into grasslands throughout Germany (POSCHLOD, 2015). Consequently, such areas may be excluded from the forest sample, although they are included in Ellenberg’s theory about natural forests.

The simulated total equilibrium basal area of around 57 m² ha⁻¹ (Table S7) is higher than expected from observations. STILLHARD *et al.*, 2022 report total basal areas of ~36 m² ha⁻¹ from pristine beech-dominated forests in Uholka-Shyrokyi Luh, Ukraine, while MORENO *et al.* (2018) project an upper limit of European forests around 50 m² ha⁻¹ (see also HEILAND *et al.*, 2023 where a JAB model based on a different selection of plots projected maximum carrying capacities below 50 m² ha⁻¹). The high basal area projections may be partly caused by the assumption of paraboloid environmental variation of the demographic rates, as indicated by the large variation in equilibrium basal areas (sd 28 m² ha⁻¹). Nevertheless, considering that our model does not account for disturbance events like fires, storms, and pathogen damage, the extrapolated equilibria fall within a realistic range and can serve as external validation of the model (e.g., CAILLERET *et al.*, 2020).

4.4.2.2 In *Fagus*' absence, *others* would also predominate at the center of environmental space

In a counterfactual simulation where *Fagus* regeneration was absent, *others* showed similar maximum abundance at the central region otherwise occupied by *Fagus* (Fig. S8 F). This demonstrates that *others* also have their physiological optimum at the center of the environmental space but are outcompeted by *Fagus*. This mechanism, whereby most species have their physiological optimum under intermediate conditions, and species turnover along environmental gradients being primarily driven by species interactions (ecological optimum), is a central principle of Ellenberg's original theory (ELLENBERG, 1952, 1963; see also HUTCHINSON, 1957; KEDDY, 2001). The theory also aligns with the stress-gradient hypothesis (BERTNESS and CALLAWAY, 1994), which proposes that as stress decreases in favourable conditions competition intensifies, as supported by empirical findings on *Fagus* by MEIER *et al.* (2011). Consequently, it can be concluded that *Fagus* predominates because its demographics are disproportionately more beneficial at the center so that it outcompetes *others*.

4.4.3 How do environmentally-varying rates control predominance?

Fagus' predominance in mesic environmental conditions is primarily driven by the environmental variation of *Fagus*' demographic rates rather than the variation of the aggregated *other* species. *Fagus* exhibits greater environmental variation of demographic rates compared to the *others* (Section 4.3.2), leading to much effects on the variation of basal area fraction (Fig. 43, Section 4.3.4).

Although the environmental variation of the log demographic rates (Table 42) already hints at the impact on the environmental response of relative abundance, the actual effect that the demographic rates have in environmental space is also dependent on the other processes in the JAB model. We therefore quantified environmental effects by comparing equilibria with the given environmentally-varying demographic rates to equilibria with flat mean rates along environmental gradient (Section 4.2.6.2, Fig. 44).

Rates that encompass limitation, rather than growth rates, had the largest *environmental variation effect* within each stage (Figure 43). Specifically, within the sapling stage (J), the competition responses (s and c_J) had a greater effect than the growth rates (r , L_p , g). In intermediate trees (A), the competition response c_A had a stronger effect than transition rate h . Among large overstory trees, the net increment b , which includes both basal area growth and density-independent mortality, had the most prominent influence along with competition response c_B . This finding aligns with previous evidence that individual growth or population growth rates alone are insufficient predictors for tree species abundance (THUILLER *et al.*, 2014; BOHNER and DIEZ, 2019; KUNSTLER *et al.*, 2021).

The variation of demographic rates in large trees (b and c_b in stage B) had the most significant impact on the predominance in environmental space. This finding may initially seem surprising, as a previous study has shown that the lower response to shading (s) is the primary factor driving the predominance of *Fagus* at the competitive equilibrium (HEILAND *et al.*, 2023; see also PETRITAN *et al.*, 2007; LEUSCHNER and ELLENBERG, 2017b; PETROVSKA *et al.*, 2021b). However, this apparent contradiction can be resolved. While variation in shade-tolerance is not the main driver of the species' abundance response in environmental space, the mechanism of shade tolerance remains crucial for *Fagus* to prevail overall. This is supported by simulated equilibria where the shading response (s) was switched between

species (Suppl. Fig. S8 G). Furthermore the recruitment rate of seedlings (r) does not have a significant environmental variation effect, which indicates that the environmental variation of seedling recruitment is better explained by variation of a species' basal area than by the variation of seedlings survival. The smaller environmental variation effect observed in seedling and sapling rates aligns with the theory that the occurrence of a particular life stage is constrained by the presence of earlier life stages due to "demographic" or "ontogenetic dependency" (HEILAND *et al.*, 2022; YOUNG *et al.*, 2005; RAMACHANDRAN *et al.*, 2023). Therefore, earlier tree life stages often have broader environmental distributions, as shown by BERTRAND *et al.* (2011); ZHU *et al.* (2014); MÁLIŠ *et al.* (2016); COPENHAVER-PARRY *et al.* (2020b).

4.4.4 Conclusions

Our study confirmed the prediction first formulated by ELLENBERG (1963), that *Fagus sylvatica*'s predominates at the competitive equilibrium in a mesic environmental range. Using model simulations based on demographic rates inferred from short time series, we showed that *Fagus* outcompetes *other* species within this environmental range, due to its disproportionately advantageous demographics. However, our predicted range slightly deviated from Ellenberg's original predictions, which could be attributed to limitations of the utilized soil water scale.

We further explained the environmental pattern of *Fagus*' predominance with the environmental variation of demographic rates by simulating environmental variation effects. On the one hand, we discovered that the variation in *Fagus* abundance is primarily driven by its own demographic rates, rather than those of *other* species. On the other hand, we identified that the most impactful environmental variation occurs at the overstory stage, despite the shade-tolerance of *Fagus* at the sapling stage being crucial for overall predominance. Finally, our results indicate that demographic rates related to a high chance of survival, rather than rapid growth, are more important for the environmental pattern of *Fagus*' abundance.

Our study presents a significant finding: Inverse calibration of a simple forest population model enables replication of plausible abundance patterns along environmental gradients and, for the first time, provides an explanation for the ecological consensus on the predominance of common beech in Central European forests using demographic rates. This suggests that indirect calibration has the potential to serve as a viable alternative to direct estimation of demographic rates along environmental gradients. For better interpretability of demographic rates, the JAB can be enhanced by incorporating more realistic environmental rates and employing informative priors. By employing our approach, ecological modelling can help gain deeper insights into the complex dynamics between species, dependent on their environment.

This dissertation has emphasized the importance of considering the environmental response of seedlings and saplings in order to fully comprehend and predict tree species occurrence and forest composition.

First, by investigating the abundance response of early life stages, we have demonstrated that juveniles frequently diverge from their conspecific adults due to ontogenetic effects (Chapter 2). The ontogenetic effects that can contribute to the observed divergences include changes of the viable environmental conditions during development (*ontogenetic niche shift, contraction, or expansion*) as well as demographic dependencies that constrain the possible occurrence of subsequent life stages (see also RAMACHANDRAN *et al.*, 2023). These insights have led us to develop a dynamic forest population model (JAB model) that specifically includes a sapling stage and its interactions with the overstory, enabling us to better understand the environmental responses of different life stages and deconstruct their ontogenetic niches (Chapter 3). We fitted this model to short forest time series, to infer environmental responses of demographic rates of different stages, to deconstruct the niches of the life stages. As a result we gained specific insights into the demographic drivers of predominance in central European forests, specifically for common beech (*Fagus sylvatica*). In particular, shade tolerance at the sapling stage was identified as a crucial factor for the overall predominance of this species, highlighting the significance of earlier life stages for forest composition (Chapter 3). But for the environmental response of *Fagus*' relative abundance, the variation of other processes were shown to be more impactful (Chapter 4). The environmental variation of *Fagus*' abundance was primarily driven by the demographic rates of adult overstory trees rather than early life stages. However, environmental variation of survival at the sapling stage had the second greatest impact. Moreover, our results suggest that survival-related demographic rates, rather than rapid growth, are important for *Fagus*' environmental abundance. Notably, the environmental variation of *Fagus* seedlings had no significant impact. The seedling recruitment rate was relatively constant across environments and did not affect the environmental abundance patterns.

With these findings, we present a novel perspective on the widespread distribution of juvenile trees, their ontogenetic niche, and their importance for forest dynamics and species composition. GRUBB (1977) established the pivotal role of the “regeneration niche” in a sem-

inal paper on species diversity. Plant regenerative processes, ranging from pollination to the seedling establishment, are highly sensitive to environmental conditions. Consequently, the special environmental conditions that enable these key processes are a crucial bottleneck of a species' niche. However, this does not imply that seedlings can only survive under narrower conditions compared to their conspecific adults along large-scale environmental gradients. In fact, Chapter 2 and several prior studies have demonstrated the more widespread environmental distributions of early tree life stages in comparison to adults (BERTRAND *et al.*, 2011; ZHU *et al.*, 2014; MÁLIŠ *et al.*, 2016; COPENHAVER-PARRY *et al.*, 2020b). This has recently sparked a discussion regarding whether juvenile trees have broader or narrower ontogenetic niches than adults (BERTRAND *et al.*, 2011; COPENHAVER-PARRY *et al.*, 2020a; NI and VELLEND, 2021). In the past, the wider occurrence of juveniles has been attributed to ontogenetic niche contraction (BERTRAND *et al.*, 2011; COPENHAVER-PARRY *et al.*, 2020a; NI and VELLEND, 2021), which can emerge through more severe mortality of adults under the same conditions because they demand more resources BERTRAND *et al.* (2011); BENNETT (2015).

However, we have shown that more widespread juvenile occurrence can also be attributed to demographic dependency between life stages, without necessitating distinct niches (Chapter 2; see also RAMACHANDRAN *et al.*, 2023). Even when juveniles and adults share identical ontogenetic niches, adults may be found in narrower environmental conditions simply because their abundance is influenced not only by their own ontogenetic niche but also by the abundance of earlier life stages (YOUNG *et al.*, 2005).

Since the occurrence of a specific life stage is also constrained by its demographic dependency on other life stages, the question about juvenile niche width cannot be solely addressed by comparing the occurrences of life stages. Instead, we employed the JAB model to compare their distinct vital performance across environmental gradients (Chapter 4). By incorporating the sapling stage into our model, we were able to make a significant contribution to the ongoing discourse, by demonstrating that the sapling niche is not the primary bottleneck in *F. sylvatica*. In fact, we revealed that the environmental variation of adult survival imposes a more important constraint on the relative abundance of this species.

In summary, this dissertation presents an innovative approach by employing a demographic species distribution model that includes a sapling stage to explain the mechanisms of forest composition along environmental gradients. By considering the environmental responses of juvenile trees, we were able to draw conclusions regarding the differentiation between juvenile and adult niches. Specifically, this enabled us to differentiate between the distinct role of saplings for forest composition overall on the one hand, and their environmental variation for abundance patterns on the other hand. This underscores the importance of integrating early tree life stages into forest models to achieve a mechanistic understanding of forest composition.

Finally, our findings on juvenile tree ecology provide hope about resilience of forest ecosystem in the face of a rapidly changing environment. The widespread occurrence of seedlings and saplings today suggests that juvenile trees may already be present in conditions that will be suitable for adults in the future.

Appendices

- **Supplementary Tables S1** published at <https://onlinelibrary.wiley.com/action/downloadSupplement?doi=10.1111%2Fecog.06042&file=ecog12848-sup-0001-AppendixS1.pdf>
 - **Table S1.1:** Simulation parameters
 - **Table S1.2:** NFI analysis data scope table
 - **Table S1.3:** NFI size classes classes for juvenile tree counts
 - **Table S1.4:** NFI analysis regression table for heat sum
 - **Table S1.5:** NFI analysis regression table for water availability
- **Supplementary Material S2:** R code for the simulations and NFI data analyses, including the data required for reproduction <https://github.com/lukasheiland/Divergence/>
- **Supplementary Material S3:** NFI analysis quantile residuals <https://github.com/lukasheiland/Divergence/tree/master/Residuals>

A Methods

A.1 NFI data

A.1.1 German NFI data

Germany is situated in the European temperate vegetation zone, with the main potential natural vegetation being beech (*F. sylvatica*) and mixed beech forests (BOHN and GOLLUB, 2006). The NFI plots used for calibration, which have been selected to include at least some observation of *Fagus*, have *Fagus* as the most abundant species with an average of about 24% of the basal area (Table S3).

The forest plots of the German NFI are arranged in clusters of four plots on a regular quadratic grid. The standard grid has clusters arranged at longitudinal and latitudinal distance of 4 km. In some federal states the grid may be intensified to either the grid centers (distance 2.83 km) or the sides (distance 2 km) of the grid quadrants (ТОМППО *et al.*, 2010). Each grid point is the position of the south-western plot within a quadratic cluster of four potential forest plots, which are arranged at distance 150 m. To fit the JAB model, we used one randomly selected forested plot of a cluster corresponds to a subpopulation. One plot per cluster was selected, instead of averaging or summing up per cluster, because the within-cluster variance of abundances was very high, yet selecting one plot per cluster still avoids potential dependencies among the plots of one cluster.

In the German NFI data, trees above 10cm dbh were sampled with the angle count method (RIEDEL *et al.*, 2017), which selects all trees that appear wider than a defined angle around a central observer at height 1.3 m (KANGAS and MALTAMO, 2006). The selected trees are then recorded together with their distance and diameter at breast height (dbh, 1.3 m). Instead of a fixed area for all tree sizes, the selection with an angle leads to a sampling area that varies with dbh. The angle count method—besides providing counts that are directly proportional to the basal area—delivers data where each counted tree has (1) a corresponding distance to the center, (2) a dbh that is equivalent to a potential sampling distance, i.e. area and sampling probability, (3) as well as a calibration factor k [$\text{m}^2 \text{ha}^{-1}$] for the sampling angle. In this study, the angle count plots were truncated to have a fixed maximum area of

14 m (for details see A.2.3). Saplings between height 20 cm and dbh 7 cm were counted on circular fixed area plots with radii dependent on size class and survey and were subsumed as size class J in the analyses (Table S2).

For analyzing potential predominance of *Fagus*, we selected plots with repeated observations that were unmanaged during the observation period: First, to rule out clear cuts, we excluded all plots that had tree observations in the first or second of the three surveys, but had only zero-observations across all tree sizes in a subsequent survey. Further, plots where management was recorded in the second or third survey were excluded. Records of management in the German NFI include unnatural forest regeneration (sowing, planting), harvested sample trees, and damage through forestry in sample trees. We also excluded plots with records of individual sample trees that went missing for “unknown reasons” in the third survey (category not available in the first and second survey). Subsequently, to make sure that the data is robust for inferring trajectories of populations over time, plots were selected that were surveyed thrice. Selecting only plots with observations in all three surveys—1987, 2002, and 2012—confines the spatial extent of the German NFI to former West Germany. Further, to make sure that only locations are selected that are likely within the fundamental niche of *Fagus sylvatica*, we limited the data to plots that had any record of *Fagus* (and *others*) in any size stage at any time and to plots at submontane elevations 100–600m (ELLENBERG, 1963). From the remaining clusters we sampled one random plot per cluster. Finally, to limit the computational expense, 1000 plots each representing one cluster were randomly sampled (compared to originally 61666 plots in 21574 clusters; Table S1).

A.1.2 Slovakian NFI data

The forested areas in Slovakia are mostly part of the European temperate vegetation zone and have similar potential natural beech and mixed beech forests (BOHN and GOLLUB, 2006) and current species composition (Tables S3–S4) as in Germany. The selected forest plots in Slovakia have *F. sylvatica* as the predominant species with about 28% of the basal area.

In the Slovakian NFI, full tree counts and circumference measurements were conducted on 500 m² fixed-area plots that are arranged on a regular quadratic grid (ŠEBEŇ, 2017). The lower size threshold for sampling trees is dbh 7 cm. Smaller seedlings and saplings with height 10 cm and greater were sampled on varying circles with increasing areas, i.e. 3.14, 7.07, 12.57, 28.27, and 50.26 m². The sampling area for seedlings and saplings was adapted depending on field estimates of the tree density so that at least 15 trees were counted.

To infer seedling recruitment rates from the Slovakian NFI, we selected only plots without records of unnatural regeneration. This reduced the number of plots from 1412 to 1402 (Table S1).

A.2 Accounting for varying sampling areas with offsets

A.2.1 Offsets for the angle count method

Count data from the angle count method (size stage A in the German NFI) were related to the count states in the JAB model by scaling with area offsets. In angle count sampling, each tree has a specific sampling area a dependent on its dbh with $a = \pi k^2 dbh^2$, where k is a constant for the sampling angle (here, $k = 25$). Thus, for the sampling area of a plot, which corresponds to the actually observed trees on a plot we use the weighted mean

$a_p = \sum_{i=1}^n w_i a_i / \sum_{i=1}^n w_i$, where the weights w_i are the respective area-standardized counts per hectare. This weighted mean has the property that—together with the actually observed counts on a plot c_p —it conveys equivalent information as the sum of all area-standardized counts per hectare on a plot $c_A = \frac{c_p}{a_p}$ [ha^{-1}]. The area a_p was used as the offset for size stage A (o in Equation 3.5).

To relate count data from the angle count method to the basal area state in the model (size stage B in the German NFI), we used an offset factor that not only includes the sampling area a_p but transforms the basal area per hectare in the JAB model to counts. This was achieved with an offset o that also included the total observed basal area ba_p on a plot: $o = a_p \frac{c_p}{ba_p}$ [ha m^{-2}]. By multiplying the model state \hat{x} [$\text{m}^2 \text{ha}^{-1}$] with this offset we transformed the model state to counts, by including the data on basal area (“how many counts are one unit of basal area?”) on the right hand side of the model statement: $x \sim a_p \frac{c_p}{ba_p} \hat{x}$.

A.2.2 Offsets for counts on fixed-area plots

Counts on fixed-area plots (seedlings in the Slovakian NFI and saplings J in the German NFI) were also standardized using area offsets. In the statistical model inferring priors for the seedling recruitment rates r from the Slovakian NFI data (see A.4), we used areas of the corresponding subplots as offsets. In the German NFI data, the size class J of the JAB model consists of multiple size classes with different sampling areas, which also change between surveys (Table S2). As in the angle count data, we calculated a weighted mean area per plot, where the different sampling areas were weighted by the counts per area within the corresponding size classes. The weighted mean area per NFI plot was used as an offset to relate the sapling counts to the area-standardized counts of J in the JAB model [ha^{-1}].

A.2.3 Offsets for zero observations

Because all NFI sampling protocols made observation areas dependent on size or abundance (see A.1.2 and A.1.1), the observation area was not readily available when there were no observations for a stage on a plot. For zero observations in the angle count data in the German NFI (size classes A and B), we used the sampling area of the other species, or, if both species had zero observations, the mean sampling area per size class and survey as an offset (for a test of the robustness of this approach, see below). To be able to compute a mean area for the largest size class B, we truncated the angle count data to a maximum sampling radius of 14 m. The truncation included dropping all trees outside the sampling radius, which is about the 98th percentile of tree counts in A and B and assigning the new maximum sampling area to all trees that were within the maximum radius but had a dbh that was originally corresponding to a sampling area greater than the new maximum area (dbh > 60 cm). Truncating the angle count data to a fixed maximum area removes a source of bias (missed tree observations at higher radii) at the cost of moderate added variance (BERGER *et al.*, 2020), and furthermore leads to a finite sampling area that can be averaged over. The mean sampling area per size class (A and B) was calculated by dividing the definite integral from 0 up to the respective maximum radius—by the maximum radius. This mean area was used as an offset for zero observations in size class A. To obtain an offset for zero observations in size class B, we also needed an additional factor that scaled the basal area to the scale of observed counts. Instead of multiplying the area with the plot-specific factor

$\frac{c_p}{ba_p}$ (as for non-zero observations, see A.2.1), we included the mean of the factor per survey and additionally per species to differentiate between their average basal areas.

We made sure that the choice of the particular area offset for zero observations did not affect the relations of the parameter estimates, nor the conclusions regarding the extrapolated equilibria, nor the importance of the “shading” parameter s , by running the entire analysis pipeline with three alternative choices for the sampling area of zero observations: the count per hectare-weighted mean of all observation areas per survey and species, as well as the analogous first quantile and the third quantile (weighted quantiles from package DescTools version 0.99.45; SIGNORELL, 2021).

Zero observations in the sapling counts of the size class J in the German NFI were assigned an equally weighted mean of all possible sampling areas for the respective set of smaller size classes within the corresponding survey (Table S2).

For zero observations in seedling counts in the Slovakian NFI there were two possible cases: If only one of *Fagus* and *others* had no seedling observation on a plot in a year, the zero observation was assigned the sampling area from the respective other species. If there was no seedling observation at all, we used the maximum possible area (50.26 m²), because the sampling protocol prescribed increasing the subplot area until sufficient seedling density was reached (see A.1.2).

A.3 Species’ regional abundance for predicting seedling input

To derive the regional species abundance \mathfrak{B}_p used to estimate the external seedling input (parameter l , see Section 3.2.1) we used thin plate spline regressions with the geographic coordinates as predictors to interpolate the species-specific basal area per hectare on the German NFI grid (Table S6, Figure S1).

For fitting the thin plate splines from the regular standard grid of the German NFI (4 km; see A.1.1), which is homogeneous across Federal states, we selected only the basal area records from the last survey (2012), because the grid had changed over surveys. We completed non-forested clusters of the regular grid, and also all of the four plots within clusters, with zero observations to obtain an unbiased sample of the geographical density of tree species. To obtain a response variable for each set of coordinates, we calculated the species abundances per cluster by averaging the basal area per hectare above the sampling threshold (BA) over the four plots. This average basal area per hectare on the completed grid was spatially smoothed with a two-dimensional geographic thin plate spline. Based on the coordinates, a “spline on sphere” was fitted with the `gam()` function from the package `mgcv` ($k = 200$; version 1.8-39; WOOD, 2021), where the average basal area per hectare was the response. The response variable had been rounded to an integer to be able to fit a negative binomial response. The predicted plot-specific regional species abundances \mathfrak{B}_p were used as a proxy for the probability of seedling input, which factors into the JAB model with a species-specific effect size l , $L_p = \mathfrak{B}_p l$. By using a strictly positive negative binomial response for \mathfrak{B}_p , it was made sure that plots were not excluded from invasion in the JAB model.

A.4 Prior inference on seedling recruitment

To infer priors for the rate r , i.e. seedling recruitment by the local basal area, we fitted a regression model with the data from the Slovakian NFI (Table S5). The Slovakian NFI

includes counts of small seedlings with height 10–20 cm, which is right below the size class J in the German NFI (height 20 cm to dbh 7 cm, Section 3.2.2.1). The density of the small seedlings on a plot was used as a proxy for the number of seedlings having appeared in a year on a plot. Although the size class height 10–20 cm neither completely covers yearlings nor excludes older or younger trees, data on seedling growth suggests that this size class can be a rough approximation for yearling count density: The common conifer *Pinus sylvestris* L., e.g., reaches average height 20.0 cm after two years (GEUDENS *et al.*, 2004), *Fagus sylvatica* and *Quercus robur* L. both have an average height between 10 and 15 cm after one year (WELANDER and OTTOSSON, 1998). As a predictor of yearling count density we used the conspecific basal area per hectare above the sampling threshold (dbh \geq 10 cm).

We fitted a joined hurdle regression model for *Fagus* and *others*, where the species-specific yearly seedling recruitment rate r is a function of the local and conspecific basal area BA . All other yearly seedling input, i.e. appearing seedlings due to long-distance or temporal dispersal, is included as an intercept k . The hurdle model is implemented as a two-component mixture where the probability density D is the sum of a Bernoulli distribution and a zero-truncated Negative Binomial distribution (ZTNB), parameterized with mean and precision ϕ , such that:

$$\hat{S}_{ps} = k_s + r_s BA_{ps} \quad (S1)$$

$$\hat{\Sigma}_p = \sum_{s=1}^2 \hat{S}_{ps} \quad (S2)$$

$$d_p = \text{Bernoulli}[1 \mid \text{logit}^{-1}(\theta_a + m\hat{\Sigma}_p)] \quad (S3)$$

$$D_{ps} = \begin{cases} d_p & \text{if } S_{ps} = 0 \\ (1 - d_p) \text{ ZTNB}(S_{ps} \mid \hat{S}_{ps}A_a, \phi_a) & \text{if } S_{ps} > 0 \end{cases} \quad (S4)$$

where S_{ps} are the observed and \hat{S}_{ps} the predicted seedling density, which are a function of intercept k and conspecific basal area BA_{ps} with slope r , and where variables vary with plot p and species s and plots can have one of the sampling area levels a . The Bernoulli density d_p describes the probability of observing no seedlings, which has an inverse logit-transformed linear predictor dependent on the latent total seedling density on a plot across species $\hat{\Sigma}_p$ with slope m , but also on the factor sampling area (parameter θ_a). The hurdle model with a separate process for zero observations was chosen to account for the deflated zeroes with small sampling areas and inflated zeroes with great sampling areas. A deflation of zeroes at smaller sampling areas that could not be explained by a Negative Binomial distribution was likely a product of the sampling protocol, where the sampling area was increased in steps when the total seedling density was too small, depending on field estimates (see A.1.2). Because the total seedling density $\hat{\Sigma}_p$ is included in the linear predictor for the probability of observing a zero d_p , other than in a classical hurdle model, the zeroes in the data also inform the predicted seedling density \hat{S}_{ps} . The zero-truncated Negative Binomial distribution, which describes the non-zero counts, is parameterized with mean \hat{S}_p multiplied by an offset for the sampling area \hat{A}_a and precision ϕ_a , which also varies with the levels of sampling area.

The model was fitted with weakly informative, normally-distributed priors for log-transformations of the parameters of interest $\log r \sim \mathcal{N}(5, 10)$, $\log k \sim \mathcal{N}(5, 10)$ —and regularizing priors

$\theta \sim \mathcal{N}(0, 2)$, $m \sim \mathcal{N}(0, 2)$, and the half-normal $\frac{1}{\sqrt{\phi}} \sim \mathcal{H}(1)$. The resulting posterior distribution of the basal area-dependent seedling recruitment rate $\log r$ was propagated as a prior for the corresponding parameter in the JAB model (Section 3.2.3.1; Tables S5 and 32).

B Code repository

All software to reproduce the study, including the JAB model, has been made openly available at <https://doi.org/10.5281/zenodo.8032461>.

C Data repository

The data supporting the findings of this study have been made available by the authors at <https://doi.org/10.5061/dryad.3ffbg79pv>.

D Supplementary tables

Table S1: Scope of the two NFIs and plot selection.

	German NFI	Slovakian NFI
No. of surveys	3	1
... years	1986–1989, 2000–2003, 2011–2013	2015–2016
No. of plots	61666	1412
... after selection	1000	1402
No. of clusters	21574	.
... after selection	1000	.

Table S2: Size classes for saplings counts and corresponding radii of sampling circles in the three surveys of the German NFI (main years 1987, 2002, 2012). The size classes up to dbh 7 cm, which were consistently sampled across all three surveys, were assigned to the size class J in fitting the JAB model.

	1987	2002	2012
height 20–50 cm	1 m	1 m	1 m
height 50–130 cm	2 m	1.75 m	2 m
height 130–∞ cm and dbh 0–5 cm	2 m	1.75 m	2 m
dbh 5–6 cm	4 m	1.75 m	2 m
dbh 6–7 cm	4 m	1.75 m	2 m
dbh 7–8 cm	4 m	.	.
dbh 8–9 cm	4 m	.	.
dbh 9–10 cm	4 m	.	.

Table S3: Taxa composition of the German NFI on the selected plots. All observed taxa are listed, ranked by the mean basal area per plot. In addition, the mean percentage of the total plot basal area is given.

	Taxon	Mean basal area [m ² ha ⁻¹]	Mean percentage of the basal area
1	<i>Fagus sylvatica</i>	6.174	24.492%
2	<i>Picea abies</i>	5.084	19.730%
3	<i>Pinus sylvestris</i>	4.139	13.145%
4	<i>Quercus petraea</i>	2.692	10.027%
5	<i>Quercus robur</i>	1.293	4.436%
6	<i>Pseudotsuga menziesii</i>	0.779	3.366%
7	<i>Larix decidua</i>	0.767	3.073%
8	<i>Carpinus betulus</i>	0.797	2.825%
9	<i>Acer pseudoplatanus</i>	0.572	2.515%
10	<i>Betula pendula</i>	0.521	2.515%
11	<i>Fraxinus excelsior</i>	0.597	2.309%
12	<i>Abies alba</i>	0.533	2.176%
13	<i>Quercus</i>	0.623	2.158%
14	<i>Prunus avium</i>	0.224	0.949%
15	<i>Tilia</i>	0.208	0.794%
16	<i>Larix</i>	0.246	0.786%
17	<i>Quercus rubra</i>	0.146	0.639%
18	<i>Populus tremula</i>	0.133	0.427%
19	<i>Alnus glutinosa</i>	0.165	0.386%
20	<i>Castanea sativa</i>	0.123	0.364%
21	<i>Acer platanoides</i>	0.061	0.319%
22	<i>Alnus</i>	0.115	0.309%
23	<i>Acer campestre</i>	0.074	0.304%
24	<i>Salix</i>	0.049	0.278%
25	<i>Robinia pseudoacacia</i>	0.107	0.203%
26	<i>Populus</i>	0.074	0.189%
27	<i>Larix kaempferi</i>	0.076	0.188%
28	<i>Pinus nigra</i>	0.068	0.179%
29	<i>Sorbus aucuparia</i>	0.035	0.133%
30	other coniferous (German NFI)	0.035	0.127%
31	<i>Sorbus</i>	0.04	0.110%
32	other <i>Abies</i> (German NFI)	0.024	0.104%
33	<i>Aesculus hippocastanum</i>	0.025	0.067%
34	<i>Ulmus</i>	0.021	0.059%
35	other deciduous (German NFI)	0.015	0.048%
36	<i>Pinus strobus</i>	0.012	0.047%
37	other <i>Acer</i> (German NFI)	0.01	0.041%
38	<i>Ilex aquifolium</i>	0.01	0.031%
39	<i>Populus nigra</i>	0.014	0.028%
40	<i>Abies grandis</i>	0.005	0.027%
41	<i>Prunus padus</i>	0.007	0.026%
42	<i>Sorbus aria</i>	0.005	0.018%
43	other <i>Pinus</i> (German NFI)	0.005	0.017%
44	<i>Thuja</i>	0.004	0.014%
45	<i>Sorbus torminalis</i>	0.003	0.008%
46	other <i>Picea</i> (German NFI)	0.001	0.007%
47	<i>Juglans</i>	0.002	0.004%

Table S4: Taxa composition of the Slovakian NFI on the selected plots. All observed taxa are listed, ranked by the mean basal area per plot. In addition, the mean percentage of the total plot basal area is given.

	Taxon	Mean basal area [m ² ha ⁻¹]	Mean percentage of the basal area
1	<i>Fagus sylvatica</i>	9.102	27.859%
2	<i>Picea abies</i>	7.578	21.290%
3	<i>Quercus petraea</i>	2.54	8.267%
4	<i>Pinus sylvestris</i>	1.92	6.325%
5	<i>Carpinus betulus</i>	1.437	6.316%
6	<i>Abies alba</i>	1.225	3.551%
7	<i>Quercus cerris</i>	0.816	2.768%
8	<i>Betula pendula</i>	0.507	2.600%
9	<i>Acer pseudoplatanus</i>	0.776	2.405%
10	<i>Robinia pseudoacacia</i>	0.519	2.231%
11	<i>Larix decidua</i>	0.638	1.937%
12	<i>Alnus glutinosa</i>	0.508	1.628%
13	<i>Fraxinus excelsior</i>	0.473	1.622%
14	<i>Salix caprea</i>	0.263	1.326%
15	<i>Acer campestre</i>	0.259	1.143%
16	<i>Cerasus avium</i>	0.177	0.882%
17	<i>Populus tremula</i>	0.201	0.864%
18	<i>Salix alba</i>	0.191	0.815%
19	<i>Tilia cordata</i>	0.186	0.675%
20	<i>Alnus incana</i>	0.147	0.591%
21	<i>Quercus robur</i>	0.157	0.556%
22	<i>Pinus nigra</i>	0.153	0.356%
23	<i>Pyrus pyraeaster</i>	0.048	0.340%
24	<i>Acer platanoides</i>	0.094	0.311%
25	<i>Malus sylvestris</i>	0.043	0.286%
26	<i>Populus x canadensis</i> cv. I 214	0.14	0.265%
27	<i>Prunus domestica</i>	0.024	0.252%
28	<i>Populus nigra</i>	0.189	0.207%
29	<i>Sorbus aucuparia</i>	0.036	0.195%
31	<i>Morus alba</i>	0.021	0.174%
32	<i>Pinus cembra</i>	0.024	0.168%
33	<i>Quercus rubra</i>	0.045	0.165%
34	<i>Sorbus aria</i>	0.046	0.150%
35	<i>Populus x canadensis</i> cv. Robusta	0.011	0.143%
37	<i>Ulmus minor</i>	0.02	0.135%
38	<i>Ulmus glabra</i>	0.034	0.132%
39	<i>Tilia platyphyllos</i>	0.042	0.129%
40	<i>Quercus pubescens</i>	0.028	0.116%
41	<i>Juglans regia</i>	0.007	0.082%
42	<i>Ulmus laevis</i>	0.006	0.071%
44	<i>Castanea sativa</i>	0.028	0.069%
45	<i>Sorbus torminalis</i>	0.015	0.053%
46	<i>Pseudotsuga menziesii</i>	0.016	0.048%
47	<i>Acer negundo</i>	0.011	0.027%
48	<i>Fraxinus ornus</i>	0.005	0.025%
49	<i>Juglans nigra</i>	0.002	0.023%
50	<i>Salix fragilis</i>	0.008	0.014%
51	<i>Celtis occidentalis</i>	0.004	0.013%
52	<i>Fraxinus angustifolia</i>	0.002	0.007%
53	<i>Acer tataricum</i>	0.001	0.005%
54	<i>Betula pubescens</i>	0.001	0.004%
55	<i>Prunus mahaleb</i>	<0.001	0.001%
56	<i>Taxus baccata</i>	<0.001	0.001%

Table S5: Model parameters of prior inference on seedling regeneration r .

		mean	median	sd	q5	q95	convergence (r)	bulk ESS
Fagus	$\log r$	4.2234	4.2262	0.1287	4.0083	4.4302	1.0006	2 855.86
	$\log k$	6.0833	6.0852	0.1904	5.7679	6.3930	0.9999	3 748.85
others	$\log r$	3.0499	3.0621	0.1993	2.6978	3.3468	0.9995	2 951.27
	$\log k$	6.6571	6.6593	0.1276	6.4407	6.8607	1.0004	3 016.92
common	$\text{logit } m$	-4.7850	-4.7356	0.7356	-6.0725	-3.6619	1.0004	3 090.75
	$\text{logit } \theta_1$	-0.4898	-0.4946	0.1387	-0.7179	-0.2618	0.9999	5 257.69
	$\text{logit } \theta_2$	-0.6620	-0.6597	0.2300	-1.0475	-0.2929	1.0010	5 166.38
	$\text{logit } \theta_3$	-0.6581	-0.6590	0.0965	-0.8148	-0.5016	1.0002	4 917.66
	$\text{logit } \theta_4$	-0.6537	-0.6532	0.1421	-0.8951	-0.4200	1.0012	5 323.25
	$\text{logit } \theta_5$	0.6506	0.6511	0.0503	0.5679	0.7319	1.0012	5 427.17
	ϕ_1	0.0175	0.0174	0.0021	0.0142	0.0212	1.0007	4 312.37
	ϕ_2	0.0637	0.0625	0.0130	0.0448	0.0870	0.9999	5 940.02
	ϕ_3	0.0477	0.0473	0.0065	0.0379	0.0592	1.0007	4 244.71
	ϕ_4	0.1637	0.1603	0.0338	0.1129	0.2239	0.9994	4 966.71
	ϕ_5	0.5898	0.5879	0.0623	0.4923	0.6985	1.0006	4 354.77

Table S6: Estimates of the thin plate spline regression for interpolation of the background basal area \mathfrak{B} of *Fagus* and *others*.

<i>Fagus sylvatica</i>				
A) parametric coefficients (Intercept)	Estimate	Std. Error	t-value	p-value
	0.1436	0.0308	4.6584	< 0.0001
B) smooth terms s(Y,X)	edf	Ref.df	F-value	p-value
	120.0256	199.0000	1411.8250	< 0.0001
<i>others</i>				
A) parametric coefficients (Intercept)	Estimate	Std. Error	t-value	p-value
	2.3541	0.0200	117.4778	< 0.0001
B) smooth terms s(Y,X)	edf	Ref.df	F-value	p-value
	65.6964	199.0000	540.0728	< 0.0001

E Supplementary figures

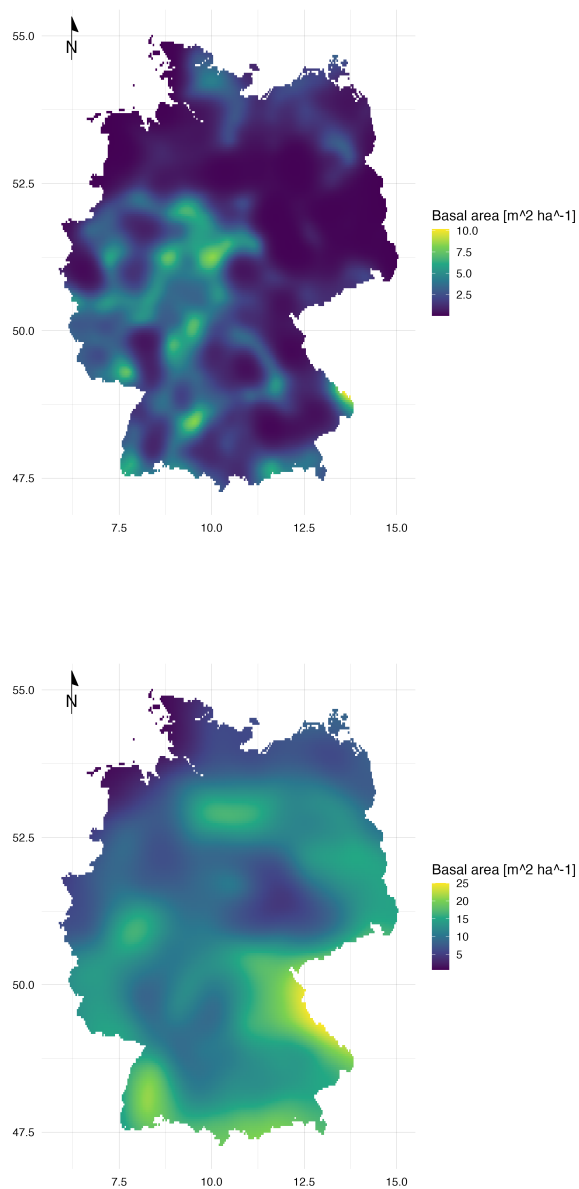


FIGURE S1: Spatial basal area smoothing splines, which were used as a proxy for background abundance for *Fagus* (A) and others (B) in Germany. For methodological details, see A.3.

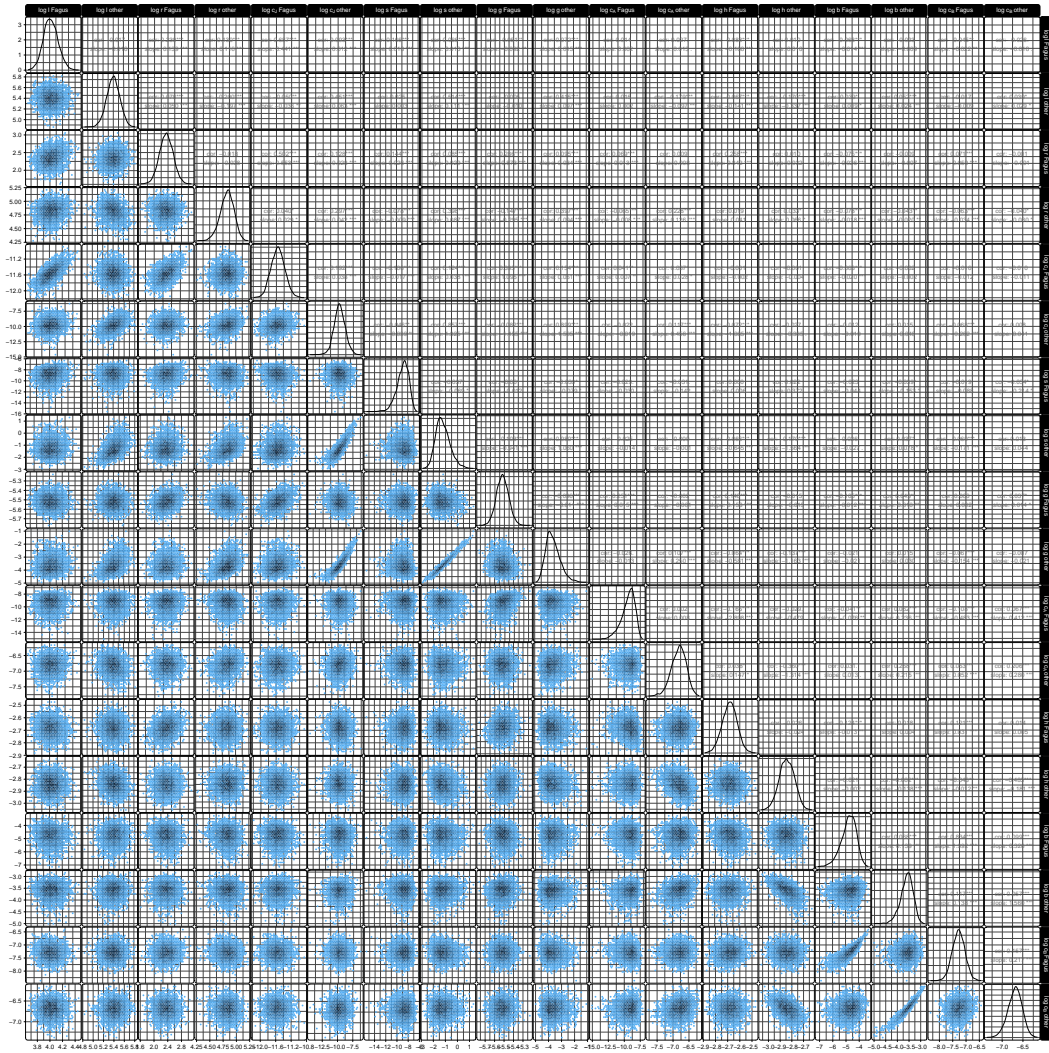


FIGURE S2: Paired scatter plots of posterior parameter distributions. The lower triangle shows the correlations of the posterior samples, where hexagonal bins are colored by the density of MCMC samples. The diagonal shows the marginal posteriors. The upper triangle quantifies the overall correlation and the slope of a linear regression between the parameters.

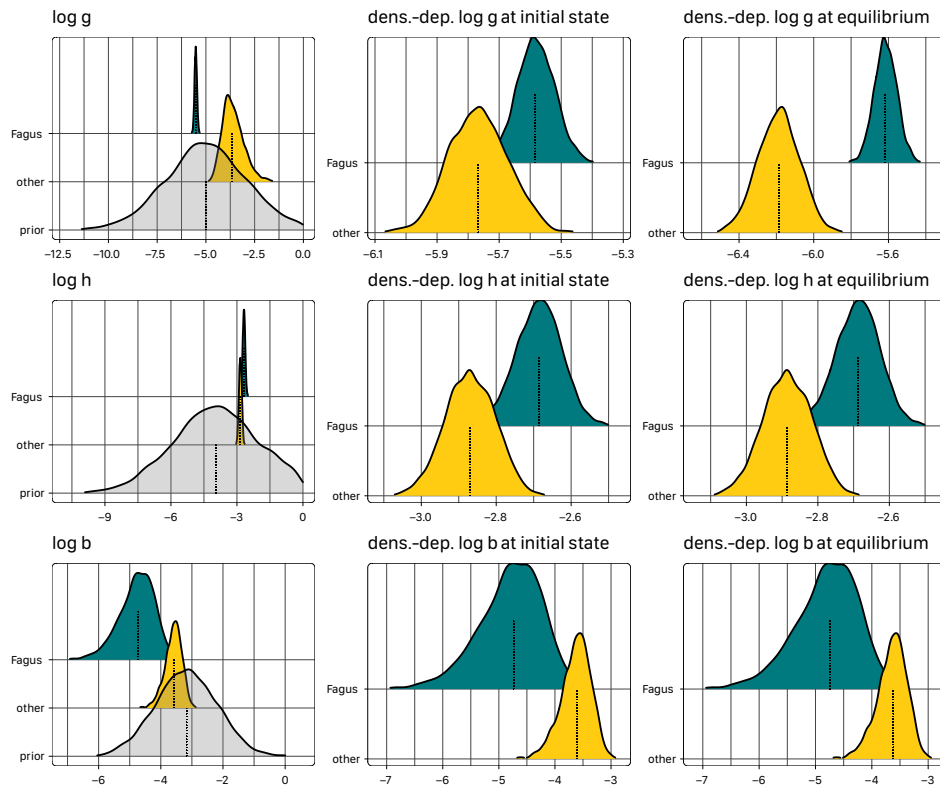


FIGURE S3: Marginal posterior distributions for parameters g , h , and b with the common priors, as in Figure 33. In addition, the corresponding density-dependent terms $\frac{g}{s \text{ sum}(BA) + c_J \text{ sum}(J)}$, $\frac{h}{c_A \text{ sum}(BA)}$, and $\frac{b}{c_B \text{ sum}(BA)}$ are provided. These terms were calculated with the sums of J and BA at both the initial state and competitive equilibrium.

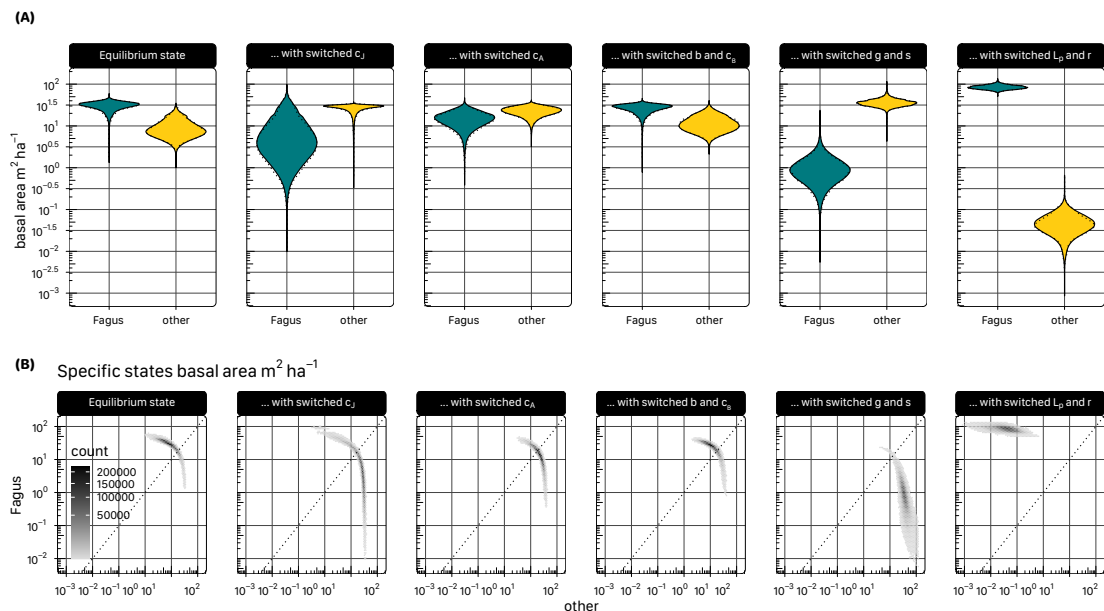


FIGURE S4: Equilibrium state and counterfactual equilibria as in Figure 35 but with additional parameters switched between species.

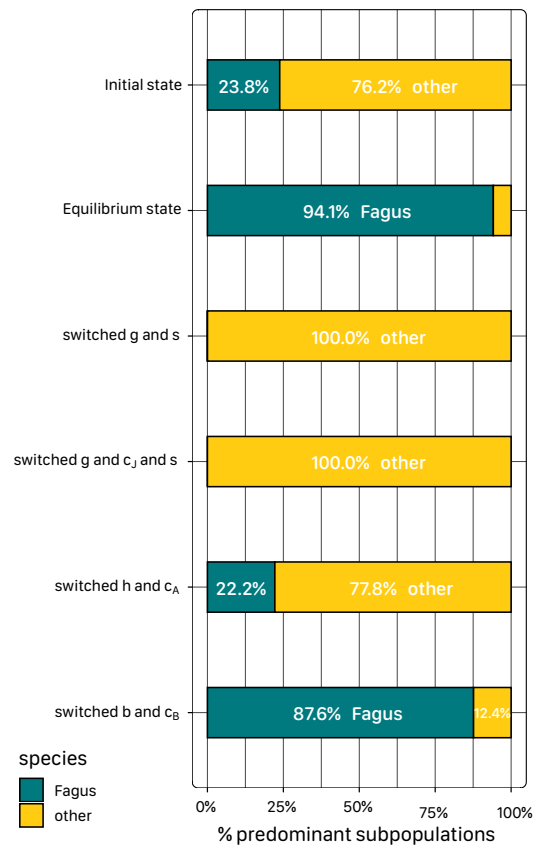


FIGURE S5: Fraction of posterior cases where either *Fagus* or *others* are the predominant species, as in Figure 36. Here, in contrast to Figure 36, the counterfactual equilibria are generated with joint switches of those parameters, that are part of one density-dependent term.

A Supplementary Methods

A.1 JAB model description

*Adapted from HEILAND *et al.* (2023).*

The JAB model is a dynamic model with competition effects that includes an explicit juvenile stage (Figure S1). The JAB model describes populations of species that are logistically limited by the same resource (GAUSE, 1932) but differs from a classical competitive Lotka-Volterra model in four main aspects: (1) size-structured populations, (2) basal area growth, (3) reduced complexity of competition effects, (4) influx from outside the populations.

In the JAB model, populations are structured into three size stages that interact: the juvenile stage J, representing the understory, and the stages A and B, jointly representing the overstory (Figure S1). Partitioning tree populations into understory and overstory, we can express asymmetric competition between the two fundamentally different forest layers (SCHWINNING, 1998): the understory is affected by the shading of the overstory, while the overstory is directly exposed to light and unaffected by the understory (VALLADARES and NIINEMETS, 2008; ANGELINI *et al.*, 2015; CORDONNIER *et al.*, 2019; DE LOMBAERDE *et al.*, 2019). The overstory (BA) is divided into A and B to enable conversion between measures of tree abundance in the sapling stage J, which is quantified as a count density, and the final stage B, which is represented in terms of basal area. The count density in J reflects the common measure of sapling inventories in NFI (see 4.2.3), whereas the basal area in the overstory stage B is a common measure for timber growth and competition (BIGING and DOBBERTIN, 1992). The size stage A functions as an intermediary between J (only counts) and B (only basal area) by having counts that are converted to basal area with a conversion factor. The JAB model represents growth as transition rates in absence of competition: from the understory stage J to the intermediary stage A (parameter g) and from A to B (parameter h). In addition to transitions from A, the final stage B has intrinsic basal area growth (parameter b ; Table 41).

To reduce the complexity of competition compared to a full Lotka-Volterra model, we represented only the differences in species' response to competition, assuming a similar com-

petition effect among species (simplifying from a matrix of n^2 parameters to parameter vectors of n competing species). More specifically, species are affected by the competition from the sum of the basal area of all species within their respective layers, i.e. they have a different competitive response to the sum of all inter- and intraspecific competition (vectors of species-specific parameters c_J, c_A, c_B). In applying this competition structure, we assume that the difference in competitive response between species is much more important than their difference in competitive effect (TILMAN, 1982; GOLDBERG and LANDA, 1991; GOLDBERG, 1996). The asymmetric competition from the overstorey BA on J is represented by the “shading” parameter s .

In the JAB model, there are two different sources of seedling recruitment: (1) local recruitment that is proportional to the local conspecific basal area (parameter r), and (2) external seedling input. The external seedling input L_p represents all long-term persistence of diaspores and long-distance dispersal into a subpopulation that is not explained by the local conspecific basal area of a plot p . It is proportional to a measure of long-term and large-scale distribution of the species \mathfrak{B}_p with the coefficient and parameter l (detailed in A.2).

Based on these principles, we implemented the JAB model as a discrete-time iteration rule in stan, with hyperbolic density dependence (see WATKINSON, 1980; ELLNER, 1984; LEVINE and REES, 2004), similar to a Lotka Volterra-type model formulation in DIN (2013). The iteration rule comprises a set of four equations (Equations 3.1–3.4) that relate states at year $t + 1$ to states at year t . Here, in accordance with the software implementation, we provide a vectorized formulation of the model, where all variables, including the parameters, and the stages J [ha^{-1}], A [$\text{m}^2 \text{ha}^{-1}$], B [$\text{m}^2 \text{ha}^{-1}$], and BA [$\text{m}^2 \text{ha}^{-1}$] are vectors with length n (number of species). These vectors are operated on with element-wise multiplication \odot and division \oslash ; the operator sum reduces the stages to a scalar, representing the total abundance of a stage across species.

$$J_{t+1} = L_p + r \odot BA_t + (J_t - g \odot J_t) \oslash [1 + c_J \text{sum}(J_t) + s \text{sum}(BA_t)] \quad (\text{S1})$$

$$A_{t+1} = g \odot J_t \oslash [1 + c_J \text{sum}(J_t) + s \text{sum}(BA_t)] + (A_t - h \odot A_t) \oslash [1 + c_A \text{sum}(BA_t)] \quad (\text{S2})$$

$$B_{t+1} = h \odot A_t \cdot \beta_{uA} \oslash [1 + c_A \text{sum}(BA_t)] + (1 + b) \odot B_t \oslash [1 + c_B \text{sum}(BA_t)] \quad (\text{S3})$$

$$BA_{t+1} = A_{t+1} \odot \beta_{mA} + B_{t+1} \quad (\text{S4})$$

All parameters ($r, c_J, s, g, c_A, h, b, c_B$, and $L_p = l\mathfrak{B}_p$) are generally assumed to be positive, so that all model states are strictly positive at any time (in fitting the model, this will be ensured by exponentiating the parameters sampled on a log-scale; Section 4.2.5.1). The four equations, representing size stages, are coupled through states of other stages, so that changes in one state propagate in discrete time steps, e.g., from BA to J to A to B. The fractions of trees that survive and grow from J to A and from A to B are expressed by the transition rates g and h ($\in (0, 1)$), respectively. The counts in A are transformed to basal area at two different occasions: (1) In the transition to B, the counts are converted by factoring in the basal area of one tree at the threshold between A and B, a species-independent scalar factor β_{uA} , which is dependent on the threshold diameter at breast height (dbh; Equation S3); (2) the combined basal area BA is calculated by multiplying the counts within A with a vector of the corresponding mean basal areas β_{mA} , which are species-specific constants from the data (Equation S4; *Fagus*: 0.015687m^2 ; *others* 0.016069m^2).

All stages (J, A, and B) are logistically limited by interspecific tree density: The sapling stage J is limited by the competitive effect from the total basal area across species BA (s) and from the total counts within the same stage (c_J), while the stages A and B are only limited by the competitive effect of BA (c_A , c_B). This limitation is implemented by dividing the states with a denominator that is slightly greater than 1: $[1 + c_J \text{sum}(J_t) + s \text{sum}(BA_t)]$ and $[1 + c_{A,B} \text{sum}(BA_t)]$, for understory and overstory respectively. The fractions of trees that transitions to the next stage, i.e. $g \cdot J$ and $h \cdot A$, are also limited by tree density so that they cannot exceed the number of trees in the current stage that is affected by limitation, e.g., the trees that transition from A to B $h \odot A_t \odot [1 + c_A \text{sum}(BA_t)]$ cannot exceed $A_t \odot [1 + c_A \text{sum}(BA_t)]$. Similarly in stage B, the density-dependent increment $B_t \odot b \odot [1 + c_B \text{sum}(BA_t)]$ cannot exceed the state-conserving term $B_t \odot [1 + c_B \text{sum}(BA_t)]$ (with $b \leq 1$). Not making $B_t \odot b$ density-dependent would allow constellations where $b \sim 1$ and $c_B \gg 0$ so that most of the state conservation would come from $B_t \odot b$. As a result, the competitive parameters c_J , s , c_A , and c_B describe, how species are differently affected by density of the respective forest layers ($\text{sum } J_t$ and $\text{sum } BA_t$) and the parameters g , h and b describe growth and survival in the absence of competition.

Overall, this leads to a system of populations that are in an arms race from a disturbed state towards a competitive equilibrium: Depending on their seedling recruitment (L_p and r), through transition (g , h) and net basal area increment (b) populations can intrinsically only grow or stagnate. This assumes that density-independent mortality is negligible in J and A, and that density-independent mortality in B is included in b and does not exceed basal area growth in the long term. Populations can, however, decline through interspecific competition (c_J , s , c_A , c_B). These properties enable the JAB model to extrapolate species composition under the assumption that species composition is mainly determined by a competitive equilibrium (ELLENBERG, 1963).

A.2 Species' regional abundance for predicting seedling input

Reproduced from HEILAND et al. (2023).

To derive the regional species abundance \mathfrak{B}_p used to estimate the external seedling input (parameter l , see Section A.1) we used thin plate spline regressions with the geographic coordinates as predictors to interpolate the species-specific basal area per hectare on the German NFI grid (see Appendix of HEILAND et al., 2023 for estimate table and plots).

For fitting the thin plate splines from the regular standard grid of the German NFI (4 km; see 4.2.3), which is homogeneous across Federal states, we selected only the basal area records from the last survey (2012), because the grid had changed over surveys. We completed non-forested clusters of the regular grid, and also all of the four plots within clusters, with zero observations to obtain an unbiased sample of the geographical density of tree species. To obtain a response variable for each set of coordinates, we calculated the species abundances per cluster by averaging the basal area per hectare above the sampling threshold (BA) over the four plots. This average basal area per hectare on the completed grid was spatially smoothed with a two-dimensional geographic thin plate spline. Based on the coordinates, a "spline on sphere" was fitted with the `gam()` function from the package `mgcv` ($k = 200$; version 1.8-39; WOOD, 2021), where the average basal area per hectare was the response. The response variable had been rounded to an integer to be able to fit a negative binomial response. The predicted plot-specific regional species abundances \mathfrak{B}_p

were used as a proxy for the probability of seedling input, which factors into the JAB model with a species-specific effect size l , $L_p = \mathfrak{B}_p l$. By using a strictly positive negative binomial response for \mathfrak{B}_p , it was made sure that plots were not excluded from invasion in the JAB model.

A.3 Offsets for scaling area-standardized model states to observed counts

Adapted from HEILAND et al. (2023).

To model tree abundances from varying sampling areas with a count process in the likelihood of the JAB model (Section 4.2.5.3), we used different offsets. In general, the offsets o convert the model states \hat{x} , which are abundances standardized per hectare, to the scale of observed counts x :

$$x \sim o \hat{x} \tag{S5}$$

Different offsets were used depending on the type of the abundances in the model and the corresponding data: for the special offsets that scaled the basal area states in the model to count data from the angle count method see A.3.1; for the offsets that scaled counts in the model to counts on different fixed areas see A.3.2. Because the sampling protocol of the German NFI made observation areas dependent on size, the offsets for zero observations had to be derived separately (see A.3.3).

These offsets account for the varying sampling intensity that also affects the variance of observations. Furthermore, using a count process with offsets is (1) preferable over modelling a continuous response for the basal area because it reflects the actual observation process with discrete numbers of trees (even when being multiplied with a tree-specific basal area), and (2) preferable over upscaling the small sampling areas to a common area because this would break distributional assumptions by deflating small counts in the data, e.g. when a plot size is one fourth of the common standard area 1 hectare, the smallest measured count per hectare would be 4.

A.3.1 Offsets for the angle count method

Count data from the angle count method (size stage A in the German NFI) were related to the count states in the JAB model by scaling with area offsets. In angle count sampling, each tree has a specific sampling area a dependent on its dbh with $a = \pi k^2 dbb^2$, where k is a constant for the sampling angle (here, $k = 25$). Thus, for the sampling area of a plot, which corresponds to the actually observed trees on a plot we use the weighted mean $a_p = \sum_{i=1}^n w_i a_i / \sum_{i=1}^n w_i$, where the weights w_i are the respective area-standardized counts per hectare. This weighted mean has the property that—together with the actually observed counts on a plot c_p —it conveys equivalent information as the sum of all area-standardized counts per hectare on a plot $c_A = \frac{c_p}{a_p}$ [ha^{-1}]. The area a_p was used as the offset for size stage A (o in Equation S5).

To relate count data from the angle count method to the basal area state in the model (size stage B in the German NFI), we used an offset factor that not only includes the sampling area a_p but transforms the basal area per hectare in the JAB model to counts. This was achieved with an offset o that also included the total observed basal area ba_p on a plot:

$o = a_p \frac{c_p}{ba_p} [\text{ha m}^{-2}]$. By multiplying the model state $\hat{x} [\text{m}^2 \text{ha}^{-1}]$ with this offset we transformed the model state to counts, by including the data on basal area (“how many counts are one unit of basal area?”) on the right hand side of the model statement: $x \sim a_p \frac{c_p}{ba_p} \hat{x}$.

A.3.2 Offsets for sapling counts on fixed-area plots

Sapling counts on fixed-area plots (size class J) were also standardized using area offsets. In the German NFI data, size class J consists of multiple size classes with different sampling areas, which also change between surveys (Table S2). As in the angle count data, we calculated a weighted mean area per plot, where the different sampling areas were weighted by the counts per area within the corresponding size classes. The weighted mean area per NFI plot was used as an offset to relate the sapling counts to the area-standardized counts of J in the JAB model $[\text{ha}^{-1}]$.

A.3.3 Offsets for zero observations

Because the sampling protocol of the German NFI made observation areas dependent on size, the observation area was not readily available when there were no observations for a stage on a plot. For zero observations in the angle count data in the German NFI (size classes A and B), we used the sampling area of the other species, or, if both species had zero observations, the mean sampling area per size class and survey as an offset (for a test of the robustness of this approach, see below). To be able to compute a mean area for the largest size class B, we truncated the angle count data to a maximum sampling radius of 15 m. The truncation included dropping all trees outside the sampling radius, which is about the 98th percentile of tree counts in A and B and assigning the new maximum sampling area to all trees that were within the maximum radius but had a dbh that was originally corresponding to a sampling area greater than the new maximum area (dbh > 60 cm). Truncating the angle count data to a fixed maximum area removes a source of bias (missed tree observations at higher radii) at the cost of moderate added variance (BERGER *et al.*, 2020), and furthermore leads to a finite sampling area that can be averaged over. The mean sampling area per size class (A and B) was calculated by dividing the definite integral from 0 up to the respective maximum radius—by the maximum radius. This mean area was used as an offset for zero observations in size class A. To obtain an offset for zero observations in size class B, we also needed an additional factor that scaled the basal area to the scale of observed counts. Instead of multiplying the area with the plot-specific factor $\frac{c_p}{ba_p}$ (as for non-zero observations, see A.3.1), we included the mean of the factor per survey and additionally per species to differentiate between their average basal areas.

Zero observations in the sapling counts of the size class J in the German NFI were assigned an equally weighted mean of all possible sampling areas for the respective set of smaller size classes within the corresponding survey (Table S2).

B Supplementary Tables

Table S1: Scope of the German NFI and plot selection.

German NFI	
No. of surveys	3
... years	1986–1989/2000–2003/2011–2013
No. of plots	61666
... after selection	795
No. of clusters	21574
... after selection	795

Table S2: Size classes for saplings counts and corresponding radii of sampling circles in the three surveys of the German NFI (main years 1987, 2002, 2012). The size classes up to dbh 7 cm, which were consistently sampled across all three surveys, were assigned to the size class J in fitting the JAB model.

	1987	2002	2012
height 20–50 cm	1 m	1 m	1 m
height 50–130 cm	2 m	1.75 m	2 m
height 130– ∞ cm and dbh 0–5 cm	2 m	1.75 m	2 m
dbh 5–6 cm	4 m	1.75 m	2 m
dbh 6–7 cm	4 m	1.75 m	2 m
dbh 7–8 cm	4 m	.	.
dbh 8–9 cm	4 m	.	.
dbh 9–10 cm	4 m	.	.

Table S3: Soil water levels from BENNING *et al.* (2016), ranking and conversion into pseudo-ratio scale. Translation according to LEUSCHNER and ELLENBERG (2017a).

Category	Description	Pseudo-ratio value	Ellenberg levels	Translation
T1	trocken	-6	trocken	dry
T1-T2	trocken bis mäßig trocken	-5		
T2	mäßig trocken	-4	mäßig trocken	moderately dry
T2-T3	mäßig trocken bis mäßig frisch	-3		
T2-T4	mäßig trocken bis frisch	-2.5		
T3	mäßig frisch	-2	mäßig frisch	moderately damp
T3-T4	mäßig frisch bis frisch	-1		
S	sehr tief sitzende Staunässe	-0.5		
T3-S1	mäßig frisch bis sehr schwach staunass / wechselfeucht	-0.25		
T4	frisch	0	frisch	damp
S0	tief sitzende Staunässe	0.25		
T4-T5	frisch bis sehr frisch	0.5		
T4-S1	frisch bis sehr schwach staunass / wechselfeucht	0.7		
T5	sehr frisch	0.8		
G0	grundfrisch	1		
S1	sehr schwach staunass / wechselfeucht	1.25		
G1	grundfrisch	1.5		
S1-S2	sehr schwach bis schwach staunass / wechselfeucht	1.7		
S2	schwach staunass / wechselfeucht	1.8		
G2	grundfeucht	2	(mäßig feucht)	(moderately moist)
S1-G2/3	sehr schwach staunass / wechselfeucht bis grundfeucht	2.2		
S1-S3	sehr schwach bis mittel staunass / wechselfeucht	2.3		
G2/3	grundfeucht	2.5		
S3	mittel staunass / wechselfeucht	2.7		
S3-G2/3	mittel staunass / wechselfeucht bis grundfeucht	2.8		
G3	grundfeucht	3		
S3-S4	mittel bis stark staunass / wechselfeucht	3.5		
G4	feucht	4	feucht	moist
G4-G5	feucht bis nass	5		
S4	stark staunass / wechselfeucht	5.5		
G4-G6	feucht bis nass	5.8		
G5	nass	6	nass	wet
S3-S6	mittel bis äußerst staunass	6.5		
S5	sehr stark staunass / wechselfeucht	7		
G6	nass	7.5		
S6	äußerst staunass	8	sehr nass	very wet

Table S4: Stratification of the two environmental gradients into seven intervals each (left: water level, top: pH) and the number of forest plots sampled within each of the 49 resulting bins.

	(2.84,3.47]	(3.47,4.09]	(4.09,4.72]	(4.72,5.34]	(5.34,5.97]	(5.97,6.59]	(6.59,7.22]
(-6.01,-4.07]	1	14	23	22	25	6	4
(-4.07,-2.14]	6	25	25	25	25	25	19
(-2.14,-0.214]	15	25	25	25	25	25	6
(-0.214,1.71]	15	25	25	25	25	25	6
(1.71,3.64]	4	13	25	25	25	12	3
(3.64,5.57]	3	21	25	25	25	21	2
(5.57,7.51]	0	4	6	6	7	5	1

Table S5: Taxa composition of the German NFI on the selected plots. All observed taxa are listed, ranked by the mean basal area per plot. In addition, the mean percentage of the total plot basal area is given.

	Taxon	Mean basal area m ² ha ⁻¹	Mean percentage of the total basal area
1	<i>Picea abies</i>	7.852	28.972%
2	<i>Pinus sylvestris</i>	5.714	18.566%
3	<i>Fagus sylvatica</i>	3.325	13.102%
4	<i>Quercus petraea</i>	1.761	6.754%
5	<i>Quercus robur</i>	1.249	4.522%
6	<i>Pseudotsuga menziesii</i>	0.886	3.391%
7	<i>Betula pendula</i>	0.692	3.161%
8	<i>Alnus glutinosa</i>	0.739	2.581%
9	<i>Fraxinus excelsior</i>	0.562	2.478%
10	<i>Larix decidua</i>	0.637	2.356%
11	<i>Carpinus betulus</i>	0.555	1.778%
12	<i>Quercus</i> spp.	0.561	1.717%
13	<i>Acer pseudoplatanus</i>	0.235	1.318%
14	<i>Abies alba</i>	0.281	1.048%
15	<i>Prunus avium</i>	0.218	0.899%
16	<i>Alnus</i> spp.	0.237	0.760%
17	<i>Salix</i> spp..	0.14	0.691%
18	<i>Populus tremula</i>	0.187	0.661%
19	<i>Tilia</i> spp.	0.181	0.649%
20	<i>Quercus rubra</i>	0.137	0.589%
21	<i>Populus nigra</i>	0.135	0.460%
22	<i>Robinia pseudoacacia</i>	0.17	0.389%
23	<i>Acer campestre</i>	0.09	0.382%
24	<i>Populus</i>	0.147	0.366%
25	<i>Larix kaempferi</i>	0.081	0.341%
26	<i>Pinus nigra</i>	0.103	0.236%
27	<i>Larix</i> spp.	0.075	0.218%
28	<i>Acer platanoides</i>	0.03	0.195%
29	<i>Alnus incana</i>	0.035	0.183%
30	<i>Pinus strobus</i>	0.039	0.156%
31	<i>Ulmus</i> spp.	0.034	0.124%
32	<i>Populus alba</i>	0.073	0.093%
33	other coniferous (German NFI)	0.029	0.088%
34	<i>Sorbus aucuparia</i>	0.012	0.083%
35	<i>Aesculus hippocastanum</i>	0.024	0.078%
36	other deciduous (German NFI)	0.017	0.070%
37	<i>Populus trichocarpa</i> x <i>maximoviczii</i>	0.03	0.065%
38	<i>Sorbus aria</i>	0.012	0.060%
39	<i>Picea sitchensis</i>	0.01	0.058%
40	<i>Sorbus torminalis</i>	0.017	0.051%
41	<i>Thuja</i> spp.	0.02	0.041%
42	<i>Prunus padus</i>	0.007	0.038%
43	<i>Betula pubescens</i>	0.005	0.035%
44	<i>Ilex aquifolium</i>	0.01	0.032%
45	<i>Frangula alnus</i>	0.005	0.030%
46	<i>Castanea sativa</i>	0.005	0.027%
47	<i>Pyrus communis</i>	0.007	0.027%
48	other <i>Pinus</i> (German NFI)	0.008	0.026%
49	<i>Sorbus</i> spp.	0.005	0.019%
50	<i>Abies grandis</i>	0.003	0.018%
51	<i>Juglans</i>	0.003	0.016%
52	<i>Malus sylvestris</i>	0.002	0.004%

Table S6: Posterior distributions of the dispersion parameter ϕ and bulk effective sample size (ESS). There are different levels of uncertainty per stage and survey.

	Level	Species	Posterior	bulk ESS
ϕ	J Initial state	Fagus	10170. \pm 152700.	3962.175
	J Initial state	others	21850. \pm 173200.	4114.269
	J 2nd survey	Fagus	0.3863 \pm 0.05948	8763.802
	J 2nd survey	others	0.2342 \pm 0.01473	7526.126
	J 3rd survey	Fagus	0.2050 \pm 0.01912	9997.296
	J 3rd survey	others	0.2066 \pm 0.01238	9309.075
	A Initial state	Fagus	5157. \pm 20760.	3520.311
	A Initial state	others	7000. \pm 36340.	4753.705
	B Initial state	Fagus	9725. \pm 165700.	3703.357
	B Initial state	others	12330. \pm 65700.	4243.675
	A 2nd/3d survey	Fagus	3.623 \pm 1.010	6371.580
	A 2nd/3d survey	others	1.980 \pm 0.1897	8463.309
	B 2nd/3d survey	Fagus	2.485 \pm 0.3213	7960.757
	B 2nd/3d survey	others	3.964 \pm 0.2868	6709.977

Table S7: Posterior distributions of initial and equilibrium abundances (stages J and A [count ha⁻¹]; B and total BA [m² ha⁻¹]) and species' predominance (mean \pm standard deviation across subpopulations and HMC samples). Equilibrium states include counterfactual simulations, where the rate s has been switched between *Fagus* and *others* or where the respective other species does not regenerate.

		Fagus	others
J	initial state data	817.05 \pm 4911.0	4414.5 \pm 11196.
	initial model state	827.12 \pm 4912.4	4436.1 \pm 11199.
	equilibrium state	7789.7 \pm 4342.6	3218.9 \pm 1575.8
A	initial state data	43.744 \pm 187.64	312.88 \pm 525.15
	initial model state	45.227 \pm 187.23	313.88 \pm 524.46
	equilibrium state	550.96 \pm 295.18	76.920 \pm 58.745
B	initial state data	2.0691 \pm 5.9266	14.140 \pm 15.510
	initial model state	2.1133 \pm 6.0062	14.258 \pm 15.678
	equilibrium state	39.382 \pm 31.583	7.7577 \pm 10.855
BA	initial state data	2.6943 \pm 7.0598	18.590 \pm 16.974
	initial model state	2.8227 \pm 7.2233	19.302 \pm 17.430
	equilibrium state	48.025 \pm 34.253	8.9937 \pm 11.752
	eq. sum across species	57.019 \pm 28.099	.
	eq. with switched s eq. without regeneration of resp. other	8.0109 \pm 20.301 58.395 \pm 30.592	32.853 \pm 12.054 38.786 \pm 2.8381
Fraction of basal area	initial model state	0.20731 \pm 0.31625	0.79269 \pm 0.31625
	equilibrium state	0.78654 \pm 0.30819	0.21346 \pm 0.30819
	eq. with switched s	0.16222 \pm 0.30936	0.16222 \pm 0.30936

C Supplementary Figures

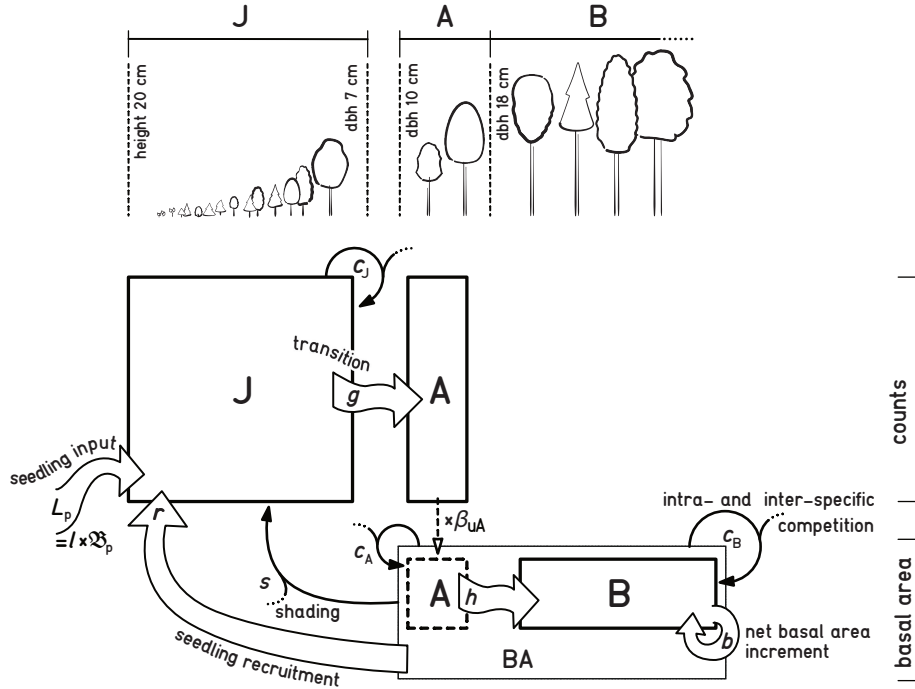


FIGURE S1: The JAB model represents three different size stages of a tree population (J, A, B) and demographic processes, including the competitive interactions between size stages and multiple species. There are processes that contribute to population growth: seedling input into the population from temporal or spatial dispersal L_p (dependent on regional basal area \mathfrak{B}_p), within-population seedling regeneration r , transitions from a smaller to a larger stage (g, h), and the basal area growth b . The processes that limit population growth comprise the competition effect from the total sum of the sapling stage J on species-specific J (c_J), the competition from the sum of A and B, i.e. the total basal area of all species BA, on A and B (c_A, c_B), as well as the asymmetric competition from BA on J (“shading” effect s). The choice of thresholds between size stages is informed by the size classes in the data. In the German NFI small trees between height 20 cm and dbh 7 cm were counted, while trees with dbh > 10 cm were additionally measured in terms of basal area, so that intermediary size stage A acts as a mediator between count data for J and the basal area data for B. The factor β_{uA} , i.e. the upper basal area of a tree in A, converts A from counts to basal area.

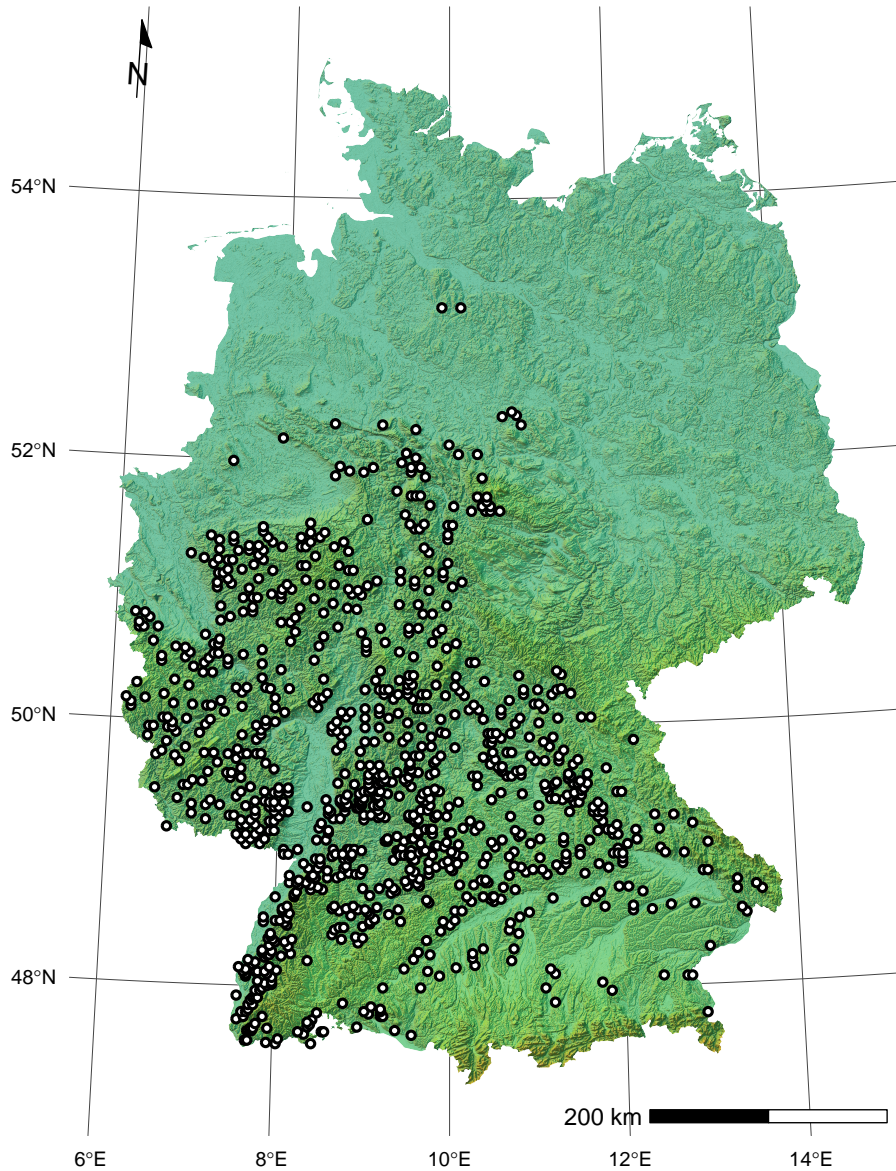


FIGURE S2: Locations of the 795 randomly selected NFI clusters in Germany. Each cluster consists of one to four sampling plots, depending on whether the location was forested. One random plot per cluster was selected if its elevation was at 100–600 m, if the observation period included all of the three surveys (1987, 2002, and 2012; which excludes former East Germany), and if there were no records of management within the period. Each selected plot (cluster) is represented by one subpopulation in the JAB model. The map projection is Lambert Conformal Conic, the color shading indicates elevation and relief.

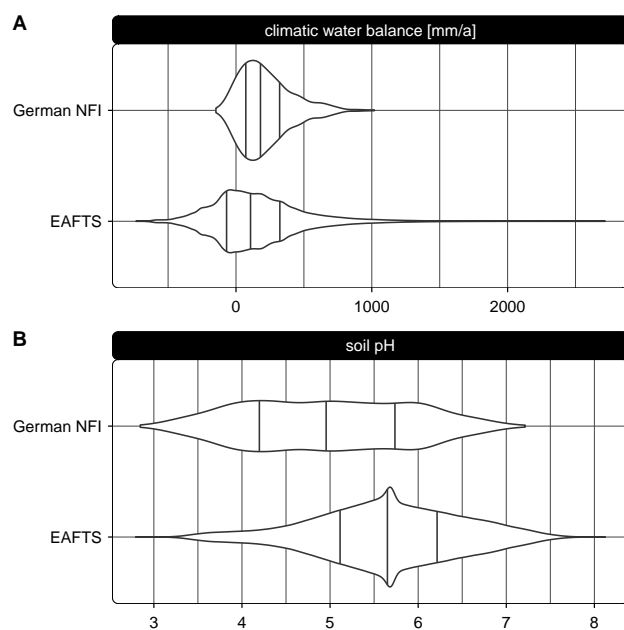


FIGURE S3: Environmental range of the German NFI and of *Fagus sylvatica* occurrence according to The European Atlas of Forest Tree Species (DE RIGO *et al.*, 2016). The German NFI has a narrower range with regard to both top soil pH in CaCl₂ (A) and climatic water balance (B). Lines correspond to quartiles.

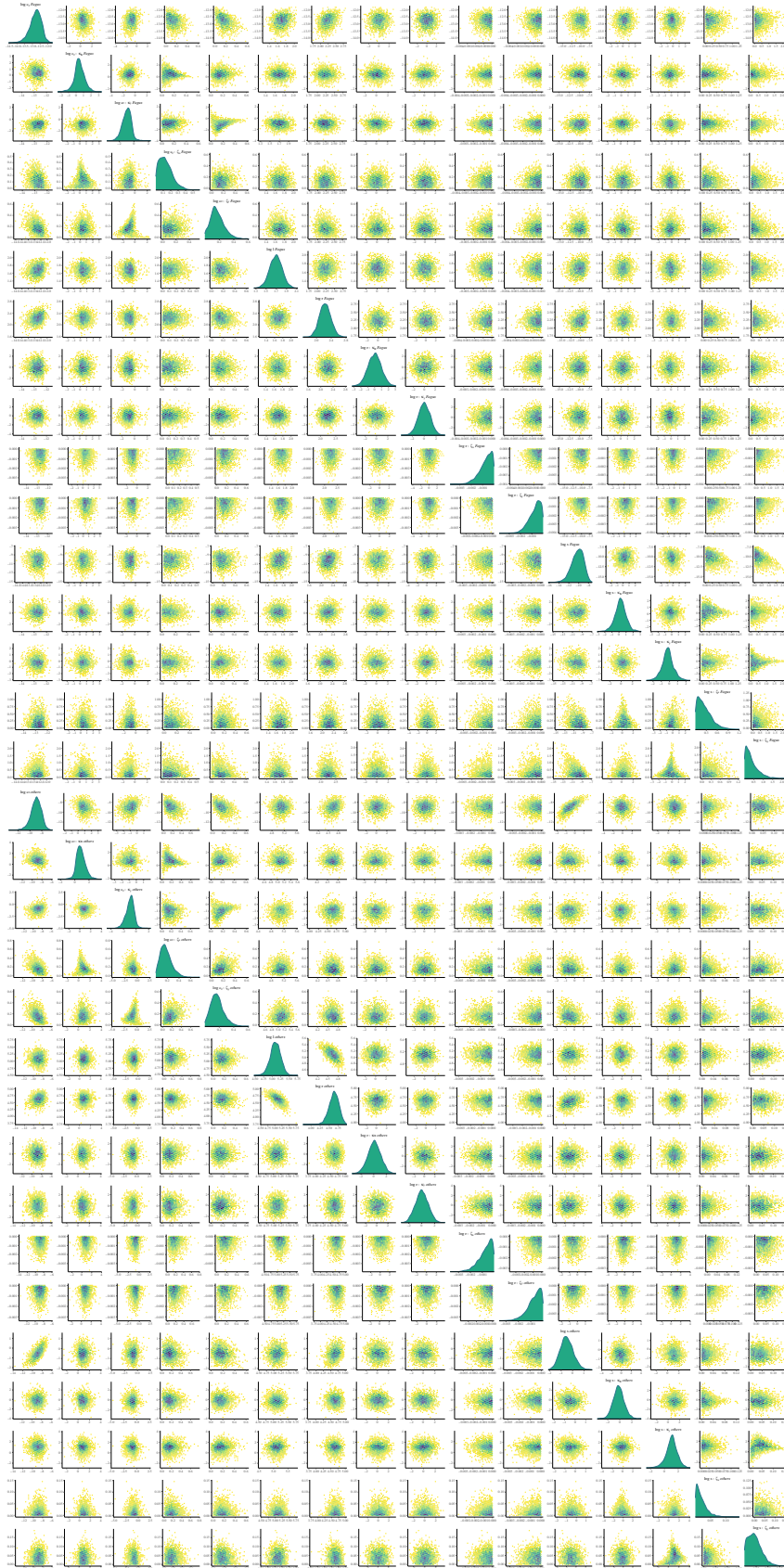


FIGURE S4: Pairs of paraboloid parameter correlations within stage J, separately for *Fagus* and *others*.

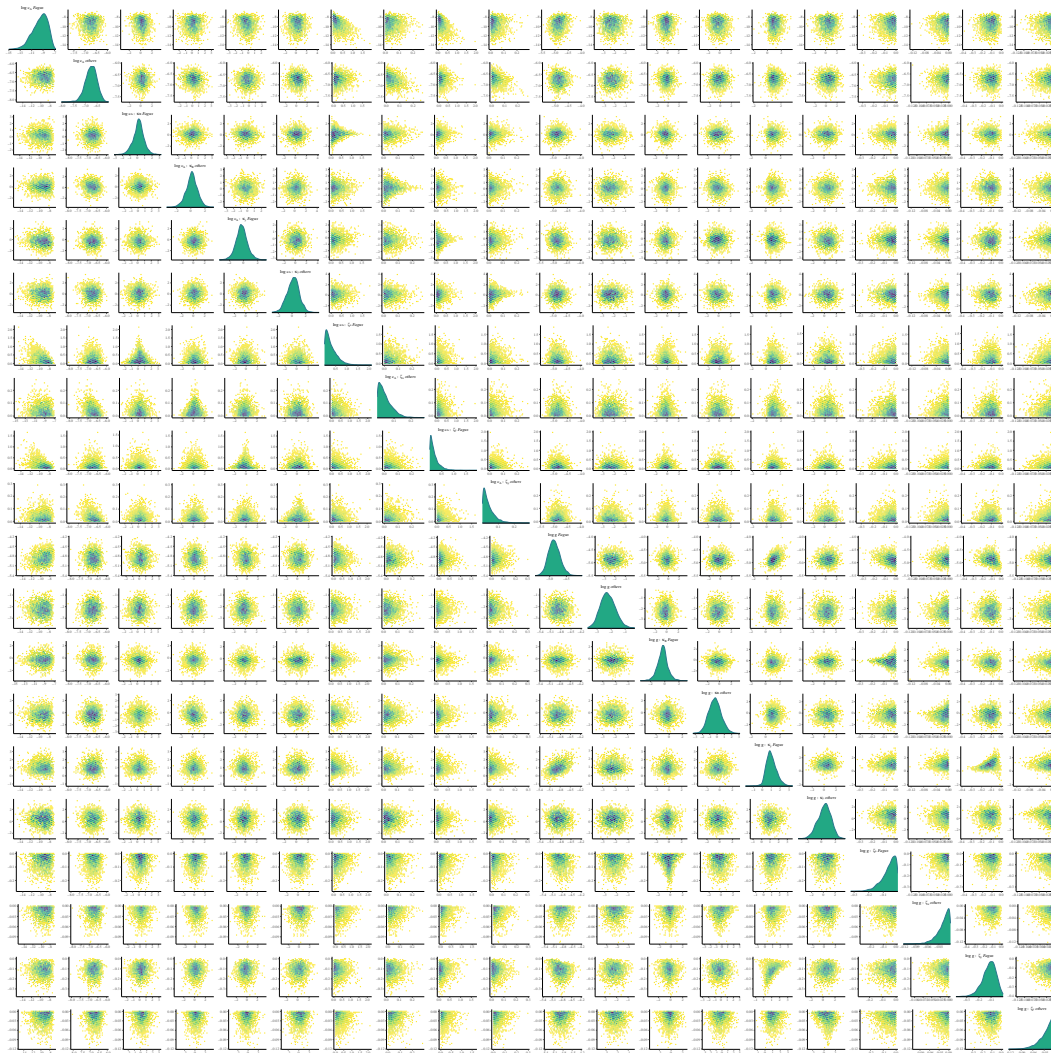


FIGURE S5: Pairs of paraboloid parameter correlations within stage A.

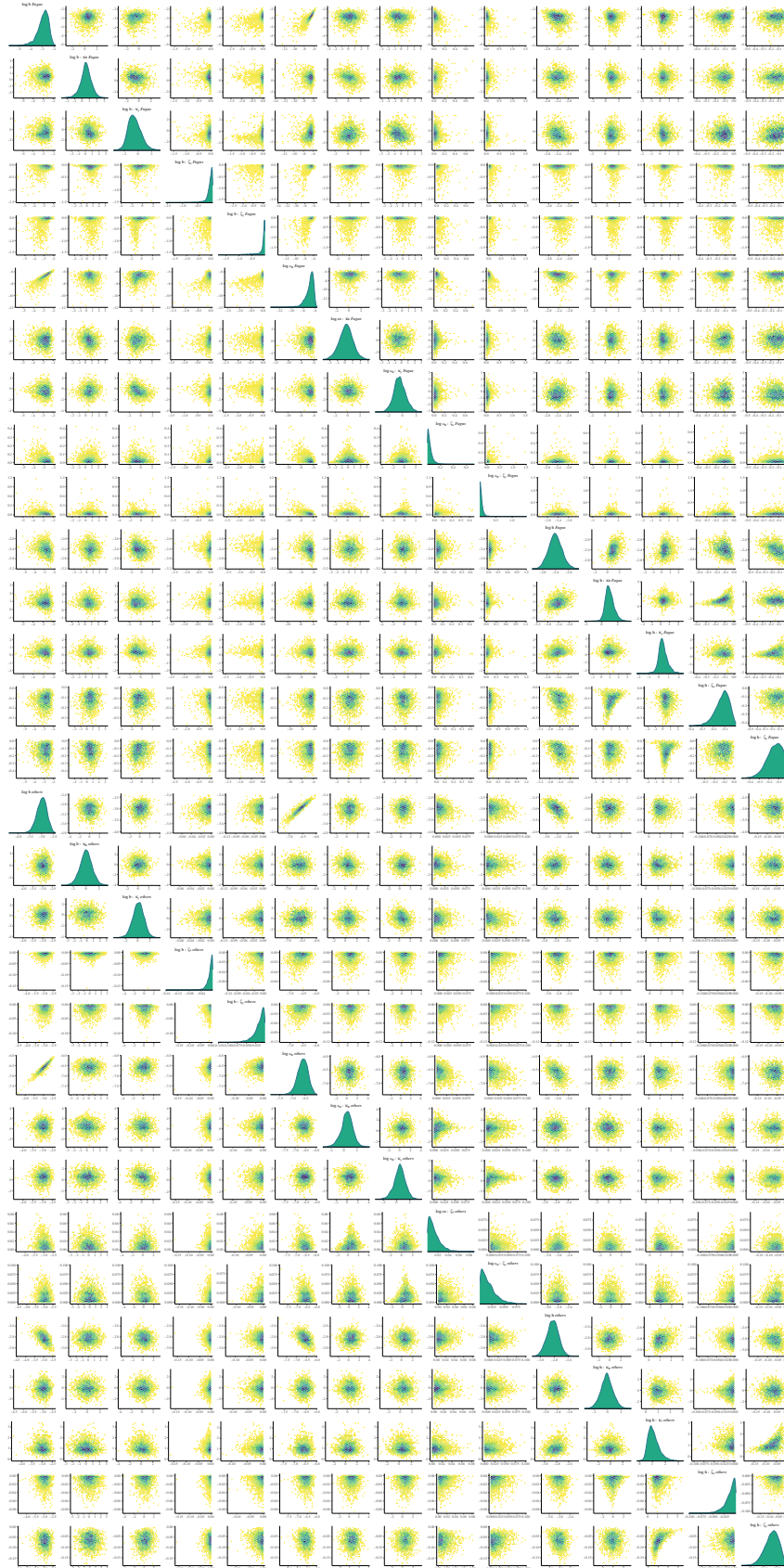


FIGURE S6: Pairs of paraboloid parameter correlations within stage B, separately for *Fagus* and *others*.

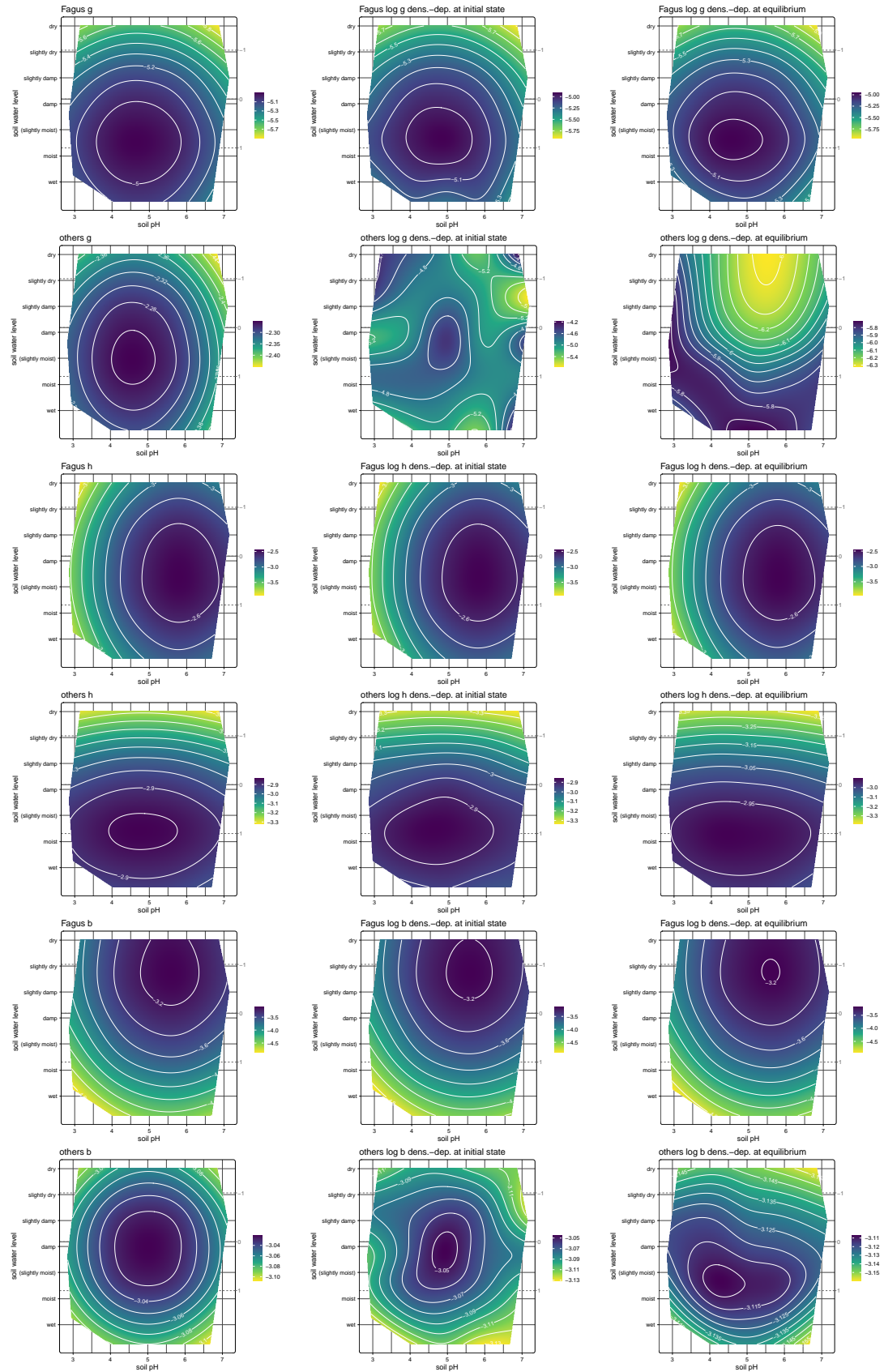


FIGURE S7: JAB model demographic rates in environmental space, including the density-dependent terms at initial and equilibrium state. The contours show predictions from smoothing splines fitted to the posterior distributions (as described in Section 4.2.6.1).

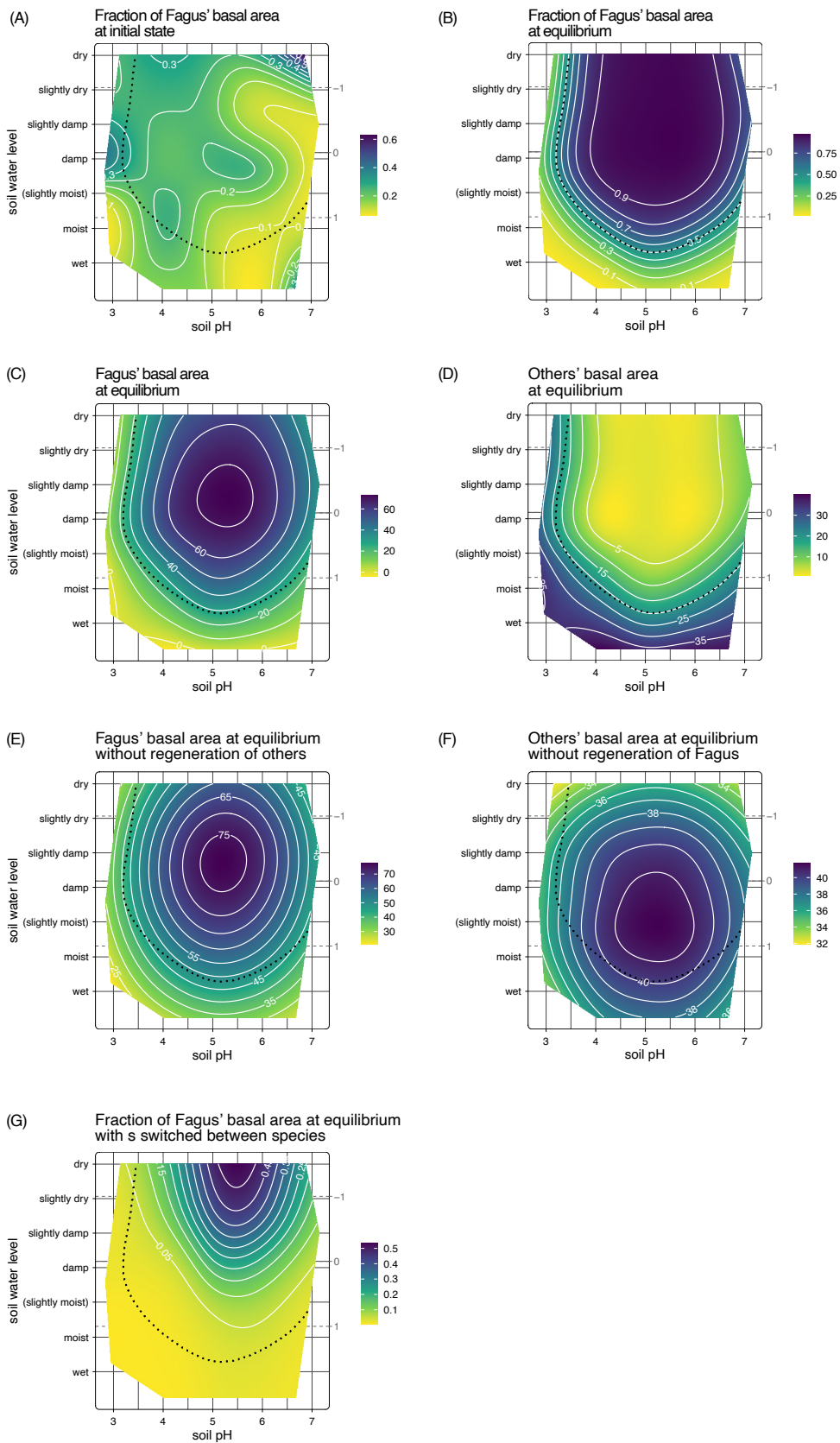


FIGURE S8: Basal areas in environmental space at initial state (A), at the competitive equilibrium (B–D). Additionally counterfactual equilibria are depicted: given that the respective other species does not reproduce (by setting l , r , and b to 0; E–F), and (G) given that the shading response (s) is switched between species. The contours show predictions from smoothing splines fitted to the posterior distributions (as described in Section 4.2.6.1)

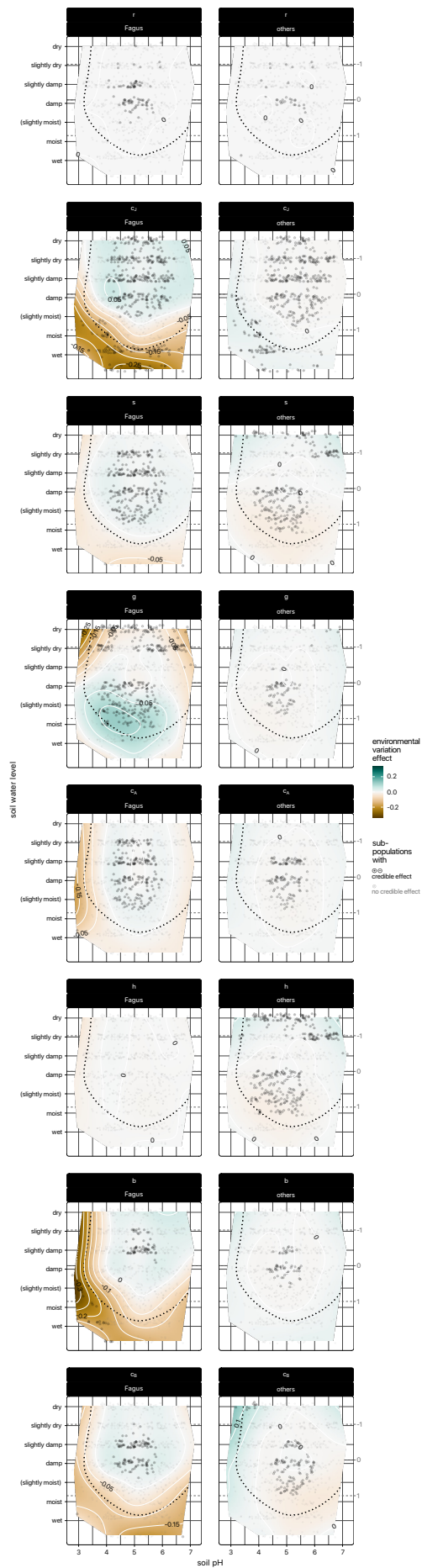


FIGURE S9: Environmental variation effect in environmental space for all rates that were determined with paraboloid parameters.

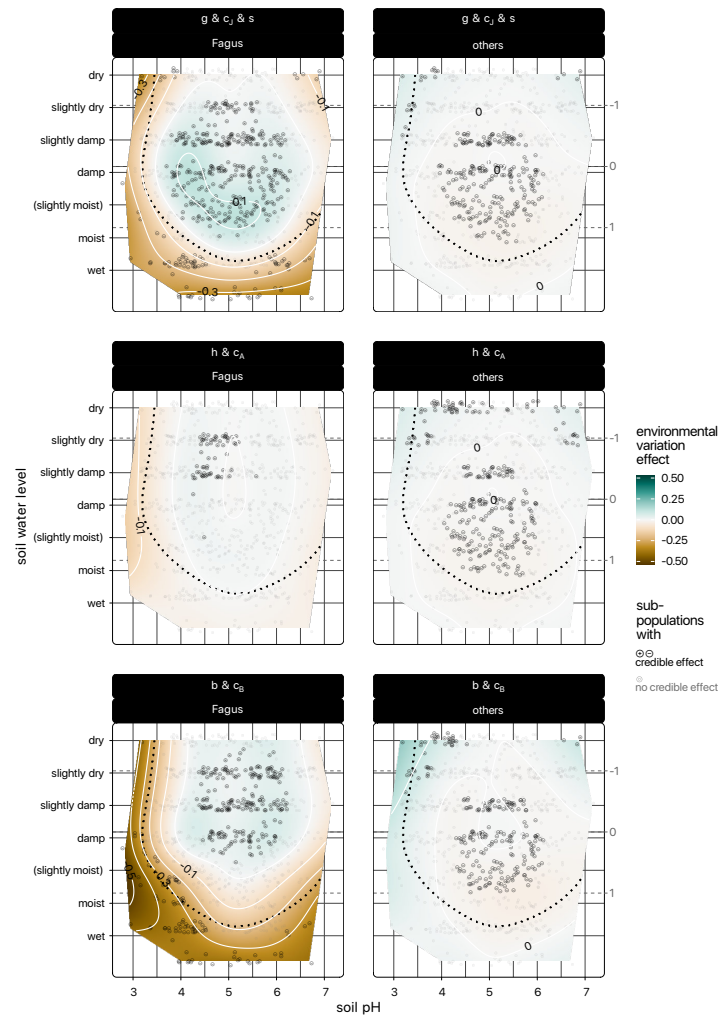


FIGURE S10: Environmental variation effect in environmental space for combinations of rates.

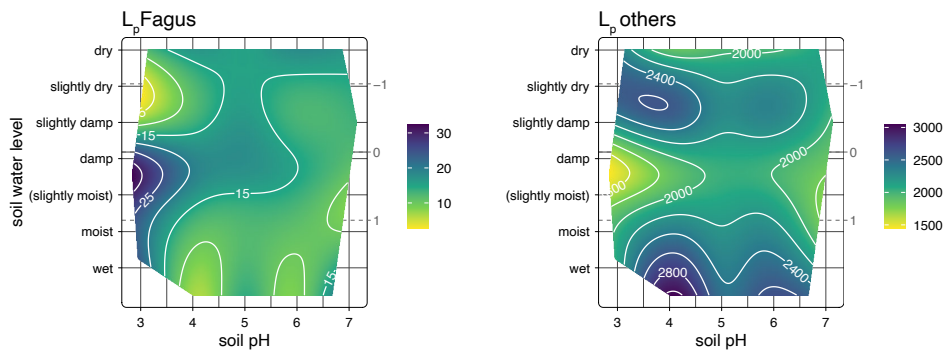


FIGURE S11: Environmental variation effect in environmental space for L_p .

Bibliography

- AMÉZTEGUI, A., L. BROTONS, and L. COLL (2010). Land-Use Changes as Major Drivers of Mountain Pine (*Pinus Uncinata* Ram.) Expansion in the Pyrenees: Land-use Changes Drive *Pinus Uncinata* Expansion. *Global Ecology and Biogeography*, **19**, 632–641. doi:10.1111/j.1466-8238.2010.00550.x.
- ANDIVIA, E., P. RUIZ-BENITO, P. DÍAZ-MARTÍNEZ, N. CARRO-MARTÍNEZ, M. A. ZAVALA, and J. MADRIGAL-GONZÁLEZ (2020). Inter-Specific Tolerance to Recurrent Droughts of Pine Species Revealed in Saplings Rather than Adult Trees. *Forest Ecology and Management*, **459**, 117848. doi:10.1016/j.foreco.2019.117848.
- ANGELINI, A., P. CORONA, F. CHIANUCCI, and L. PORTOGHESI (2015). Structural Attributes of Stand Overstory and Light under the Canopy. *Annals of Silvicultural Research*, **39**(1), 23–31. doi:10.12899/asr-993.
- AUGSPURGER, C. K. and E. A. BARTLETT (2003). Differences in Leaf Phenology between Juvenile and Adult Trees in a Temperate Deciduous Forest. *Tree Physiology*, **23**(8), 517–525. doi:10.1093/treephys/23.8.517.
- AXER, M., S. MARTENS, R. SCHLICHT, and S. WAGNER (2021). Modelling Natural Regeneration of European Beech in Saxony, Germany: Identifying Factors Influencing the Occurrence and Density of Regeneration. *European Journal of Forest Research*. doi:10.1007/s10342-021-01377-w.
- BADECK, F.-W., H. LISCHKE, H. BUGMANN, K. HÖNNINGER, P. LASCH, M. J. LEXER, F. MOUILLOT, J. SCHABER, and B. SMITH (2001). Tree Species Composition in European Pristine Forests: Comparison of Stand Data to Model Predictions. *Climatic Change*, **51**, 307–347. doi:10.1023/A:1012577612155.
- BAJOCCO, S., C. FERRARA, M. BASCIETTO, A. ALIVERNINI, R. CHIRICHELLA, A. CUTINI, and F. CHIANUCCI (2021). Characterizing the Climatic Niche of Mast Seeding in Beech: Evidences of Trade-Offs between Vegetation Growth and Seed Production. *Ecological Indicators*, **121**, 107139. doi:10.1016/j.ecolind.2020.107139.
- BALLABIO, C., E. LUGATO, O. FERNÁNDEZ-UGALDE, A. ORGIAZZI, A. JONES, P. BORRELLI, L. MONTANARELLA, and P. PANAGOS (2019). Mapping LUCAS Topsoil Chemical Properties at European Scale Using Gaussian Process Regression. *Geoderma*, **355**, 113912. doi:10.1016/j.geoderma.2019.113912.
- BAUR, G. (1957). Nature and Distribution of Rain-Forests in New South Wales. *Australian Journal of Botany*, **5**(2), 190. doi:10.1071/BT9570190.

- BEGUERÍA, S. and S. M. VICENTE-SERRANO (2017). *SPEI: Calculation of the Standardised Precipitation–Evapotranspiration Index*.
- BELL, D. M., J. B. BRADFORD, and W. K. LAUENROTH (2014). Early Indicators of Change: Divergent Climate Envelopes between Tree Life Stages Imply Range Shifts in the Western United States. *Global Ecology and Biogeography*, 23(2), 168–180. doi:10.1111/geb.12109.
- BENNETT, A. C. (2015). Larger Trees Suffer Most during Drought in Forests Worldwide. *Nature Plants*, 1, 5.
- BENNING, R., R. PETZOLD, and J. DANIGEL (2019). *BWI 2012 Umweltdatenbank Bodenprofile*. Johann Heinrich von Thünen-Institut, DE.
- BENNING, R., R. PETZOLD, J. DANIGEL, R. GEMBALLA, and H. ANDREAE (2016). Generating characteristic soil profiles for the plots of the National Forest Inventory in Saxony and. *Waldökologie, Landschaftsforschung und Naturschutz*, 16(2016).
- BERGER, A., T. GSCHWANTNER, and K. SCHADAUER (2020). The Effects of Truncating the Angle Count Sampling Method on the Austrian National Forest Inventory. *Annals of Forest Science*, 77(1), 16. doi:10.1007/s13595-019-0907-y.
- BERTNESS, M. D. and R. CALLAWAY (1994). Positive Interactions in Communities. *Trends in Ecology & Evolution*, 9(5), 191–193. doi:10.1016/0169-5347(94)90088-4.
- BERTRAND, R., J.-C. GÉGOUT, and J.-D. BONTEMPS (2011). Niches of Temperate Tree Species Converge towards Nutrient-Richer Conditions over Ontogeny. *Oikos*, 120(10), 1479–1488. doi:10.1111/j.1600-0706.2011.19582.x.
- BIGING, G. S. and M. DOBBERTIN (1992). A Comparison of Distance-Dependent Competition Measures for Height and Basal Area Growth of Individual Conifer Trees. *Forest Science*, 38(3), 695–720. arXiv:<https://academic.oup.com/forestscience/article-pdf/38/3/695/22544552/forestscience0695.pdf>, doi:10.1093/forestscience/38.3.695.
- BOHN, U. and G. GOLLUB (2006). The Use And Application Of The Map Of The Natural Vegetation Of Europe With Particular Reference To Germany. *Biology and Environment: Proceedings of the Royal Irish Academy*, 106B(3), 199–213. arXiv:20728594.
- BOHNER, T. and J. DIEZ (2019). Extensive Mismatches between Species Distributions and Performance and Their Relationship to Functional Traits. *Ecology Letters*, ele.13396. doi:10.1111/ele.13396.
- BOISVERT-MARSH, L., C. PÉRIÉ, and S. DE BLOIS (2014). Shifting with Climate? Evidence for Recent Changes in Tree Species Distribution at High Latitudes. *Ecosphere*, 5(7), art83. doi:10.1890/ES14-00111.1.
- BRISCOE, N. J., J. ELITH, R. SALGUERO-GÓMEZ, J. J. LAHOZ-MONFORT, J. S. CAMAC, K. M. GILJOHANN, M. H. HOLDEN, B. A. HRADSKY, M. R. KEARNEY, S. M. MCMAHON, B. L. PHILLIPS, T. J. REGAN, J. R. RHODES, P. A. VESK, B. A. WINTLE, J. D. L. YEN, and G. GUILLERA-ARROITA (2019). Forecasting Species Range Dynamics with Process-Explicit Models: Matching Methods to Applications. *Ecology Letters*, 22(11), 1940–1956. doi:10.1111/ele.13348.

- BRONCANO, M. J., M. VILÀ, and M. BOADA (2005). Evidence of *Pseudotsuga Menziesii* Naturalization in Montane Mediterranean Forests. *Forest Ecology and Management*, **211**(3), 257–263. doi:10.1016/j.foreco.2005.02.055.
- BROOKS, M. E., K. KRISTENSEN, K. J. VAN BENTHEM, A. MAGNUSSON, C. W. BERG, A. NIELSEN, H. J. SKAUG, M. MAECHLER, and B. M. BOLKER (2017). glmmTMB Balances Speed and Flexibility among Packages for Zero-Inflated Generalized Linear Mixed Modeling. *The R Journal*, **9**(2), 378–400.
- BRUNO, J. F., J. J. STACHOWICZ, and M. D. BERTNESS (2003). Inclusion of Facilitation into Ecological Theory. *Trends in Ecology & Evolution*, **18**(3), 119–125. doi:10.1016/S0169-5347(02)00045-9.
- BUCKLEY, L. B., M. C. URBAN, M. J. ANGILLETTA, L. G. CROZIER, L. J. RISSLER, and M. W. SEARS (2010). Can Mechanism Inform Species' Distribution Models? *Ecology Letters*, **13**(8), 1041–1054. doi:10.1111/j.1461-0248.2010.01479.x.
- BUGMANN, H. K. M. and A. M. SOLOMON (2000). Explaining Forest Composition and Biomass across Multiple Biogeographical Regions. *Ecological Applications*, **10**(1), 95–114. doi:10.1890/1051-0761(2000)010[0095:EFCABA]2.0.CO;2.
- BURAS, A., C. SCHUNK, C. ZEITRÄG, C. HERRMANN, L. KAISER, H. LEMME, C. STRAUB, S. TAEGER, S. GÖSSWEIN, H.-J. KLEMMT, and A. MENZEL (2018). Are Scots Pine Forest Edges Particularly Prone to Drought-Induced Mortality? *Environmental Research Letters*, **13**(2), 025001. doi:10.1088/1748-9326/aaa0b4.
- BURDEN, R. and J. FAIRES (1993). *Numerical Analysis*. Mathematics Series. PWS-Kent Publishing Company, Whitstable.
- CAILLERET, M., N. BIRCHER, F. HARTIG, H. BUGMANN, and L. HU (2020). Bayesian Calibration of a Growth-dependent Tree Mortality Model to Simulate the Dynamics of European Temperate Forests. *Ecological Applications*, **30**(1), 17.
- CANHAM, C. D. (1989). Different Responses to Gaps Among Shade-tolerant Tree Species. *Ecology*, **70**(3), 548–550. doi:10.2307/1940200.
- CANHAM, C. D., R. K. KOBE, E. F. LATTY, and R. L. CHAZDON (1999). Interspecific and Intraspecific Variation in Tree Seedling Survival: Effects of Allocation to Roots versus Carbohydrate Reserves. *Oecologia*, **121**(1), 1–11. doi:10.1007/s004420050900.
- CAVENDER-BARES, J. and F. A. BAZZAZ (2000). Changes in Drought Response Strategies with Ontogeny in *Quercus Rubra*: Implications for Scaling from Seedlings to Mature Trees. *Oecologia*, **124**(1), 8–18. doi:10.1007/PL00008865.
- CHEN, I.-C., J. K. HILL, R. OHLEMULLER, D. B. ROY, and C. D. THOMAS (2011). Rapid Range Shifts of Species Associated with High Levels of Climate Warming. *Science*, **333**(6045), 1024–1026. doi:10.1126/science.1206432.
- CLARK, J. S., C. L. SCHER, and M. SWIFT (2020). The Emergent Interactions That Govern Biodiversity Change. *Proceedings of the National Academy of Sciences*, **117**(29), 17074–17083. doi:10.1073/pnas.2003852117.

- CLEMENTS, F. E., H. C. HANSON, and J. E. WEAVER (1929). *Plant Competition; an Analysis of Community Functions*, volume XVI of *Carnegie Institution of Washington Publication*. Carnegie Institution of Washington, Washington.
- COOMES, D. A. and R. B. ALLEN (2007). Effects of Size, Competition and Altitude on Tree Growth. *Journal of Ecology*, **95**(5), 1084–1097. doi:10.1111/j.1365-2745.2007.01280.x.
- COOMES, D. A. and P. J. GRUBB (2000). Impacts of Root Competition in Forests and Woodlands: A Theoretical Framework and Review of Experiments. *Ecological Monographs*, **70**(2), 171–207. doi:10.1890/0012-9615(2000)070[0171:IORCIF]2.0.CO;2.
- COPENHAVER-PARRY, P. E., C. J. W. CARROLL, P. H. MARTIN, and M. V. TALLUTO (2020a). Multi-scale Integration of Tree Recruitment and Range Dynamics in a Changing Climate. *Global Ecology and Biogeography*, **29**(1), 102–116. doi:10.1111/geb.13012.
- COPENHAVER-PARRY, P. E., C. J. W. CARROLL, P. H. MARTIN, and M. V. TALLUTO (2020b). Multi-scale Integration of Tree Recruitment and Range Dynamics in a Changing Climate. *Global Ecology and Biogeography*, **29**(1), 102–116. doi:10.1111/geb.13012.
- CORDONNIER, T., C. SMADI, G. KUNSTLER, and B. COURBAUD (2019). Asymmetric Competition, Ontogenetic Growth and Size Inequality Drive the Difference in Productivity between Two-Strata and One-Stratum Forest Stands. *Theoretical Population Biology*, **130**, 83–93. doi:10.1016/j.tpb.2019.07.001.
- CRIMMINS, S. M., S. Z. DOBROWSKI, J. A. GREENBERG, J. T. ABATZOGLOU, and A. R. MYNSBERGE (2011). Changes in Climatic Water Balance Drive Downhill Shifts in Plant Species' Optimum Elevations. *Science*, **331**(6015), 324–327. doi:10.1126/science.1199040.
- CUDLÍN, P., R. TOGNETTI, F. MALIS, C. ALADOS, P. BEBI, K. GRUNEWALD, M. ZHIYANSKI, V. ANDONOWSKI, N. LA PORTA, S. BRATANOVA-DONCHEVA, E. KACHAUNOVA, M. EDWARDS-JONÁŠOVÁ, J. NINOT, A. RIGLING, A. HOFGAARD, T. HLÁSNY, P. SKALÁK, and F. WIELGOLASKI (2017). Drivers of Treeline Shift in Different European Mountains. *Climate Research*, **73**(1-2), 135–150. doi:10.3354/cr01465.
- DAMGAARD, C. (2019). A Critique of the Space-for-Time Substitution Practice in Community Ecology. *Trends in Ecology & Evolution*, **34**(5), 416–421. doi:10.1016/j.tree.2019.01.013.
- DE LOMBAERDE, E., K. VERHEYEN, H. VAN CALSTER, and L. BAETEN (2019). Tree Regeneration Responds More to Shade Casting by the Overstorey and Competition in the Understorey than to Abundance per Se. *Forest Ecology and Management*, **450**, 117492. doi:10.1016/j.foreco.2019.117492.
- DE RIGO, D., G. CAUDULLO, T. HOUSTON DURRANT, and J. SAN-MIGUEL-AYANZ (2016). *The European Atlas of Forest Tree Species: Modelling, Data and Information on Forest Tree Species*, e01aa69+. Publications Office of the European Union, Luxembourg.
- DIN, Q. (2013). Dynamics of a Discrete Lotka-Volterra Model. *Advances in Difference Equations*, **2013**(95), 1–13. doi:10.1186/1687-1847-2013-95.

- DORMANN, C. F., S. J. SCHYMANSKI, J. CABRAL, I. CHUINE, C. GRAHAM, F. HARTIG, M. KEARNEY, X. MORIN, C. RÖMERMANN, B. SCHRÖDER, and A. SINGER (2012b). Correlation and Process in Species Distribution Models: Bridging a Dichotomy. *Journal of Biogeography*, **39**(12), 2119–2131. doi:10.1111/j.1365-2699.2011.02659.x.
- DORMANN, C. F., S. J. SCHYMANSKI, J. CABRAL, I. CHUINE, C. GRAHAM, F. HARTIG, M. KEARNEY, X. MORIN, C. RÖMERMANN, B. SCHRÖDER, and A. SINGER (2012a). Correlation and Process in Species Distribution Models: Bridging a Dichotomy: Bridging the Correlation-Process Dichotomy. *Journal of Biogeography*, **39**(12), 2119–2131. doi:10.1111/j.1365-2699.2011.02659.x.
- DOUNAVI, A., N. KOUTSIAS, M. ZIEHE, and H. H. HATTEMER (2010). Spatial Patterns and Genetic Structures within Beech Populations (*Fagus Sylvatica* L.) of Forked and Non-Forked Individuals. *European Journal of Forest Research*, **129**(6), 1191–1202. doi:10.1007/s10342-010-0409-9.
- DU, H., J. LIU, M.-H. LI, U. BÜNTGEN, Y. YANG, L. WANG, Z. WU, and H. S. HE (2018). Warming-induced Upward Migration of the Alpine Treeline in the Changbai Mountains, Northeast China. *Global Change Biology*, **24**(3), 1256–1266. doi:10.1111/gcb.13963.
- ELLENBERG, H. (1952). Physiologisches Und Ökologisches Verhalten Derselben Pflanzenarten. *Berichte der Deutschen Botanischen Gesellschaft*, **65**(10), 350–361. doi:10.1111/j.1438-8677.1953.tb00671.x.
- ELLENBERG, H. (1963). *Vegetation Mitteleuropas Mit Den Alpen*. In *Kausaler, Dynamischer Und Historischer Sicht.*, volume IV/2 of *Einführung in Die Phytologie*. Ulmer, Stuttgart, first edition.
- ELLNER, S. (1984). Asymptotic Behavior of Some Stochastic Difference Equation Population Models. *Journal Of Mathematical Biology*, **19**(2), 169–200. doi:10.1007/BF00277745.
- EMBOG, J. (1998). Understorey Light Conditions and Regeneration with Respect to the Structural Dynamics of a Near-Natural Temperate Deciduous Forest in Denmark. *Forest Ecology and Management*, **106**(2-3), 83–95. doi:10.1016/S0378-1127(97)00299-5.
- ERIKSSON, O. (2002). Ontogenetic Niche Shifts and Their Implications for Recruitment in Three Clonal *Vaccinium* Shrubs: *Vaccinium Myrtillus*, *Vaccinium Vitis-Idaea*, and *Vaccinium Oxycoccus*. *Canadian Journal of Botany*, **80**, 635–641. doi:10.1139/b02-044.
- EWALD, J. (2007). Ein pflanzensoziologisches Modell der Schattentoleranz von Baumarten in den Bayerischen Alpen - A Phytosociological Model of Shade Tolerance of Tree Species in the Bavarian Alps. *Forum geobotanicum*, **3**. doi:10.3264/FG.2007.0803.
- FEEHAN, J., M. HARLEY, and J. MINNEN (2009). Climate Change in Europe. 1. Impact on Terrestrial Ecosystems and Biodiversity. A Review. *Agronomy for Sustainable Development*, **29**(3), 409–421. doi:10.1051/agro:2008066.
- FERNER, E., H. RENNENBERG, and J. KREUZWIESER (2012). Effect of Flooding on C Metabolism of Flood-Tolerant (*Quercus Robur*) and Non-Tolerant (*Fagus Sylvatica*) Tree Species. *Tree Physiology*, **32**(2), 135–145. doi:10.1093/treephys/tps009.

- FERRARI, S. and F. CRIBARI-NETO (2004). Beta Regression for Modelling Rates and Proportions. *Journal of Applied Statistics*, **31**(7), 799–815. doi:10.1080/0266476042000214501.
- FICHTNER, A., K. STURM, C. RICKERT, W. HÄRDTLE, and J. SCHRAUTZER (2012). Competition Response of European Beech *Fagus Sylvatica* L. Varies with Tree Size and Abiotic Stress: Minimizing Anthropogenic Disturbances in Forests. *Journal of Applied Ecology*, **49**(6), 1306–1315. doi:10.1111/j.1365-2664.2012.02196.x.
- FLOYD, A. G. (1990). *Australian Rainforests in New South Wales*. Surrey Beatty & Sons, Chipping Norton.
- FRIDMAN, J., S. HOLM, M. NILSSON, P. NILSSON, A. RINGVALL, and G. STÅHL (2014). Adapting National Forest Inventories to Changing Requirements – the Case of the Swedish National Forest Inventory at the Turn of the 20th Century. *Silva Fennica*, **48**(3). doi:10.14214/sf.1095.
- GABRY, J. and R. ČEŠNOVAR (2021). Cmdstanr: R Interface to CmdStan. <https://mc-stan.org/cmdstanr/reference/index.html>.
- GATSUK, L. E., O. V. SMIRNOVA, L. I. VORONTZOVA, L. B. ZAUGOLNOVA, and L. A. ZHUKOVA (1980). Age States of Plants of Various Growth Forms: A Review. *The Journal of Ecology*, **68**(2), 675. arXiv:2259429, doi:10.2307/2259429.
- GAUSE, G. F. (1932). Experimental Studies on the Struggle for Existence: I. Mixed Population of Two Species of Yeast. *Journal of experimental biology*, **9**(4), 389–402. doi:10.1242/jeb.9.4.389.
- GEUDENS, G., J. STAELENS, V. KINT, R. GORIS, and N. LUST (2004). Allometric Biomass Equations for Scots Pine (*Pinus Sylvestris* L.) Seedlings during the First Years of Establishment in Dense Natural Regeneration. *Annals of Forest Science*, **61**(7), 653–659. doi:10.1051/forest:2004067.
- GIBSON-REINEMER, D. K. and F. J. RAHEL (2015). Inconsistent Range Shifts within Species Highlight Idiosyncratic Responses to Climate Warming. *PLOS ONE*, **10**(7), e0132103. doi:10.1371/journal.pone.0132103.
- GIVNISH, T. (1988). Adaptation to Sun and Shade: A Whole-Plant Perspective. *Functional Plant Biology*, **15**(2), 63. doi:10.1071/PP9880063.
- GOLDBERG, D. E. (1996). Competitive Ability: Definitions, Contingency and Correlated Traits. *Philosophical Transactions of the Royal Society of London. Series B: Biological Sciences*, **351**(1345), 1377–1385. doi:10.1098/rstb.1996.0121.
- GOLDBERG, D. E. and A. M. BARTON (1992). Patterns and Consequences of Interspecific Competition in Natural Communities: A Review of Field Experiments with Plants. *The American Naturalist*, **139**(4), 771–801. doi:10.1086/285357.
- GOLDBERG, D. E. and K. LANDA (1991). Competitive Effect and Response: Hierarchies and Correlated Traits in the Early Stages of Competition. *The Journal of Ecology*, **79**(4), 1013. arXiv:2261095, doi:10.2307/2261095.

- GRIME, J. P. (2001). *Plant Strategies: Vegetation Processes and Ecosystem Properties*. Wiley, Chichester, second edition.
- GRUBB, P. J. (1977). Maintenance of Species-Richness in Plant Communities - Importance of Regeneration Niche. *Biological Reviews of the Cambridge Philosophical Society*, **52**(1), 107–145. doi:10.1111/j.1469-185X.1977.tb01347.x.
- GUENNEBAUD, G. and B. JACOB (2010). Eigen V3.
- GUISAN, A., N. E. ZIMMERMANN, J. ELITH, C. H. GRAHAM, S. PHILLIPS, and A. T. PETERSON (2007). What Matters for Predicting The Occurrences of Trees: Techniques, Data, or Species' Characteristics? *Ecological Monographs*, **77**(4), 615–630. doi:10.1890/06-1060.1.
- HANBURY-BROWN, A. R., R. E. WARD, and L. M. KUEPPERS (2022). Forest Regeneration within Earth System Models: Current Process Representations and Ways Forward. *New Phytologist*, nph.18131. doi:10.1111/nph.18131.
- HÄRDITZ, W., G. VON OHEIMB, A. FRIEDEL, H. MEYER, and C. WESTPHAL (2004). Relationship between pH-values and Nutrient Availability in Forest Soils – the Consequences for the Use of Ecograms in Forest Ecology. *Flora - Morphology, Distribution, Functional Ecology of Plants*, **199**(2), 134–142. doi:10.1078/0367-2530-00142.
- HARGREAVES, G. H. (1994). Defining and Using Reference Evapotranspiration. *Journal of Irrigation and Drainage Engineering*, **120**(6), 1132–1139. doi:10.1061/(ASCE)0733-9437(1994)120:6(1132).
- HART, T. B. (1995). Seed, Seedling and Sub-Canopy Survival in Monodominant and Mixed Forests of the Ituri Forest, Africa. *Journal of Tropical Ecology*, **11**(3), 443–459. arXiv:2560227.
- HARTIG, F. (2020). DHARMA: Residual Diagnostics for Hierarchical (Multi-Level / Mixed) Regression Models. <http://florianhartig.github.io/DHARMA/>.
- HARTIG, F., C. DISLICH, T. WIEGAND, and A. HUTH (2014). Technical Note: Approximate Bayesian Parameterization of a Process-Based Tropical Forest Model. *Biogeosciences*, **11**(4), 1261–1272. doi:10.5194/bg-11-1261-2014.
- HARTIG, F., J. DYKE, T. HICKLER, S. I. HIGGINS, R. B. O'HARA, S. SCHEITER, and A. HUTH (2012). Connecting Dynamic Vegetation Models to Data - an Inverse Perspective. *Journal of Biogeography*, **39**(12), 2240–2252. doi:10.1111/j.1365-2699.2012.02745.x.
- HEILAND, L., G. KUNSTLER, P. RUIZ-BENITO, A. BURAS, J. DAHLGREN, and L. HÜLSMANN (2022). Divergent Occurrences of Juvenile and Adult Trees Are Explained by Both Environmental Change and Ontogenetic Effects. *Ecography*, **2022**(3), e06042. doi:10.1111/ecog.06042.
- HEILAND, L., G. KUNSTLER, V. ŠEBEŇ, and L. HÜLSMANN (2023). Which Demographic Processes Control Competitive Equilibria? Bayesian Calibration of a Size-Structured Forest Population Model. *Ecology and Evolution*.

- HIGGINS, S. I., R. B. O'HARA, O. BYKOVA, M. D. CRAMER, I. CHUINE, E.-M. GERSTNER, T. HICKLER, X. MORIN, M. R. KEARNEY, G. F. MIDGLEY, and S. SCHEITER (2012). A Physiological Analogy of the Niche for Projecting the Potential Distribution of Plants. *Journal of Biogeography*, **39**(12), 2132–2145. doi:10.1111/j.1365-2699.2012.02752.x.
- HIJMANS, R. J. (2020). Raster: Geographic Data Analysis and Modeling. <https://CRAN.R-project.org/package=raster>.
- HODGSON, J. G., J. P. GRIME, P. J. WILSON, K. THOMPSON, and S. R. BAND (2005). The Impacts of Agricultural Change (1963–2003) on the Grassland Flora of Central England: Processes and Prospects. *Basic and Applied Ecology*, **6**(2), 107–118. doi:10.1016/j.baae.2005.01.009.
- HUTCHINSON, G. E. (1957). Concluding Remarks. *Cold Spring Harbor Symposia on Quantitative Biology*, **22**(0), 415–427. doi:10.1101/sqb.1957.022.01.039.
- JANSEN, S. and T. GEBUREK (2016). Historic Translocations of European Larch (*Larix Decidua* Mill.) Genetic Resources across Europe – A Review from the 17th until the Mid-20th Century. *Forest Ecology and Management*, **379**, 114–123. doi:10.1016/j.foreco.2016.08.007.
- JULIO CAMARERO, J. and E. GUTIÉRREZ (2007). Response of *Pinus Uncinata* Recruitment to Climate Warming and Changes in Grazing Pressure in an Isolated Population of the Iberian System (NE Spain). *Arctic, Antarctic, and Alpine Research*, **39**(2), 210–217. doi:10.1657/1523-0430(2007)39[210:ROPURT]2.0.CO;2.
- KÄBER, Y., P. MEYER, J. STILLHARD, E. DE LOMBAERDE, J. ZELL, G. STADELMANN, H. BUGMANN, and C. BIGLER (2021). Tree Recruitment Is Determined by Stand Structure and Shade Tolerance with Uncertain Role of Climate and Water Relations. *Ecology and Evolution*, ece3.7984. doi:10.1002/ece3.7984.
- KANGAS, A. and M. MALTAMO (2006). *Forest Inventory. Methodology and Applications*. Number 10 in Managing Forest Ecosystems. Springer, Dordrecht.
- KARGER, D. N., O. CONRAD, J. BÖHNER, T. KAWOHL, H. KREFT, R. W. SORIA-AUZA, N. E. ZIMMERMANN, H. P. LINDER, and M. KESSLER (2017). Climatologies at High Resolution for the Earth's Land Surface Areas. *Scientific Data*, **4**(1), 170122. doi:10.1038/sdata.2017.122.
- KEDDY, P. A. (2001). *Competition*. Number v. 26 in Population and Community Biology Series. Kluwer Academic Publishers, Dordrecht ; Boston, second edition.
- KITAJIMA, K. (1994). Relative Importance of Photosynthetic Traits and Allocation Patterns as Correlates of Seedling Shade Tolerance of 13 Tropical Trees. *Oecologia*, **98**(3-4), 419–428. doi:10.1007/BF00324232.
- KNAPP, H. (2008). *Naturerbe Buchenwälder: Situationsanalyse Und Handlungserfordernisse*. Number 240 in BfN-Skripten. Bundesamt für Naturschutz, Bonn.
- KNOERZER, D. (1999). *Zur Naturverjüngung der Douglasie im Schwarzwald: Inventur und Analyse von Umwelt- und Konkurrenzfaktoren sowie eine naturschutzfachliche Bewertung*. Number 306 in Dissertationes botanicae. Cramer, Berlin.

- KOBE, R., S. PACALA, J. SILANDER, and C. CANHAM (1995). Juvenile Tree Survivorship as a Component of Shade Tolerance. *Ecological Applications*, 5(2), 517–532. doi:10.2307/1942040.
- KÖNIG, L. A., F. MOHREN, M.-J. SCHELHAAS, H. BUGMANN, and G.-J. NABUURS (2022). Tree Regeneration in Models of Forest Dynamics – Suitability to Assess Climate Change Impacts on European Forests. *Forest Ecology and Management*, 520, 120390. doi:10.1016/j.foreco.2022.120390.
- KORZUKHIN, M. D., M. T. TER-MIKAELIAN, and R. G. WAGNER (1996). Process versus Empirical Models: Which Approach for Forest Ecosystem Management? *Canadian Journal of Forest Research*, 26(5), 879–887. doi:10.1139/x26-096.
- KOTTEK, M., J. GRIESER, C. BECK, B. RUDOLF, and F. RUBEL (2006). World Map of the Köppen-Geiger Climate Classification Updated. *Meteorologische Zeitschrift*, 15(3), 259–263. doi:10.1127/0941-2948/2006/0130.
- KUNSTLER, G., D. A. COOMES, and C. D. CANHAM (2009). Size-Dependence of Growth and Mortality Influence the Shade Tolerance of Trees in a Lowland Temperate Rain Forest. *Journal of Ecology*, 97(4), 685–695. doi:10.1111/j.1365-2745.2009.01482.x.
- KUNSTLER, G., T. CURT, M. BOUCHAUD, and J. LEPART (2005). Growth, Mortality, and Morphological Response of European Beech and Downy Oak along a Light Gradient in Sub-Mediterranean Forest. *Canadian Journal of Forest Research*, 35(7), 1657–1668. doi:10.1139/x05-097.
- KUNSTLER, G., A. GUYENNON, S. RATCLIFFE, N. RÜGER, P. RUIZ-BENITO, D. Z. CHILDS, J. DAHLGREN, A. LEHTONEN, W. THUILLER, C. WIRTH, M. A. ZAVALA, and R. SALGUERO-GOMEZ (2021). Demographic Performance of European Tree Species at Their Hot and Cold Climatic Edges. *Journal of Ecology*, 109(2), 1041–1054. doi:10.1111/1365-2745.13533.
- KUNSTLER, G., W. THUILLER, T. CURT, M. BOUCHAUD, R. JOUVIE, F. DERUETTE, and J. LEPART (2007). *Fagus Sylvatica* L. Recruitment across a Fragmented Mediterranean Landscape, Importance of Long Distance Effective Dispersal, Abiotic Conditions and Biotic Interactions: *Fagus Sylvatica* L. Recruitment across a Fragmented Mediterranean Landscape. *Diversity and Distributions*, 13(6), 799–807. doi:10.1111/j.1472-4642.2007.00404.x.
- LARCHER, W. (2003). *Physiological Plant Ecology: Ecophysiology and Stress Physiology of Functional Groups*, volume 4. Springer, Berlin.
- LENOIR, J., J.-C. GÉGOUT, A. GUISAN, P. VITTOZ, T. WOHLGEMUTH, N. E. ZIMMERMANN, S. DULLINGER, H. PAULI, W. WILLNER, and J.-C. SVENNING (2010). Going against the Flow: Potential Mechanisms for Unexpected Downslope Range Shifts in a Warming Climate. *Ecography*, 33, 295–303. doi:10.1111/j.1600-0587.2010.06279.x.
- LENOIR, J., J. C. GEGOUT, P. A. MARQUET, P. DE RUFFRAY, and H. BRISSE (2008). A Significant Upward Shift in Plant Species Optimum Elevation During the 20th Century. *Science*, 320(5884), 1768–1771. doi:10.1126/science.1156831.

- LENOIR, J., J.-C. GÉGOUT, J.-C. PIERRAT, J.-D. BONTEMPS, and J.-F. DHÔTE (2009). Differences between Tree Species Seedling and Adult Altitudinal Distribution in Mountain Forests during the Recent Warm Period (1986–2006). *Ecography*, **32**(5), 765–777. doi:10.1111/j.1600-0587.2009.05791.x.
- LEUSCHNER, C. (2020). Drought Response of European Beech (*Fagus Sylvatica* L.)—A Review. *Perspectives in Plant Ecology, Evolution and Systematics*, **47**, 125576. doi:10.1016/j.ppees.2020.125576.
- LEUSCHNER, C. and H. ELLENBERG (2017a). *Ecology of Central European Forests: Vegetation Ecology of Central Europe, Volume I*. Springer International Publishing, Cham. doi:10.1007/978-3-319-43042-3.
- LEUSCHNER, C. and H. ELLENBERG (2017b). *Ecology of Central European Non-Forest Vegetation: Coastal to Alpine, Natural to Man-Made Habitats: Vegetation Ecology of Central Europe, Volume II*. Springer International Publishing, Cham. doi:10.1007/978-3-319-43048-5.
- LEUSCHNER, C. and I. C. MEIER (2018). The Ecology of Central European Tree Species: Trait Spectra, Functional Trade-Offs, and Ecological Classification of Adult Trees. *Perspectives in Plant Ecology, Evolution and Systematics*, **33**, 89–103. doi:10.1016/j.ppees.2018.05.003.
- LEVINE, J. M. and M. REES (2004). Effects of Temporal Variability on Rare Plant Persistence in Annual Systems. *The American Naturalist*, **164**(3), 350–363. doi:10.1086/422859.
- LINDNER, M., M. MAROSCHEK, S. NETHERER, A. KREMER, A. BARBATI, J. GARCIA-GONZALO, R. SEIDL, S. DELZON, P. CORONA, M. KOLSTRÖM, M. J. LEXER, and M. MARCHETTI (2010). Climate Change Impacts, Adaptive Capacity, and Vulnerability of European Forest Ecosystems. *Forest Ecology and Management*, **259**(4), 698–709. doi:10.1016/j.foreco.2009.09.023.
- LINES, E. R., M. A. ZAVALA, D. W. PURVES, and D. A. COOMES (2012). Predictable Changes in Aboveground Allometry of Trees along Gradients of Temperature, Aridity and Competition: Predictable Variation in Tree Aboveground Allometry. *Global Ecology and Biogeography*, **21**(10), 1017–1028. doi:10.1111/j.1466-8238.2011.00746.x.
- LINES, E. R., M. A. ZAVALA, P. RUIZ-BENITO, and D. A. COOMES (2019). Capturing Juvenile Tree Dynamics from Count Data Using Approximate Bayesian Computation. *Ecography*, ecog.04824. doi:10.1111/ecog.04824.
- LORTIE, C. J., R. W. BROOKER, P. CHOLER, Z. KIKVIDZE, R. MICHALET, F. I. PUGNAIRE, and R. M. CALLAWAY (2004). Rethinking Plant Community Theory. *Oikos*, **107**(2), 433–438. doi:10.1111/j.0030-1299.2004.13250.x.
- LUNDQVIST, L. (1995). Simulation of Sapling Population Dynamics in Uneven-aged *Picea Abies* Forests. *Annals of Botany*, **76**(4), 371–380. doi:10.1006/anbo.1995.1110.

- LUSK, C. H. (2004). Leaf Area and Growth of Juvenile Temperate Evergreens in Low Light: Species of Contrasting Shade Tolerance Change Rank during Ontogeny. *Functional Ecology*, **18**(6), 820–828. doi:10.1111/j.0269-8463.2004.00897.x.
- MACARTHUR, R. H. (1972). *Geographical Ecology: Patterns in the Distribution of Species*. Harper & Row, New York.
- MAGRI, D. (2008). Patterns of Post-Glacial Spread and the Extent of Glacial Refugia of European Beech (*Fagus Sylvatica*). *Journal of Biogeography*, **35**(3), 450–463. doi:10.1111/j.1365-2699.2007.01803.x.
- MAGUIRE, B. (1973). Niche Response Structure and the Analytical Potentials of Its Relationship to the Habitat. *The American Naturalist*, **107**(954), 213–246. arXiv:2459795, doi:10.1086/282827.
- MALCHOW, A.-K., F. HARTIG, J. REEG, M. KÉRY, and D. ZURELL (2022). Demography-Environment Relationships Improve Mechanistic Understanding of Range Dynamics under Climate Change. Preprint, Ecology. doi:10.1101/2022.09.23.509134.
- MÁLIŠ, F., M. KOPECKÝ, P. PETŘÍK, J. VLADOVIČ, J. MERGANIČ, and T. VIDA (2016). Life Stage, Not Climate Change, Explains Observed Tree Range Shifts. *Global Change Biology*, **22**(5), 1904–1914. doi:10.1111/gcb.13210.
- MARÉCHAUX, I., F. LANGERWISCH, A. HUTH, H. BUGMANN, X. MORIN, C. P. REYER, R. SEIDL, A. COLLALTI, M. DANTAS DE PAULA, R. FISCHER, M. GUTSCH, M. J. LEXER, H. LISCHKE, A. RAMMIG, E. RÖDIG, B. SAKSCHEWSKI, F. TAUBERT, K. THONICKE, G. VACCHIANO, and F. J. BOHN (2021). Tackling Unresolved Questions in Forest Ecology: The Past and Future Role of Simulation Models. *Ecology and Evolution*, ece3.7391. doi:10.1002/ece3.7391.
- MATHYS, A., N. COOPS, S. SIMARD, R. WARING, and S. AITKEN (2018). Diverging Distribution of Seedlings and Mature Trees Reflects Recent Climate Change in British Columbia. *Ecological Modelling*, **384**, 145–153. doi:10.1016/j.ecolmodel.2018.06.008.
- MCGRATH, M. J., S. LUYSSAERT, P. MEYFROIDT, J. O. KAPLAN, M. BÜRGI, Y. CHEN, K. ERB, U. GIMMI, D. MCINERNEY, K. NAUDTS, J. OTTO, F. PASZTOR, J. RYDER, M.-J. SCHELHAAS, and A. VALADE (2015). Reconstructing European Forest Management from 1600 to 2010. *Biogeosciences*, **12**(14), 4291–4316. doi:10.5194/bg-12-4291-2015.
- MEIER, E. S., T. C. EDWARDS JR, F. KIENAST, M. DOBBERTIN, and N. E. ZIMMERMANN (2011). Co-Occurrence Patterns of Trees along Macro-Climatic Gradients and Their Potential Influence on the Present and Future Distribution of *Fagus Sylvatica* L.: Influence of Co-Occurrence Patterns on *Fagus Sylvatica*. *Journal of Biogeography*, **38**(2), 371–382. doi:10.1111/j.1365-2699.2010.02405.x.
- MELLERT, K. H., J. EWALD, D. HORNSTEIN, I. DORADO-LIÑÁN, M. JANTSCH, S. TAEGER, C. ZANG, A. MENZEL, and C. KÖLLING (2016). Climatic Marginality: A New Metric for the Susceptibility of Tree Species to Warming Exemplified by *Fagus Sylvatica* (L.) and Ellenberg's Quotient. *European Journal of Forest Research*, **135**(1), 137–152. doi:10.1007/s10342-015-0924-9.

- MEROW, C., A. M. LATIMER, A. M. WILSON, S. M. McMAHON, A. G. REBELO, and J. A. SILANDER (2014). On Using Integral Projection Models to Generate Demographically Driven Predictions of Species' Distributions: Development and Validation Using Sparse Data. *Ecography*, **37**(12), 1167–1183. doi:10.1111/ecog.00839.
- MILLERÓN, M., U. LÓPEZ DE HEREDIA, Z. LORENZO, J. ALONSO, A. DOUNAVI, L. GIL, and N. NANOS (2013). Assessment of Spatial Discordance of Primary and Effective Seed Dispersal of European Beech (*Fagus Sylvatica* L.) by Ecological and Genetic Methods. *Molecular Ecology*, **22**(6), 1531–1545. doi:10.1111/mec.12200.
- MIRITI, M. N. (2006). Ontogenetic Shift from Facilitation to Competition in a Desert Shrub. *Journal of Ecology*, **94**(5), 973–979. doi:10.1111/j.1365-2745.2006.01138.x.
- MONLEON, V. J. and H. E. LINTZ (2015). Evidence of Tree Species' Range Shifts in a Complex Landscape. *PLOS ONE*, **10**(1), e0118069. doi:10.1371/journal.pone.0118069.
- MORENO, A., M. NEUMANN, and H. HASENAUER (2018). Climate Limits on European Forest Structure across Space and Time. *Global and Planetary Change*, **169**, 168–178. doi:10.1016/j.gloplacha.2018.07.018.
- MORIN, X. and W. THUILLER (2009). Comparing Niche- and Process-Based Models to Reduce Prediction Uncertainty in Species Range Shifts under Climate Change. *Ecology*, **90**(5), 1301–1313. doi:10.1890/08-0134.1.
- MÜLLEROVÁ, J., R. HÉDL, and P. SZABÓ (2015). Coppice Abandonment and Its Implications for Species Diversity in Forest Vegetation. *Forest Ecology and Management*, **343**, 88–100. doi:10.1016/j.foreco.2015.02.003.
- NESTBY, R. D. J. (2020). The Status of *Prunus Padus* L. (Bird Cherry) in Forest Communities throughout Europe and Asia. *Forests*, **11**(5), 497. doi:10.3390/f11050497.
- NI, M. and M. VELLEND (2021). Space-for-time Inferences about Range-edge Dynamics of Tree Species Can Be Influenced by Sampling Biases. *Global Change Biology*, gcb.15524. doi:10.1111/gcb.15524.
- NIINEMETS, U. (2006). The Controversy over Traits Conferring Shade-Tolerance in Trees: Ontogenetic Changes Revisited. *Journal of Ecology*, **94**(2), 464–470. doi:10.1111/j.1365-2745.2006.01093.x.
- NIKLAS, K. J. and E. D. COBB (2010). Ontogenetic Changes in the Numbers of Short- vs. Long-Shoots Account for Decreasing Specific Leaf Area in *Acer Rubrum* (Aceraceae) as Trees Increase in Size. *American Journal of Botany*, **97**(1), 27–37. doi:10.3732/ajb.0900249.
- NORMAND, S., N. E. ZIMMERMANN, F. M. SCHURR, and H. LISCHKE (2014). Demography as the Basis for Understanding and Predicting Range Dynamics. *Ecography*, **37**(12), 1149–1154. doi:10.1111/ecog.01490.
- O'SULLIVAN, K. S. W., P. RUIZ-BENITO, J.-C. CHEN, and A. S. JUMP (2020). Onward but Not Always Upward: Individualistic Elevational Shifts of Tree Species in Subtropical Montane Forests. *Ecography*, ecog.05334. doi:10.1111/ecog.05334.

- PAGEL, J. and F. M. SCHURR (2012). Forecasting Species Ranges by Statistical Estimation of Ecological Niches and Spatial Population Dynamics: Statistical Estimation of Dynamic Range Models. *Global Ecology and Biogeography*, **21**(2), 293–304. doi:10.1111/j.1466-8238.2011.00663.x.
- PARISH, J. A. D. and F. A. BAZZAZ (1985). Ontogenetic Niche Shifts in Old-Field Annuals. *Ecology*, **66**(4), 1296–1302. doi:10.2307/1939182.
- PEÑUELAS, J., R. OGAYA, M. BOADA, and A. S. JUMP (2007). Migration, Invasion and Decline: Changes in Recruitment and Forest Structure in a Warming-Linked Shift of European Beech Forest in Catalonia (NE Spain). *Ecography*, **30**(6), 829–837. doi:10.1111/j.2007.0906-7590.05247.x.
- PERRING, M. P., M. BERNHARDT-RÖMERMANN, L. BAETEN, G. MIDOLO, H. BLONDEEL, L. DEPAUW, D. LANDUYT, S. L. MAES, E. DE LOMBAERDE, M. M. CARÓN, M. VEL-LEND, J. BRUNET, M. CHUDOMELOVÁ, G. DECOCQ, M. DIEKMANN, T. DIRNBÖCK, I. DÖRFLER, T. DURAK, P. DE FRENNE, F. S. GILLIAM, R. HÉDL, T. HEINKEN, P. HOMMEL, B. JAROSZEWICZ, K. J. KIRBY, M. KOPECKÝ, J. LENOIR, D. LI, F. MÁLIŠ, F. J. MITCHELL, T. NAAF, M. NEWMAN, P. PETŘÍK, K. RECZYŃSKA, W. SCHMIDT, T. STANDOVÁR, K. ŚWIERKOSZ, H. VAN CALSTER, O. VILD, E. R. WAGNER, M. WULF, and K. VERHEYEN (2018). Global Environmental Change Effects on Plant Community Composition Trajectories Depend upon Management Legacies. *Global Change Biology*, **24**(4), 1722–1740. doi:10.1111/gcb.14030.
- PETRITAN, A. M., B. VON LUPKE, and I. C. PETRITAN (2007). Effects of Shade on Growth and Mortality of Maple (*Acer Pseudoplatanus*), Ash (*Fraxinus Excelsior*) and Beech (*Fagus Sylvatica*) Saplings. *Forestry*, **80**(4), 397–412. doi:10.1093/forestry/cpm030.
- PETROVSKA, R., P. BRANG, A. GESSLER, H. BUGMANN, and M. L. HOBI (2021a). Grow Slowly, Persist, Dominate—Explaining Beech Dominance in a Primeval Forest. *Ecology and Evolution*, ece3.7800. doi:10.1002/ece3.7800.
- PETROVSKA, R., H. BUGMANN, M. L. HOBI, S. GHOSH, and P. BRANG (2021b). Survival Time and Mortality Rate of Regeneration in the Deep Shade of a Primeval Beech Forest. *European Journal of Forest Research*. doi:10.1007/s10342-021-01427-3.
- PICKETT, S. T. A. (1980). Non-Equilibrium Coexistence of Plants. *Bulletin of the Torrey Botanical Club*, **107**(2), 238. arXiv:2484227, doi:10.2307/2484227.
- PIRONON, S., J. VILLELLAS, W. THUILLER, V. ECKHART, M. GEBER, D. A. MOELLER, and M. GARCÍA (2017). The 'Hutchinsonian Niche' as an Assemblage of Demographic Niches: Implications for Species Geographic Ranges. *Ecography*. doi:10.1111/ecog.03414.
- POSCHLOD, P. (2015). *Geschichte der Kulturlandschaft: Entstehungsursachen und Steuerungsfaktoren der Entwicklung der Kulturlandschaft, Lebensraum- und Artenvielfalt in Mitteleuropa; 38 Tabellen*. Ulmer, Stuttgart (Hohenheim).
- PRENTICE, C. I., M. T. SYKES, and W. CRAMER (1993). A Simulation Model for the Transient Effects of Climate Change on Forest Landscapes. *Ecological Modelling*, **65**(1), 51–70. doi:10.1016/0304-3800(93)90126-D.

- PRETZSCH, H., G. SCHÜTZE, and E. UHL (2013). Resistance of European Tree Species to Drought Stress in Mixed *versus* Pure Forests: Evidence of Stress Release by Inter-Specific Facilitation: Drought Stress Release by Inter-Specific Facilitation. *Plant Biology*, **15**(3), 483–495. doi:10.1111/j.1438-8677.2012.00670.x.
- PRICE, D. T., N. E. ZIMMERMANN, P. J. VAN DER MEER, M. J. LEXER, P. LEADLEY, I. T. M. JORRITSMA, J. SCHABER, D. F. CLARK, P. LASCH, S. McNULTY, J. WU, and B. SMITH (2001). Regeneration in Gap Models: Priority Issues for Studying Forest Responses to Climate Change. *Climatic Change*, **51**(3), 475–508. doi:10.1023/A:1012579107129.
- PUTZ, F. and C. CANHAM (1992). Mechanisms of Arrested Succession in Shrublands: Root and Shoot Competition between Shrubs and Tree Seedlings. *Forest Ecology and Management*, **49**(3-4), 267–275. doi:10.1016/0378-1127(92)90140-5.
- QUERO, J. L., L. GÓMEZ-APARICIO, R. ZAMORA, and F. T. MAESTRE (2008). Shifts in the Regeneration Niche of an Endangered Tree (*Acer Opalus* Ssp. *Granatense*) during Ontogeny: Using an Ecological Concept for Application. *Basic and Applied Ecology*, **9**(6), 635–644. doi:10.1016/j.baae.2007.06.012.
- R CORE TEAM (2020). *R: A Language and Environment for Statistical Computing*. R Foundation for Statistical Computing, Vienna, Austria.
- R CORE TEAM (2021). *R: A Language and Environment for Statistical Computing*. R Foundation for Statistical Computing, Vienna, Austria.
- RABASA, S. G., E. GRANDA, R. BENAVIDES, G. KUNSTLER, J. M. ESPELTA, R. OGAYA, JOSEP. PEÑUELAS, M. SCHERER-LORENZEN, W. GIL, W. GRODZKI, S. AMBROZY, J. BERGH, J. A. HÓDAR, R. ZAMORA, and F. VALLADARES (2013). Disparity in Elevational Shifts of European Trees in Response to Recent Climate Warming. *Global Change Biology*, **19**(8), 2490–2499. doi:10.1111/gcb.12220.
- RAMACHANDRAN, A., J. D. HUXLEY, S. McFAUL, L. SCHAUER, J. DIEZ, R. BOONE, T. MADSEN-HEPP, E. McCANN, J. FRANKLIN, D. LOGAN, M. B. ROSE, and M. J. SPASOJEVIC (2023). Integrating Ontogeny and Ontogenetic Dependency into Community Assembly. *Journal of Ecology*, 1365–2745.14132. doi:10.1111/1365-2745.14132.
- RIEDEL, T., P. HENNIG, F. KROIHER, H. POLLEY, F. SCHMITZ, and F. SCHWITZGEBEL (2017). *Die Dritte Bundeswaldinventur (BWI 2012). Inventur- Und Auswertemethoden*. Thünen-Institut, Braunschweig.
- RIPLEY, B. (2022). MASS: Support Functions and Datasets for Venables and Ripley’s MASS. <http://www.stats.ox.ac.uk/pub/MASS4/>.
- ROGERS, R. S. (1978). Forests Dominated by Hemlock (*Tsuga Canadensis*): Distribution as Related to Site and Postsettlement History. *Canadian Journal of Botany*, **56**(7), 843–854. doi:10.1139/b78-096.
- ROSBAKH, S., E. PACINI, M. NEPI, and P. POSCHLOD (2018). An Unexplored Side of Regeneration Niche: Seed Quantity and Quality Are Determined by the Effect of Temperature on Pollen Performance. *Frontiers in Plant Science*, **9**, 1036. doi:10.3389/fpls.2018.01036.

- RUIZ-BENITO, P., L. GÓMEZ-APARICIO, and M. A. ZAVALA (2012). Large-Scale Assessment of Regeneration and Diversity in Mediterranean Planted Pine Forests along Ecological Gradients: Planted Pine Forests in the Mediterranean. *Diversity and Distributions*, **18**(11), 1092–1106. doi:10.1111/j.1472-4642.2012.00901.x.
- RUIZ-BENITO, P., J. MADRIGAL-GONZÁLEZ, S. RATCLIFFE, D. A. COOMES, G. KÄNDLER, A. LEHTONEN, C. WIRTH, and M. A. ZAVALA (2014). Stand Structure and Recent Climate Change Constrain Stand Basal Area Change in European Forests: A Comparison Across Boreal, Temperate, and Mediterranean Biomes. *Ecosystems*, **17**(8), 1439–1454. doi:10.1007/s10021-014-9806-0.
- RUIZ-BENITO, P., S. RATCLIFFE, A. S. JUMP, L. GÓMEZ-APARICIO, J. MADRIGAL-GONZÁLEZ, C. WIRTH, G. KÄNDLER, A. LEHTONEN, J. DAHLGREN, J. KATTGE, and M. A. ZAVALA (2017). Functional Diversity Underlies Demographic Responses to Environmental Variation in European Forests: Tree Diversity and Demography in European Forests. *Global Ecology and Biogeography*, **26**(2), 128–141. doi:10.1111/geb.12515.
- SCHULTZ, E. L., L. HÜLSMANN, M. D. PILLET, F. HARTIG, D. D. BRESHEARS, S. RECORD, J. D. SHAW, R. J. DEROSE, P. A. ZUIDEMA, and M. E. K. EVANS (2022). Climate-driven, but Dynamic and Complex? A Reconciliation of Competing Hypotheses for Species' Distributions. *Ecology Letters*, **25**(1), 38–51. doi:10.1111/ele.13902.
- SCHURR, F. M., J. PAGEL, J. S. CABRAL, J. GROENEVELD, O. BYKOVA, R. B. O'HARA, F. HARTIG, W. D. KISSLING, H. P. LINDER, G. F. MIDGLEY, B. SCHRÖDER, A. SINGER, and N. E. ZIMMERMANN (2012). How to Understand Species' Niches and Range Dynamics: A Demographic Research Agenda for Biogeography. *Journal of Biogeography*, **39**(12), 2146–2162. doi:10.1111/j.1365-2699.2012.02737.x.
- SCHWINNING, S. (1998). Mechanisms Determining the Degree of Size Asymmetry in Competition among Plants. *Oecologia*, **113**, 447–455. doi:10.1007/s004420050397.
- ŠEBEŇ, V. (2017). *Národná Inventarizácia a Monitoring Lesov SR 2015–2016 (Slovak National Forest Inventory)*. *Informácie, Metódy, Výsledky (Information's, Methods, Results)*. National Forest Centre, Zvolen (Slovakia).
- SEEMANN, D., V. BOUFFIER, R. KEHR, A. WULF, T. SCHRÖDER, and J. UNGER (2001). Die Esskastanie (*Castanea sativa* Mill.) in Deutschland und ihre Gefährdung durch den Kastanienrindenkrebs (*Cryphonectria parasitica* [Murr.] Barr). *Nachrichtenbl. Deut. Pflanzenschutzd.*, **53**(3), 12.
- SEIJO, F., B. CESPEDES, and G. ZAVALA (2018). Traditional Fire Use Impact in the Aboveground Carbon Stock of the Chestnut Forests of Central Spain and Its Implications for Prescribed Burning. *Science of The Total Environment*, **625**, 1405–1414. doi:10.1016/j.scitotenv.2017.12.079.
- SIGNORELL, A. (2021). DescTools: Tools for Descriptive Statistics. <https://CRAN.R-project.org/package=DescTools>.
- SIMHA, A., C. P.-D. LA HOZ, and L. CARLEY (2022). Moving beyond the “Diversity Paradox”: The Limitations of Competition-Based Frameworks in Understanding Species Diversity. *The American Naturalist*, 89–100. doi:10.1086/720002.

- SITTARO, F., A. PAQUETTE, C. MESSIER, and C. A. NOCK (2017). Tree Range Expansion in Eastern North America Fails to Keep Pace with Climate Warming at Northern Range Limits. *Global Change Biology*, **23**(8), 3292–3301. doi:10.1111/gcb.13622.
- SMITH, V. H., G. D. TILMAN, and J. C. NEKOLA (1999). Eutrophication: Impacts of Excess Nutrient Inputs on Freshwater, Marine, and Terrestrial Ecosystems. *Environmental Pollution*, **100**(1-3), 179–196.
- SMITHERS, B. V., M. P. NORTH, C. I. MILLAR, and A. M. LATIMER (2018). Leap Frog in Slow Motion: Divergent Responses of Tree Species and Life Stages to Climatic Warming in Great Basin Subalpine Forests. *Global Change Biology*, **24**(2), e442–e457. doi:10.1111/gcb.13881.
- SOBERÓN, J. and A. T. PETERSON (2005). Interpretation of Models of Fundamental Ecological Niches and Species' Distributional Areas. *Biodiversity Informatics*, **2**. doi:10.17161/bi.v2i0.4.
- SOETAERT, K., T. PETZOLDT, and R. W. SETZER (2010). Solving Differential Equations in R: Package deSolve. *Journal of Statistical Software*, **33**(9), 1–25. doi:10.18637/jss.v033.i09.
- SPINONI, J., J. VOGT, and P. BARBOSA (2015). European Degree-Day Climatologies and Trends for the Period 1951-2011. *International Journal of Climatology*, **35**(1), 25–36. doi:10.1002/joc.3959.
- STAGGE, J. H., D. G. KINGSTON, L. M. TALLAKSEN, and D. M. HANNAH (2017). Observed Drought Indices Show Increasing Divergence across Europe. *Scientific Reports*, **7**(1), 14045. doi:10.1038/s41598-017-14283-2.
- STAN DEVELOPMENT TEAM (2022). Stan Modeling Language Users Guide and Reference Manual. <https://mc-stan.org>.
- STARFINGER, U., I. KOWARIK, M. RODE, and H. SCHEPKER (2003). From Desirable Ornamental Plant to Pest to Accepted Addition to the Flora? – The Perception of an Alien Tree Species Through the Centuries. *Biological Invasions*, **5**(4), 323–335. doi:10.1023/B:BINV.0000005573.14800.07.
- STILLHARD, J., M. L. HOBI, P. BRANG, U.-B. BRÄNDLI, M. KOROL, V. POKYNCHEREDA, and M. ABEGG (2022). Structural Changes in a Primeval Beech Forest at the Landscape Scale. *Forest Ecology and Management*, **504**, 119836. doi:10.1016/j.foreco.2021.119836.
- STOHLGREN, T. J., R. R. BACHAND, Y. ONAMI, and D. BINKLEY (1998). Species-Environment Relationships and Vegetation Patterns: Effects of Spatial Scale and Tree Life-Stage. *Plant Ecology*, **135**, 14.
- SUTHERLAND, W. J., R. P. FRECKLETON, H. C. J. GODFRAY, S. R. BEISSINGER, T. BENTON, D. D. CAMERON, Y. CARMEL, D. A. COOMES, T. COULSON, M. C. EMMERSON, R. S. HAILS, G. C. HAYS, D. J. HODGSON, M. J. HUTCHINGS, D. JOHNSON, J. P. G. JONES, M. J. KEELING, H. KOKKO, W. E. KUNIN, X. LAMBIN, O. T. LEWIS, Y. MALHI, N. MIESZKOWSKA, E. J. MILNER-GULLAND, K. NORRIS, A. B. PHILLIMORE, D. W. PURVES, J. M. REID, D. C. REUMAN, K. THOMPSON, J. M. J. TRAVIS, L. A. TURNBULL,

- D. A. WARDLE, and T. WIEGAND (2013). Identification of 100 Fundamental Ecological Questions. *Journal of Ecology*, **101**(1), 58–67. doi:10.1111/1365-2745.12025.
- SYKES, M. T., I. C. PRENTICE, and W. CRAMER (1996). A Bioclimatic Model for the Potential Distributions of North European Tree Species Under Present and Future Climates. *Journal of Biogeography*, **23**(2), 203–233. arXiv:2845812.
- TER BRAAK, C. J. and I. C. PRENTICE (1988). A Theory of Gradient Analysis. In: *Advances in Ecological Research*, volume 18, 271–317. Elsevier. doi:10.1016/S0065-2504(08)60183-X.
- THOMAS, S. C. and W. E. WINNER (2002). Photosynthetic Differences between Saplings and Adult Trees: An Integration of Field Results by Meta-Analysis. *Tree Physiology*, **22**(2-3), 117–127. doi:10.1093/treephys/22.2-3.117.
- THORNTON, C. W. (1948). An Approach toward a Rational Classification of Climate. *Geographical Review*, **38**(1), 55–94.
- THUILLER, W., T. MÜNKEMÜLLER, S. LAVERGNE, D. MOUILLOT, N. MOUQUET, K. SCHIFFERS, and D. GRAVEL (2013). A Road Map for Integrating Eco-Evolutionary Processes into Biodiversity Models. *Ecology Letters*, **16**, 94–105. doi:10.1111/ele.12104.
- THUILLER, W., T. MÜNKEMÜLLER, K. H. SCHIFFERS, D. GEORGES, S. DULLINGER, V. M. ECKHART, T. C. EDWARDS, D. GRAVEL, G. KUNSTLER, C. MEROW, K. MOORE, C. PIEDALLU, S. VISSAULT, N. E. ZIMMERMANN, D. ZURELL, and F. M. SCHURR (2014). Does Probability of Occurrence Relate to Population Dynamics? *Ecography*, **37**(12), 1155–1166. doi:10.1111/ecog.00836.
- TILMAN, D. (1982). *Resource Competition and Community Structure*. Number 17 in Monographs in Population Biology. Princeton University Press, Princeton, N.J.
- TOMPO, E., T. GSCHWANTNER, and M. L. P. FOR COMMON (2010). *National Forest Inventories*. Springer, Heidelberg Dordrecht London New York.
- TURNER, B. L., E. F. LAMBIN, and A. REENBERG (2007). The Emergence of Land Change Science for Global Environmental Change and Sustainability. *Proceedings of the National Academy of Sciences*, **104**(52), 20666–20671. doi:10.1073/pnas.0704119104.
- URBIETA, I. R., L. V. GARCÍA, M. A. ZAVALA, and T. MARAÑÓN (2011). Mediterranean Pine and Oak Distribution in Southern Spain: Is There a Mismatch between Regeneration and Adult Distribution?: Pine and Oak Adult and Regeneration Distribution. *Journal of Vegetation Science*, **22**(1), 18–31. doi:10.1111/j.1654-1103.2010.01222.x.
- VALDEZ, J. W., F. HARTIG, S. FENNEL, and P. POSCHLOD (2019). The Recruitment Niche Predicts Plant Community Assembly Across a Hydrological Gradient Along Plowed and Undisturbed Transects in a Former Agricultural Wetland. *Frontiers in Plant Science*, **10**. doi:10.3389/fpls.2019.00088.
- VALLADARES, F. and Ü. NIINEMETS (2008). Shade Tolerance, a Key Plant Feature of Complex Nature and Consequences. *Annual Review of Ecology, Evolution, and Systematics*, **39**(1), 237–257. doi:10.1146/annurev.ecolsys.39.110707.173506.

- VANDERWEL, M. C., D. M. A. ROZENDAAL, and M. E. K. EVANS (2017). Predicting the Abundance of Forest Types across the Eastern United States through Inverse Modelling of Tree Demography. *Ecological Applications*, **27**(7), 2128–2141. doi:10.1002/eap.1596/full.
- VECCHIO, S. D., E. FANTINATO, M. ROSCINI, A. T. R. ACOSTA, G. BACCHETTA, and G. BUFFA (2020). The Germination Niche of Coastal Dune Species as Related to Their Occurrence along a Sea–Inland Gradient. *Journal of Vegetation Science*, **n/a**(n/a). doi:10.1111/jvs.12899.
- VEHTARI, A., A. GELMAN, D. SIMPSON, B. CARPENTER, and P.-C. BÜRKNER (2021). Rank-Normalization, Folding, and Localization: An Improved R for Assessing Convergence of MCMC (with Discussion). *Bayesian Analysis*, **16**(2), 667–718. doi:10.1214/20-BA1221.
- VELLEND, M. (2010). Conceptual Synthesis in Community Ecology. *The Quarterly Review of Biology*, **85**(2), 183–206. doi:10.1086/652373.
- VITASSE, Y. (2013). Ontogenic Changes Rather than Difference in Temperature Cause Understory Trees to Leaf out Earlier. *New Phytologist*, **198**(1), 149–155. doi:10.1111/nph.12130.
- VOSPERNIK, S. (2021). Basal Area Increment Models Accounting for Climate and Mixture for Austrian Tree Species. *Forest Ecology and Management*, **480**, 118725. doi:10.1016/j.foreco.2020.118725.
- WALTHER, G.-R., E. POST, P. CONVEY, A. MENZEL, C. PARMESAN, T. J. C. BEEBEE, J.-M. FROMENTIN, O. HOEGH-GULDBERG, and F. BAIRLEIN (2002). Ecological Responses to Recent Climate Change. *Nature*, **416**(6879), 389–395. doi:10.1038/416389a.
- WASON, J. W. and M. DOVCIAK (2017). Tree Demography Suggests Multiple Directions and Drivers for Species Range Shifts in Mountains of Northeastern United States. *Global Change Biology*, **23**(8), 3335–3347. doi:10.1111/gcb.13584.
- WATKINSON, A. (1980). Density-Dependence in Single-Species Populations of Plants. *Journal of Theoretical Biology*, **83**(2), 345–357. doi:10.1016/0022-5193(80)90297-0.
- WATKINSON, A. R. (1985). On the Abundance of Plants Along an Environmental Gradient. *The Journal of Ecology*, **73**(2), 569. arXiv:2260494, doi:10.2307/2260494.
- WATT, A. S. (1923). On the Ecology of British Beechwoods with Special Reference to Their Regeneration. *The Journal of Ecology*, **11**(1), 1. arXiv:2255601, doi:10.2307/2255601.
- WELANDER, N. T. and B. OTTOSSON (1998). The Influence of Shading on Growth and Morphology in Seedlings of *Quercus Robur* L. and *Fagus Sylvatica* L. *Forest Ecology and Management*, **107**, 117–126.
- WERNER, E. E. (1984). The Ontogenetic Niche and Species Interactions in Size-Structured Populations. *Annual Review of Ecology and Systematics*, **15**, 393–425.
- WHITMORE, T. C. (1989). Canopy Gaps and the Two Major Groups of Forest Trees. *Ecology*, **70**(3), 536–538. doi:10.2307/1940195.

- WHITTAKER, R. H. (1967). Gradient Analysis of Vegetation. *Biological Reviews*, **42**(2), 207–264. doi:10.1111/j.1469-185X.1967.tb01419.x.
- WILKINSON, G. N. and C. E. ROGERS (1973). Symbolic Description of Factorial Models for Analysis of Variance. *Applied Statistics*, **22**(3), 392. arXiv:10.2307/2346786, doi:10.2307/2346786.
- WOOD, S. (2021). Mgcvm: Mixed GAM Computation Vehicle with Automatic Smoothness Estimation. <https://CRAN.R-project.org/package=mgcv>.
- WOODALL, C., C. OSWALT, J. WESTFALL, C. PERRY, M. NELSON, and A. FINLEY (2009). An Indicator of Tree Migration in Forests of the Eastern United States. *Forest Ecology and Management*, **257**(5), 1434–1444. doi:10.1016/j.foreco.2008.12.013.
- WOODALL, C., K. ZHU, J. WESTFALL, C. OSWALT, A. D'AMATO, B. WALTERS, and H. LINTZ (2013). Assessing the Stability of Tree Ranges and Influence of Disturbance in Eastern US Forests. *Forest Ecology and Management*, **291**, 172–180. doi:10.1016/j.foreco.2012.11.047.
- WOODWARD, F. I. (1987). *Climate and Plant Distribution*. Cambridge University Press.
- WOODWARD, F. I. (1988). Temperature and the Distribution of Plant Species. *Symposia of the Society for Experimental Biology*, **42**, 59–75.
- WOODWARD, F. I. and B. G. WILLIAMS (1987). Climate and Plant Distribution at Global and Local Scales. *Vegetatio*, **69**(1-3), 189–197. doi:10.1007/BF00038700.
- YOUNG, T. P., D. A. PETERSEN, and J. J. CLARY (2005). The Ecology of Restoration: Historical Links, Emerging Issues and Unexplored Realms. *Ecology Letters*, **8**(6), 662–673. doi:10.1111/j.1461-0248.2005.00764.x.
- ZHU, K., C. W. WOODALL, S. GHOSH, A. E. GELFAND, and J. S. CLARK (2014). Dual Impacts of Climate Change: Forest Migration and Turnover through Life History. *Global Change Biology*, **20**(1), 251–264. doi:10.1111/gcb.12382.
- ZURELL, D., V. GRIMM, E. ROSSMANITH, N. ZBINDEN, N. E. ZIMMERMANN, and B. SCHRÖDER (2012). Uncertainty in Predictions of Range Dynamics: Black Grouse Climbing the Swiss Alps. *Ecography*, **35**(7), 590–603. doi:10.1111/j.1600-0587.2011.07200.x.
- ZURELL, D., W. THULLER, J. PAGEL, J. S. CABRAL, T. MÜNKEMÜLLER, D. GRAVEL, S. DULLINGER, S. NORMAND, K. H. SCHIFFERS, K. A. MOORE, and N. E. ZIMMERMANN (2016). Benchmarking Novel Approaches for Modelling Species Range Dynamics. *Global Change Biology*, **22**(8), 2651–2664. doi:10.1111/gcb.13251.